Structural evolution of the lower Agardhfjellet Formation, in Central Spitsbergen:

Implications for caprock integrity

Lise Nakken

UNIS

The University Centre in Svalbard

Thesis submitted for the degree of
Master in Geoscience
(Structural Geology)
60 credits

Department of Geoscience
Faculty of mathematics and natural sciences

UNIVERSITY OF OSLO

Spring 2020

Structural evolution of the lower Agardhfjellet Formation, in Central Spitsbergen:

Implications for caprock integrity

Lise Nakken

Structural evolution of the lower Agardhfjellet Formation, in Central Spitsbergen:

http://www.duo.uio.no/

Printed: X-press printing house

Acknowledgement

First and foremost, I extend my thanks to my two main supervisors. Mark Mulrooney (UiO), thank you for your guidance during fieldwork and for your tedious work during my thesis writing, which has significantly improved the outcome of my work. Kim Senger (UNIS), thank you for enabling me to continue my studies in the amazing Svalbard scenery and for always being supportive and helpful. All your constructive remarks and suggestions are much appreciated. I also want to thank my co-supervisor Elin Skurtveit (NGI) for hosting my thesis in the NCCS project.

I would like to thank the Department of Geoscience at the University of Oslo, Svalbard Science Forum and Jan Christensens Legat for financial support, enabling me to complete two successful field campaigns and thesis work on Svalbard.

Data access granted by the UNIS CO_2 Lab is highly appreciated. Also, thanks to Niklas Schaaf for providing me with his collected data.

I am very grateful for all help I have received from field assistants Astrid Vikingstad, Matthjis Nuus, Peter Betlem, Rakul Johanessen and Tom Birchall. The data collection would not have been manageable without your help and the polar beer encounters would not have felt so safe.

Big thanks to all my UiO friends and to all the amazing people I have gotten to know in Svalbard, especially my quarantine buddies in Nybyen. Thanks to Martin Vika Gjesteland for fruitful discussions and supportive phone calls. Finally, I am forever grateful for Karoline Løvlie for being my co-student and best friend for the past five years. You have helped me become the geologist I am today!

Finally, thanks to my loving family for always supporting me throughout my studies.

Abstract

This study documents the presence of faults and fractures in the shale dominated lower Agardhfjellet Formation in central Spitsbergen, Svalbard. Results from two drill cores and outcrops are presented with the ultimate goal of understanding the nature and abundance of analysed faults and fractures present in the upper Jurassic formation. The structural evaluation herein presents an emphasis of the geological evolution responsible for the development of the analysed structures. The Agardhfjellet Formation is considered a caprock for UNIS CO_2 Lab project. Accordingly, this study aims to assess the implications the analysed structures have on integrity of the lowermost caprock interval for CO_2 storage purposes.

A normal fault array trending northeast-southwest has been analysed with the maximum offset of 8 meters, argued to have formed in during the Paleogene Western Spitsbergen fold-and-thrust-belt. This study suggests potential formation mechanisms of the extensional faults in an overall contractional regime. The key control of fracture formation in the lower Agardhfjellet Formation is suggested to be caused by the same tectonic event. This is documented through low angled shear fractures analysed in drill cores and predominantly ENE-WSW-tending, steep dipping, open fractures from outcrops.

Detailed fault core architecture analysis were conducted, aiming to reveal potential migration pathways. The results suggest that the fault core itself will act baffle for fluids. However, increased fracturing in damage zones adjacent to the faults are considered a potential risk for creating migration pathways.

The modification of petrophysical properties in the lower Agardhfjellet Formation is significantly affected by the analysed structures presented herein. Swarms of increased steep fractures adjacent to faults in combination with the low angled shear fractures is considered the main risk for fluid migration through the lower Agardhfjellet Formation. However, based on the current subsuface conditions, with contrasting pore pressures in the lower Agardhfjellet Formation and in an aquifer overlying the complete caprock succession, there are indications that the caprock succession as a whole is an efficient seal for CO_2 sequestration purposes.

Contents

List of Tables

List of Figures

Chapter 1

Introduction

1.1 Thesis outline

This thesis will present a field based study conducted on central Spitsbergen in Svalbard. The investigations target the lower to mid Agardhfjellet Formation of Upper Jurassic age. The shale-rich formation is considered a caprock for CO_2 sequestration in the UNIS CO_2 Lab project. The main motivation for this study was to assess the nature and evolution of the geological structures present in the lowermost interval of the caprock (i.e. lower Agardhfjellet Formation). Further, the caprock succession on Svalbard can be used as an analogue for the time equivalent shales of Hekking Formation in the Barents Sea and the Draupne Formation in the North Sea. As this project forms part of the larger SINTEF-hosted NCCS (Norwegian CCS Research Center) project, the goal was to understand the potential risks structural discontinuities might have on caprock integrity.

A combination of classical geological techniques and modern tools were used in order to map the fracture network and fault array, present in the Oppdalen, Lardyfjellet and Oppdalsåata members of the Agardhfjellet Formation. The results herein presents structural mapping of fractures and meso-scale extensional faults from outcrops. Further, drill core analyses from this study presents detailed fracture characterisation. Insights from drill cores and outcrops are integrated to conduct a complete assessment of the lowermost caprock succession in order to predict potential structures that might compromise the caprock integrity.

1.2 Motivations

The Norwegian CCS Research Center (NCCS) initiative aims to ensure Norway's position in CCS research and to support an industry driven full-scale CCS chain. The project includes all aspects; capturing CO_2 from various onshore industries, transporting it by ship and inject it for permanent storage below the seabed in the North Sea. The Intergovernmental Panel on Climate Change (IPCC) recommended CCS as a necessary measure to reach any goals of lowering anthropogenic emissions to keep global warming

to 1.5°C (Metz et al., 2005). The importance of geology is related to the storage site for the captured CO_2. The same components are needed as in a classical petroleum system. This includes a porous and permeable storage formation, where the captured CO_2 will be injected, and a robust caprock to ensure safe and lasting storage of the CO_2. UNIS CO_2 Lab was an academic driven project initiated in 2006, aiming to evaluate the subsurface in central Spitsbergen as a potential geological storage cite. The Triassic storage formation comprised of the Wilhelmøya Subgroup has been thoroughly analysed by Bohloli et al. (2014); Braathen et al. (2012); Ogata et al. (2014b) and others. The same authors and Schaaf (2017) have conducted work to assess the sealing properties of the Agardhfjellet Formation, but a complete analysis of the structures within the caprock succession was yet to be conducted.

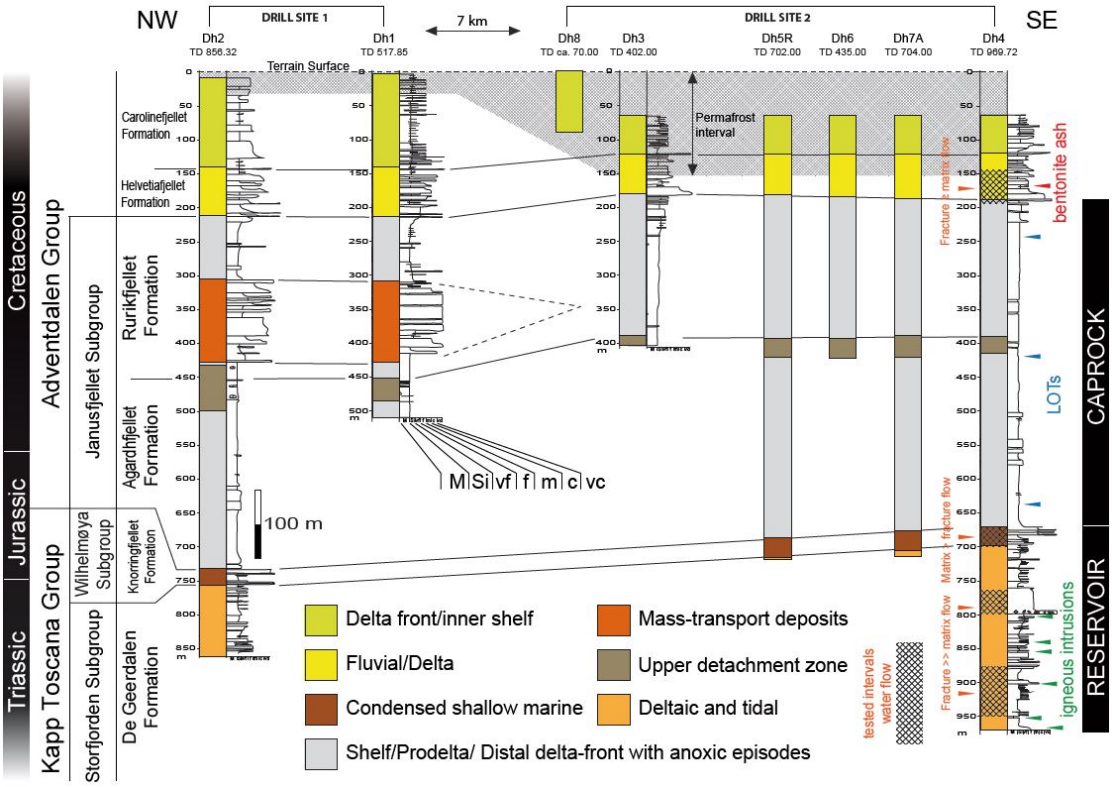

Figure 1.1: Figure from Ogata et al. (2014b) presenting the targeted subsurface formations in the UNIS CO_2 Lab project, with the storage formation comprised by the Wilhelmøya Subgroup and the caprock (i.e. Agardhfjellet and Rurikfjellet formations).

1.2.1 Utilising Svalbard as an analogue to offshore Norway

In terms of stratigraphy, there is a correlation between Svalbard, the Barents Sea and the North Sea (Stoker et al., 2017). Hence, the onshore geology in Svalbard is a window into the offshore subsurface geology. The rock record varies from North Sea, Barents Sea and Svalbard because of their geographic positions. However, some periods of time equivalent deposition have similar characteristics. The targeted Upper Jurassic is one of these (Dypvik and Harris, 2001; Abay et al., 2017), which increases the application of the results from this study to investigations of the time equivalents in the North Sea and in the Barent Sea.

1.3 Introduction to study area

The present-day outcrops of the Agardhfjellet Formation are predominantly found in central Spitsbergen (Fig. 1.2). The site selection for this study was chosen because the entire caprock succession is present in the subsurface and in outcrops, both in proximity to Longyearbyen (Fig. 1.2). Subsurface data from two drill holes in Adventdalen were used. These wells are located approximately eight kilometers apart.

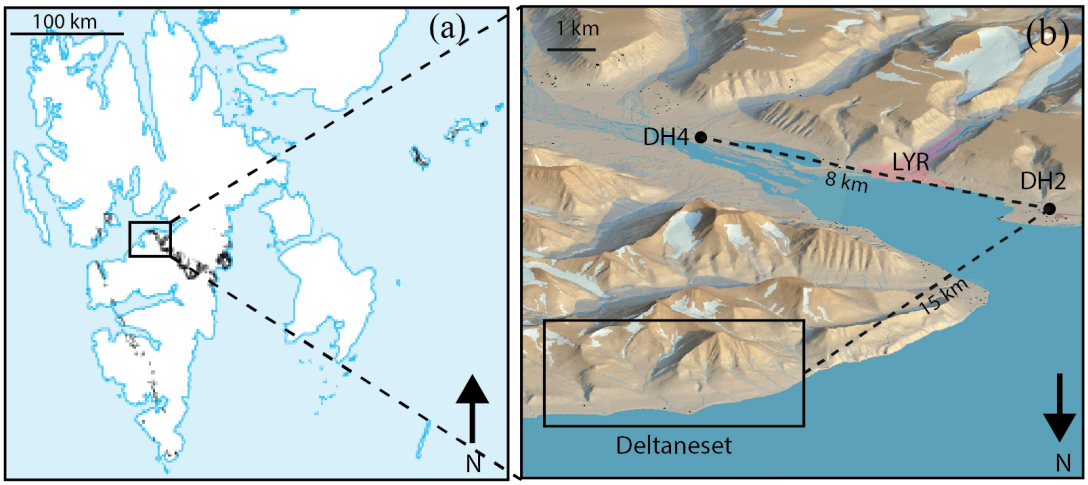

Figure 1.2: (a) Present day outcrops of the Agardhfjellet Formation, modified from Mørk et al. (1999a). (b) 3D map of the study area for this study with marked location of DH2 and DH4 in relation to the field site near Deltaneset (map retrieved from toposvalbard.no).

1.4 Objectives

Preliminary investigations of the for UNIS CO_2 Lab caprock have identified faults and fractures that in the lower Agardhfjellet Formation. To gain a complete understanding of the occurrence of these structures, as well as their implications for caprock integrity, this study aims to:

- Determine which geological event formed the fracture networks and the extensional faults in the lower Agardhfjellet Formation.
- Conduct detailed analysis of normal faults in outcrops, in order to assess the faults vertical and lateral extent, as well as defining fault core architecture.
- Assess how the structural elements in the lower Agardhfjellet Formation influence cap rock integrity.

Chapter 2

Geological setting

In this chapter, a summary of the tectonostratigraphic development of the NW Barents Shelf and Svalbard will be given. The outcrops in Svalbard gives access to the Barents shelf geology as it is uplifted. Further, more detailed description of the deposition of the Agardhfjellet Formation with an emphasis of the members studies herein will be outlined. Further, post depositional geological events that has affected the targeted Mesozoic strata in central Spitsbergen will be presented. Finally, previous studies recording normal faulting in the Agardhfjellet Formation will be presented.

Svalbard is comprised of a mostly continuous geological succession ranging in age from the Proterozoic to present (Fig. 2.1a; Worsley (1986); Dallmann (1999); Mørk et al. (1999a)). Major north–south trending basement-rooted fault zones were reactivated repeatedly and controlled the positions of major depocentres. These structural elements are long-lived, initially forming during the Caledonian Orogeny, and reactivating as contractional faults in the Devonian, extensional faults in the Carboniferous and contractional faults, again, in the Paleogene (Mcwhae, 1952; Bergh et al., 1997; Braathen and Bergh, 1995; Braathen et al., 1999a; Leever et al., 2011; Bælum and Braathen, 2012).

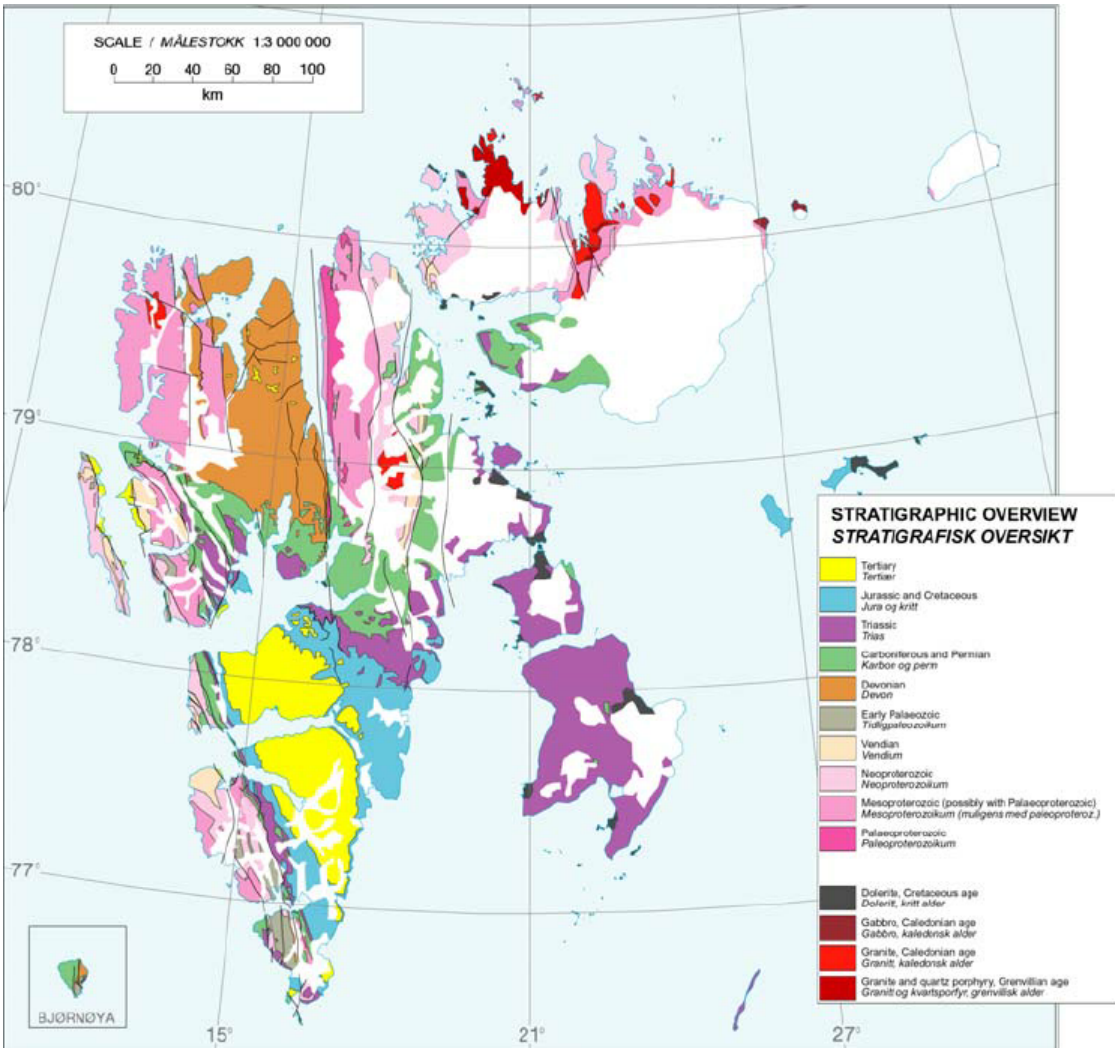

Figure 2.1: Geological map of Svalbard from Dallmann et al. (2015).

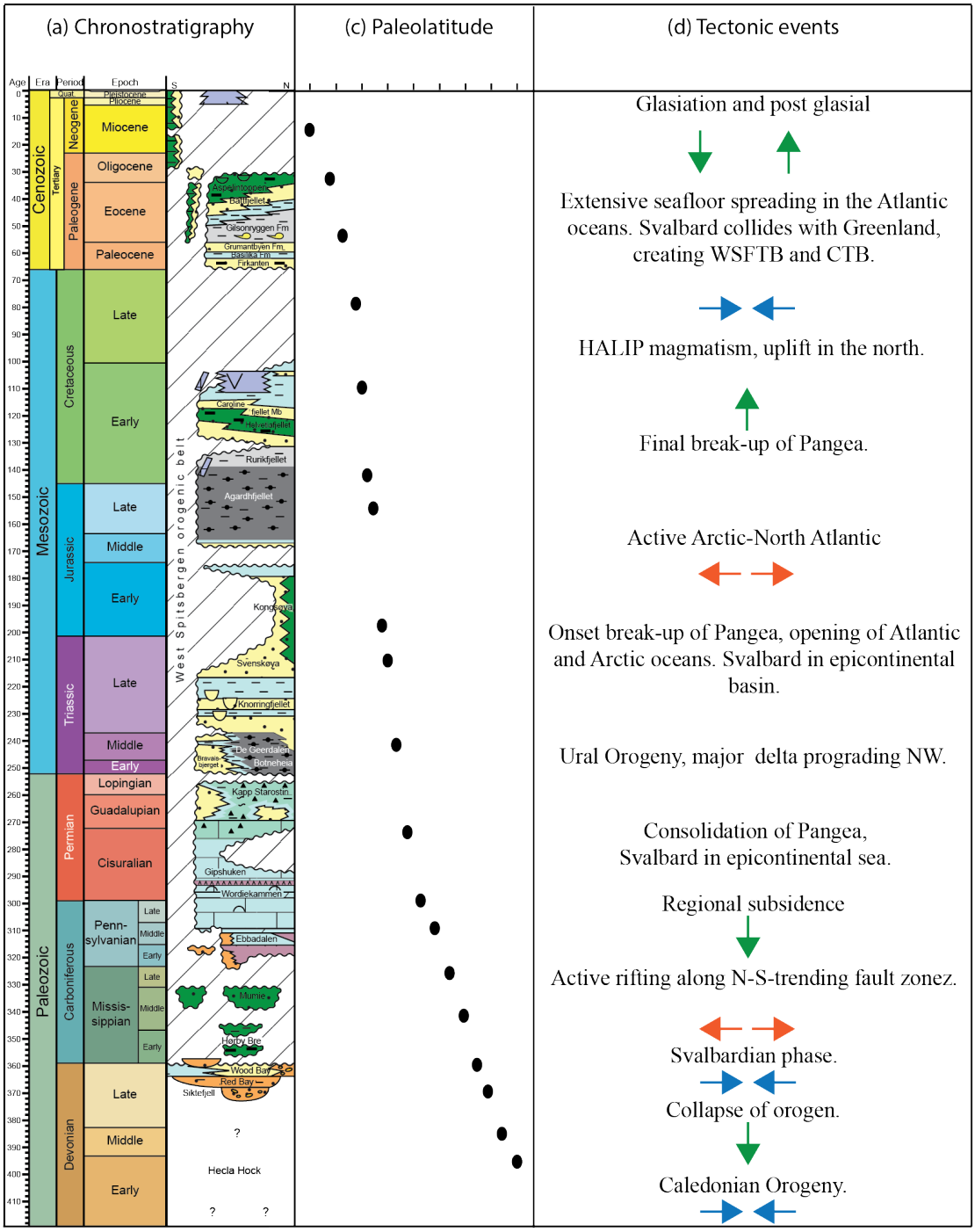

Figure 2.2: (a) Chronostratigraphy and (b) lithology (NPD). (c) Paleogeographic reconstructions, modified from (Dallmann et al., 2015). (d) Brief summary of key events for the geological evolution, compiled from Dallmann et al. (2015) and Faleide et al. (2010).

2.1 Deposition of Agardhfjellet Formation

Following the break-up of Pangea, seafloor spreading commenced in the Middle Jurassic opening the North Atlantic and Arctic oceans (Skogseid et al., 2000; Brekke et al., 2001; Faleide et al., 2010). Increased seafloor spreading rates in the Kimmeridgian was accompanied by high eustatic sea level rise which flooded extensive areas. (Fig. 2.3; Brekke et al. (2001); Faleide et al. (2010)). This major transgression led to regional deposition of the shale dominated Agardhfjellet Formation and the Barents Sea and North Sea time equivalents, the Hekkingen and Draupne formations respectively (Dypvik, 1984; **?**). The global time equivalent is the Kimmeridge Clay (Dypvik, 1984; Torsvik et al., 2002).

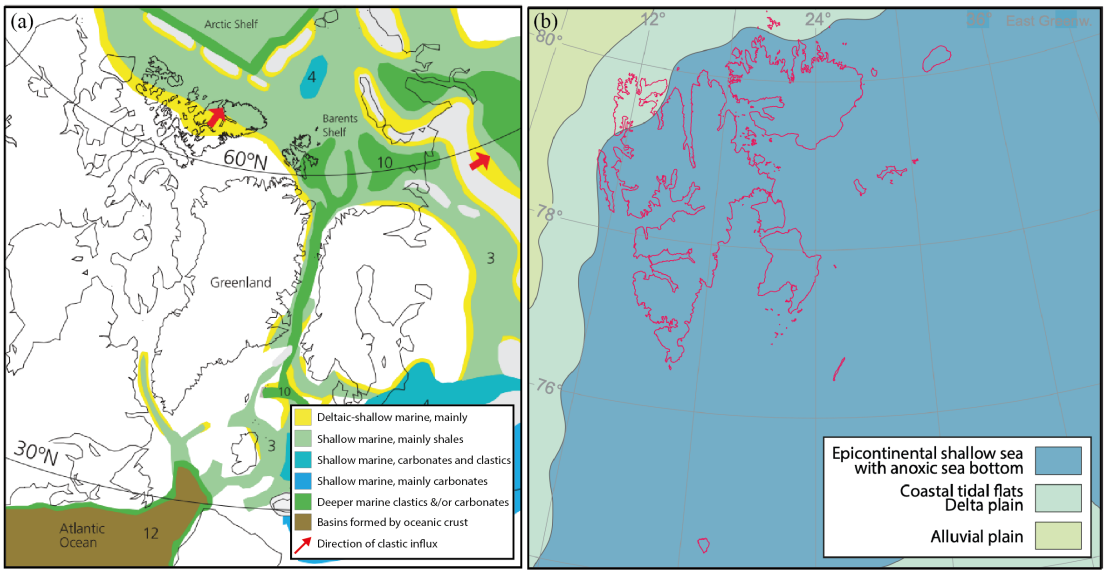

Figure 2.3: (a) Late Jurassic (Oxfordian-Tithonian) extent of the Kimmeridge Clay. Modified from Torsvik et al. (2002). (b) Paleogeographic reconstruction from Upper Jurassic (Kimmeridgian). Modified from Dallmann et al. (2015).

The Agardhfjellet Formation is divided into four members, from oldest to youngest; the Oppdalen, Lardyfjellet, Oppdalssåta and Slottsmøys members (Dypvik et al., 1991; Mørk et al., 1999a; Koevoets et al., 2019; Rismyhr et al., 2019). The lowermost boundary to the Agardhfjellet Formation is defined as the first siltstone bed overlying the phosphatic, conglomeratic Brentskardhaugen Bed (Bäckström and Nagy, 1985; Krajewski, 1990; Mørk et al., 1999a; Krajewski et al., 2001; Krajewski, 2004; Koevoets et al., 2019). The following Oppdalen Member is mainly comprised of siltstones with fossiliferous siderite beds, deposited in a shallow marine environment (Birkenmajer et al., 1982;

Bäckström and Nagy, 1985; Dypvik et al., 1991; Mørk et al., 1999a; Koevoets et al., 2019). The oolitic Marhøgda Bed is comprising the lowermost interval of the Oppdalen Member (Krajewski, 1990). Lardyfjellet Member consists of darker shales, with only few siderite horizons or lenses Dypvik et al. (1991); Mørk et al. (1999a); Koevoets et al. (2019). The third Oppdalssåta Member is the coarsest interval of the Agardhfjellet Formation, comprised by shale, siltstone and sandstone in 10-15 meter thick intervals that are coarsening upward (Dypvik et al., 1991; Dypvik and Harris, 2001; Koevoets et al., 2019). The Lardyfjellet and Oppdalssåta members were deposited on an open marine shelf with with periodically restricted water circulation. This led to anoxic conditions and hence high organic content (up to 11% TOC; Krajewski (2004); Koevoets et al. (2019)). Sideride beds and lenses has formed in carbonate rich beds throughout the Agardhfjellet Formation during diagenesis (Bjærke et al., 1980; Krajewski et al., 2001).

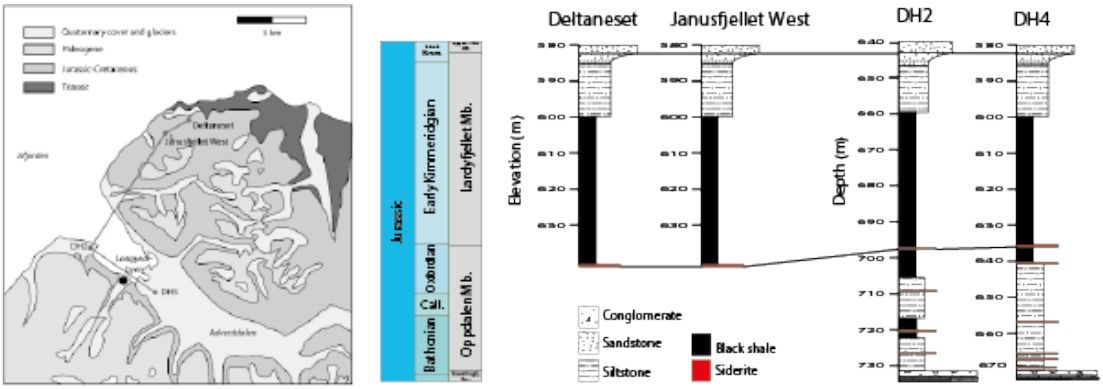

Figure 2.4: (a) Map with location of the logs, modified from Koevoets et al. (2019). (b) Sedimentary logs from the investigated areas in this study. Modified from Koevoets et al. (2016).

2.2 Post depositional events

2.2.1 Early Cretaceous High Arctic Large Igneous Province

In the Early Cretaceous, the opening of the Amerasia Basin resulted in the High Arctic Large Igneous Province (HALIP) affecting Svalbard and areas further north (Maher, 2001; Midtkandal et al., 2007; Nejbert et al., 2011; Minakov et al., 2012; Corfu et al., 2013; Senger et al., 2014b; Polteau et al., 2016; Maher et al., 2020). This led to magmatic activity on Svalbard, which is primarily expressed as doleritic sills that intrude the Mesozoic succession. Associated regional thermal uplift to the north in a response to

the magmatic activity has resulted in a major hiatus on Svalbard (Dörr et al., 2012; Smelror[1] and Larssen, 2016; Jochmann et al., 2019).

2.2.2 Paleogene West Spitsbergen fold-and-thrust-belt

The Paleogene West Spitsbergen fold-and-thrust-belt (WSTFB) has been extensively studied (e.g., Braathen and Bergh (1995); Bergh et al. (1997); Leever et al. (2011); Maher Jr et al. (1995); Worsley (1986)). The tectonic framework is well-established and summarised in 2.5. Extension in the Labrador Sea and Baffin Bay was followed by subsequent sea floor spreading related to the opening of the Arctic- and North Atlantic Ocean (Faleide et al., 2010; Dallmann et al., 2015). The WSFTB developed as a result of transpressional movement between Greenland and Spitsbergen, with the initial principal stress trending NNE-SSW progressive to subsequent NE-SW shortening (Braathen and Bergh, 1995; Bergh et al., 1997; Braathen et al., 1999b; Leever et al., 2011; Gasser, 2014). Subsequently, opening of the North Atlantic Ocean continued, finally separating Spitsbergen and Greenland.

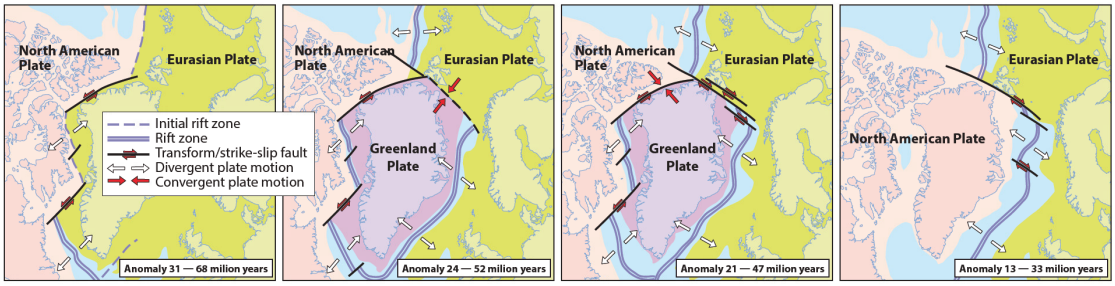

Figure 2.5: West Spitsbergen fold-and-thrust-belt reconstruction. Modified from Dallmann et al. (2015).

The impact of the Paleogene WSFTB is preserved in the rock record throughout Spitsbergen. The thick-skinned deformation,i.e., involving basement structures, was concentrated in the fold-and-thrust-belt in the west (Fig. 2.6; Braathen and Bergh (1995); Bergh et al. (1997); Braathen et al. (1999b); Leever et al. (2011)). The deformation propagated eastward through thin-skinned deformation where detachement or decollement zones exploited shale rich and gypsum units (Bergh and Andresen, 1990; Andresen et al., 1992).The shale detachments developed in the Botneheia, Agardhfjellet and Rurikfjellet formations respectively (Haremo et al., 1990; Andresen et al., 1992). Further, inversion of preexisting structures (Haremo and Andresen, 1992; Welbon and Maher Jr, 1992; Leever et al., 2011; Bælum and Braathen, 2012). As the orogen formed,

increased loading induced flexural subsidence creating a foreland basin i.e., the Central Tertiary Basin (Steel et al., 1985).

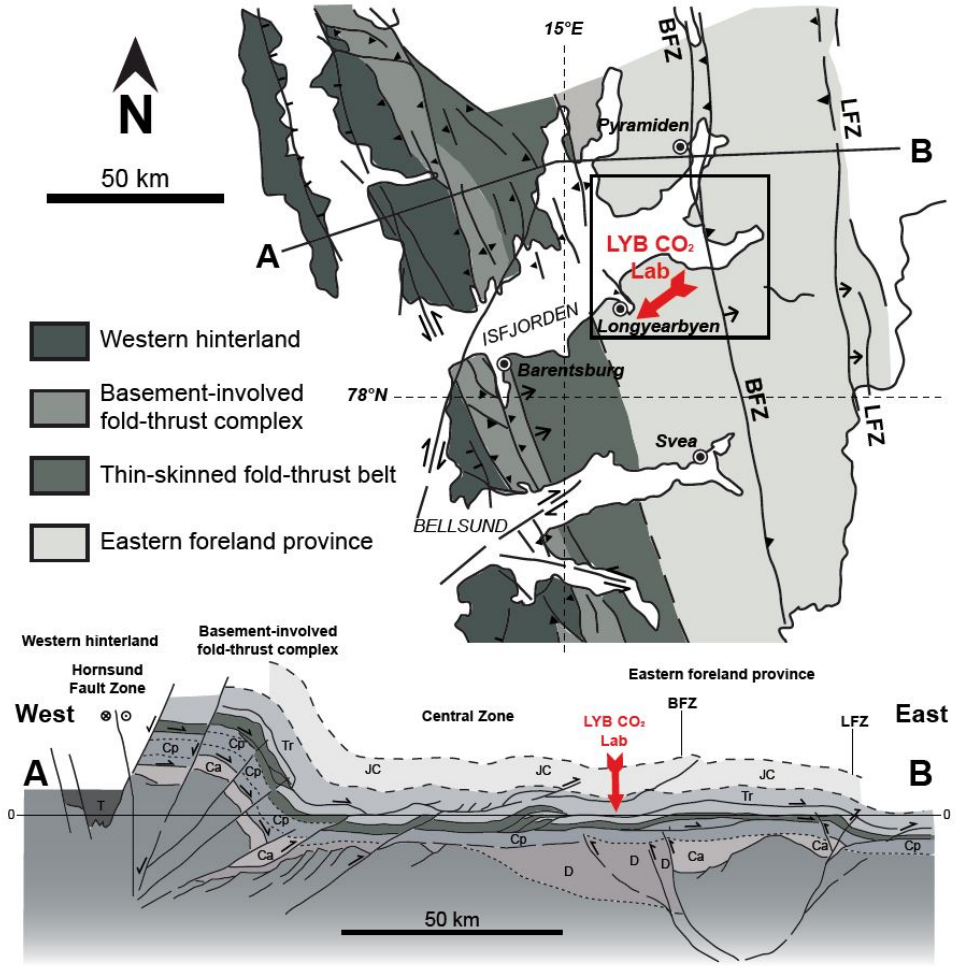

Figure 2.6: West Spitsbergen fold-and-thrust-belt reconstruction. Modified from Dallmann et al. (2015).

2.2.3 Quaternary glaciation and deglaciation

The Barents Sea and Svalbard experienced uplift and erosion due to repeated glaciation from the Oligocene to Quaternary Dimakis et al. (1998); Bohloli et al. (2014). Glacial isostatic rebound likely resulted in a few kilometers uplift Dimakis et al. (1998). Severe underpressure recorded in the storage formation and lowermost Agardhfjellet Formation for the UNIS CO2 Lab (Bohloli et al., 2014) is suggested to develop due to repeated glaciations, followed by isostatic rebound and subsequent erosion (Wangen et al., 2016).

Chapter 3

Scientific background

This chapter provides the scientific background on the formation and classification of structural discontinuities, and their implications for fluid flow. Firstly, the mechanisms causing deformation of rocks are outlined. Secondly, the terminology used to describe faults and fractures in this study is presented. Finally, the implications of faults and fractures for caprock integrity will be presented.

3.1 Driving mechanisms for deformation

Driving mechanisms for brittle deformation are controlled by basin subsidence (i.e. loading and diagenesis), uplift and subsequent erosion (i.e. decompaction) or external tectonic forces (Freund, 1998; Nelson, 2001; Schultz and Fossen, 2008). These processes change the stress relations acting on a rock. When external forces exceeds the internal strength of a rock, the rock will mechanically fail accordingly. Hydraulic fractures develop as a result of pore pressure exceeding the internal strength of a rock (Engelder and Lacazette, 1990). As a result, the stress acting on the rock normalises and pore pressure decreases. Uplift is coupled with erosion and hence, rocks elevated from depth will experience decreased stress (Nelson, 2001). Accordingly, generation of new or opening of preexisting fractures can take place response to decompaction.

3.2 Kinematics and terminology

Figure 3.1a present the kinematic of fracture development in relation to principal stresses. Three modes of fracturing can be defined based on the relative movement (Freund, 1998; Nelson, 2001; Schultz and Fossen, 2008). Mode I is tension fractures, forming parallel to the maximum stress axis (Fig. 3.1b). Veins are mode I fractures, which later has precipitated minerals in the voids (Schultz and Fossen, 2008). Mode II and III are shear fractures, which commonly develop conjugate fractures at 20-40 $^\circ$ from the maximum stress axis. Figure 3.1c show how the shear movement can be in plane (mode II), whereas Figure 3.1d show shear movement out of the plane (mode III). Shear fractures commonly display slickensided fracture surfaces, which are striations forming due to movement

along the fracture during deformation (Nelson, 2001). The nature of fractures can deduce which kinematics formed them (Freund, 1998; Nelson, 2001; Schultz and Fossen, 2008). However, the nature of a fracture can change due to progressive processes acting, such as other tectonic events, subsidence (i.e. compaction) and decompaction after uplift and erosion (Ameen, 1995).

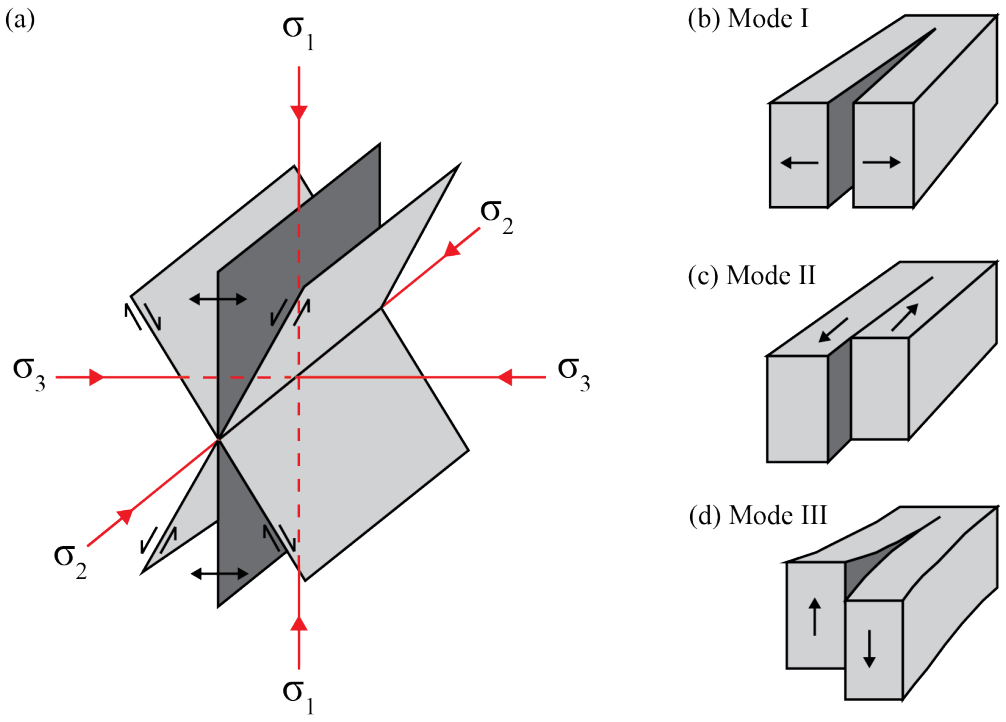

Figure 3.1: (a) Kinematic of fracture development in relation to principal stresses. (b) Three modes of fracturing can be defined based on the relative movement. Redrawn and modified from Nelson (2001)

Lithology and bed thickness affects the mechanical competency of a layer and fractures populate with respect to this (Hanks et al., 1997; Laubach et al., 2009; Peacock and Mann, 2005). However, fracturing can be highly influenced by local controls, such as proximity to faults Braathen et al. (2009); Peacock and Mann (2005). Continued deformation can results in fractures linking up to produce a bigger discontinuity, a fault, where strata is moving relative to one another (Schultz and Fossen, 2008). The kinematics of fractures can significantly improve the understanding of paleostresses.

A fault plane is a discontinuity with greater displacement than fractures (Schultz and Fossen, 2008), developing in response to the principal stress axes (Fig. 3.2). For normal

faults, the hanging wall move down relative to the foot wall (Anderson, 1905). Fault displacement is at its maximum in the centre of the fault and will decrease towards the fault tips (Kim and Sanderson, 2005; Nicol et al., 2017; Rotevatn et al., 2019). Hence, fault length can be predicted when recording its maximum displacement.

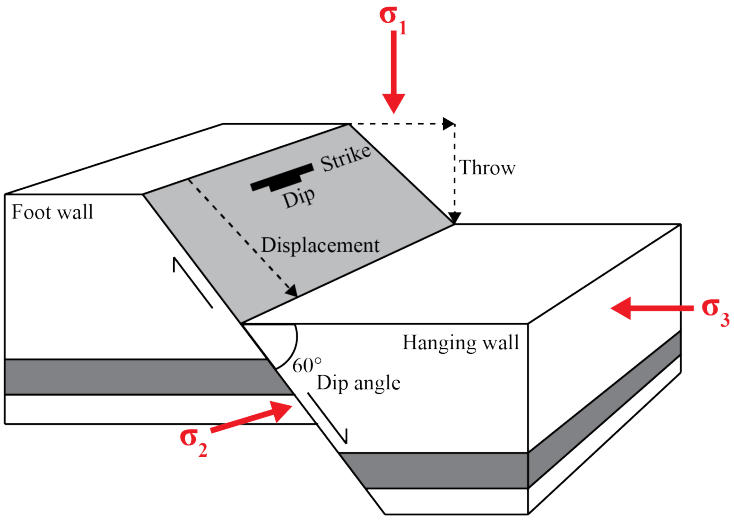

Figure 3.2: Formation of a normal fault in relation to principal stresses, with fault terminology. Throw is the vertical offset of a marker bed, while the oblique distance from the same bed in the foot wall and hanging wall is the displacement. Illustration is based on Anderson (1905); Braathen et al. (2009)

3.2.1 Fault architecture

In addition to the displacement of stratigraphy, faults impact extends to modify the properties of a volume of the host rock (Braathen et al., 2009). Kim et al. (2004) present three damage zones that develop in relation to fault propagation. Firstly, fault tip damage zone develop around fault tips as a result of high stress concentrated at the tips. Secondly, linking damage zones develop where fault tips interact and link (vertically or laterally). Thirdly, wall damage zone develop along the fault when deformation extends to the adjacent rock volume. This damage zone increase with progressive slip of the fault. To describe the amount and characteristics of strain in relation to faults, fault facies are utilized (Braathen et al., 2009).

Braathen et al. (2009) divides structures that develop in response to a fault into three categories; discrete structures, lenses and membranes respectively. The formation of lenses is mainly fault segments or slip surface linkage (Braathen et al., 2009). The

lenses are often elongated parallel to the fault axis. With continued deformation, these lenses are crushed to fault rock, creating membranes (Childs et al., 2009; Gabrielsen and Clausen, 2001), forming parallel with the fault. The membranes can dependent on the continuity of it be defined from continuous to patchy.

3.3 Implications on caprock properties

For a hydrocarbon reservoir or CO_2 storage formation, enhanced fluid flow can be beneficial. However, conduits for fluid flow will compromise the integrity of a caprock (Færseth et al., 2007; Torabi and Berg, 2011; Gale et al., 2014). Fluid flow in shale dominated units are governed by structural discontinuities, as porosity and permeability is low and fluid migration through pore space is limited (Aplin et al., 1999). Three scenarios of leakage through the caprock are commonly addressed (Aplin et al., 1999). Firstly, preexisting structures can work conduits or baffles. Open fracture networks can cause migration in otherwise impermeable rocks. Depending on their extent and connectivity, fluids can migrate through the caprock. Faults can works as both conduits and baffles (Aplin et al., 1999; Færseth et al., 2007; Torabi and Berg, 2011; Gale et al., 2014). The petrophysical properties of the host rock changes in a fault core and damage zone in response to deformation (Braathen et al., 2009; Færseth et al., 2007; Gale et al., 2014). Depending on the architectural elements present, this can lead to across fault and up fault leakage (Færseth et al., 2007; Torabi et al., 2015). The permeability of a fault core is predominantly low in shale dominated units Aplin et al. (1999). Porosity and permeability will increase in fractured damage zones (Braathen et al., 2009; Singhal and Gupta, 2010).

When CO_2 is injected into a storage formation, the pore pressure increases. If the pore pressure exceeds the capillary entry pressure, CO_2 can migrate though the tight pore spaces in the caprock (Ingram and Urai, 1999). The fluid migration will eventually normalise the pressure and the leakage will cease. Further, the acting stresses in a storage formation will increase in response to higher pore pressure (Hubbert and Willis, 1972; Engelder and Lacazette, 1990). Accordingly, the caprock can fail by creating new, open fractures (i.e. hydraulic fracturing). Further, reactivation of preexisting faults and fractures can occur, as it is easier to reactivate preexisting structures than to initiate new failure. Reactivation of faults during CO_2 injection can result in further deformation of the fault core and damage zones (Aplin et al., 1999). Hence, active deformation can increase fluid flow in faults.

Chapter 4

Data and methods

In this chapter, the data sets, methods for collecting the data, as well as the methods used for processing, interpreting and analysing the data sets used in this study are outlined. Firstly, an overview of the data collected for this study is provided. Secondly, each step of data collection and processing for fieldwork, core logging and borehole data is outlined. Finally, the workflow for integration of subsurface outcrop data is presented.

4.1 Data sets and software

A range of software were utilized in order to process, interpret and analyse the data set collected for this study (Table 4.1).

Table 4.1: Software used in this study.

Software	Developer	Function
Agisoft Metashap	Agisoft	Photogrammetry
LIME	VOG Group	Interpret virtual outcrops and quantitative measurements
Stereonet 10	Richard W. Allmendinger	Visualisation and processing of fault/fracture data
FieldMOVE	Petex	Georeferenced field notes

4.2 Fieldwork

4.2.1 Sedimentary logging and structural mapping

Sketch logging was conducted in order to ensure correct stratigraphic positioning of the structural measurements collected. Boundaries and marker beds were taken from relevant literature. The structural analyses mainly targeted faults and fractures in Konusdalen West. All identified structures were characterised using criteria outlined in chapter 3. Fault displacement and orientation was measured, and detailed characterisation of the fault core was conducted in order to define the fault architecture. Seven scanlines (i.e. the 1-D line intersection method, after Singhal and Gupta (2010)) comprising a total of

421 measurements (fracture orientation and relative spacing) were collected and display the horizontal fracture frequency. The scanlines stations encompassed fault damage envelopes in order to determine the control of faults on fracture frequency. The FieldMove smart device application was used to georeference notes, whereas a manual clinometer compass was used for fracture orientations given it provided better accuracy over the digital alternative. The right hand rule was used consistently throughout this study.

4.3 Core logging

Detailed structural logging after Singhal and Gupta (2010) has been performed in drill cores from DH2, retrieved from 655-734 meter depth. This was done in order to record the amount of fractures and their distribution in the lower Agardhfjellet Formation (i.e. the Oppdalen and Lardyfjellet members). The fracture characteristic collected were; stratigraphic positions, spacing and frequency, dip angle, surface asperity, coating and infilling (if present). Drilling induced fractures were also collected. The distinction between a drilling induced fracture and a natural fracture was made due to their appearance and based on criteria by Kulander et al. (1977). Previous investigations conducted by Schaaf (2017) provided a structural log of the fractures present in the lowermost Agardhfjellet Formation interval in DH4, present at 580-668 meter depth. In total, 180 meters of logged drill core is presented in this study.

4.4 Virtual outcrop analysis

4.4.1 Acquisition and processing

During fieldwork, a drone with built-in GPS, was used to photograph the outcrops. Following the acquisition methods outlined in Westoby et al. (2012), pictures from different angles and distance to the outcrop with 90% overlap was ensured. After photo acquisition, the photogrammetry processing of 3D models (referred to as virtual outcrop models herein) was conducted using Agisoft Metashape (Fig. 4.1). This was conducted in order to make further qualitative and quantitative analyses of faults. Georeferenceing of models was enabled by GPS positioning of the pictures taken in the field. This enabled the models to quantify strike and dip measurements from planar surfaces e.g. faults or large through-going fractures.

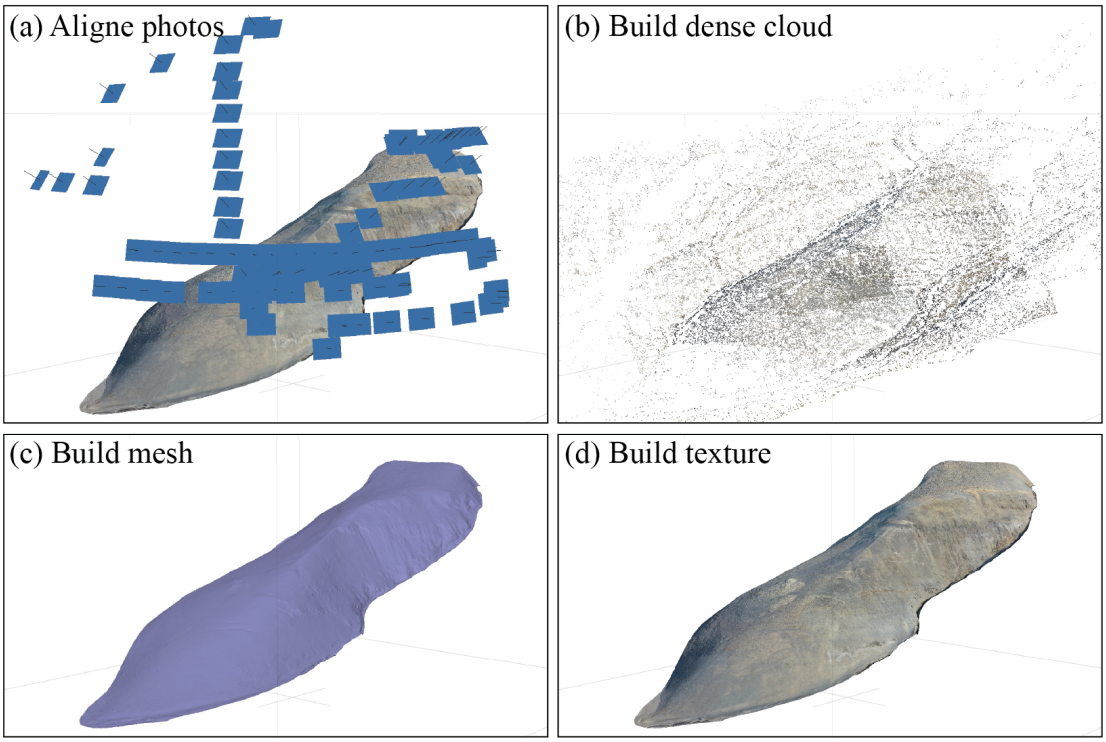

Figure 4.1: Photogrammetry workflow temporary.

4.4.2 Quantitative interpretation

In order to visualize and conduct interpretations of the virtual outcrop models, the software LIME was used. The software enables quantitative measurement collection, such as distance (i.e. conducting throw and displacement measurements), orientation and dip angles of the faults. Interpreting marker beds across the entire outcrop ensured interpretation of all faults present in the Konusdalen West and Konusdalen outcrops.

4.5 Integrating results

Integration of the results from vertical scanlines collected in drill cores and horizontal collected from fieldwork enabled comparison of fracture frequencies, spacing, dip angles, fracture type. Acoustic televiewer data provided by the UNIS CO_2 Lab (Elvebakk, 2010), containing fracture frequencies, spacing, orientation and dip angles was utilized. Further, interpreted core box photos (Braathen et al., 2012), including fracture frequencies and dip angles was compared to the manual logging conducted for this study.

Chapter 5

Results

This chapter will firstly present techtonostratigraphy of the field site near Deltaneset. The brief stratigraphic overview places the field site in correlation with the drill sites (Fig. 5.1). The analysed geological structures will be presented as meso-scale fault systems in outcrops, fractures from outcrops and fractures in drill cores. Finally, results from outcrops, drill cores and borehole data will be integrated.

5.1 Stratigraphic context of the field site

The investigations targeted normal faults and fractures recognized in the Lower to Middle Agardhfjellet Formation, i.e., in the Oppdalen, Lardyfjellet and Oppdalsåta members Lubrano-Lavadera et al. (2019); Mulrooney et al. (2019); Ogata et al. (2014b). The weathered exposures of these shale-rich intervals proved stratigraphic positioning difficult but coarser siltstone beds and lenticular sand-prone layers were used as stratigraphical marker beds across the study area. Sedimentological context of the field site and drill cores were derived from Koevoets et al. (2016). On the basis of this, stratigraphic positioning of the structural investigations in the different field site location was possible.

The base Agardhfjellet Formation, which is also the base Oppdalen Member, was identified in Konusdalen, based on sedimentary logs from Dallmann (1999), Mørk et al. (1999b), Koevoets et al. (2016) and Rismyhr et al. (2019). It is defined as the first siltstone bed following conglomerates of the Brentskardhaugen Bed, which is easily recognizable in field (Fig. 5.1e). The overlying shale rich intervals of the Oppdalen and Lardyfjellet members were also identified Konusdalen (Fig. 5.1d). A coarser interval marks the transition from Lardyfjellet Member to Oppdalsåta Members. This marker bed was possible to follow along the study area and the same interval was recognised between Konusdalen and Criaserasdalen (Fig. 5.1c) and in Konusdalen West (Fig. 5.1b). In Konusdalen West, four additional coarser intervals were correlated to the sedimentary logs from Koevoets et al. (2016).

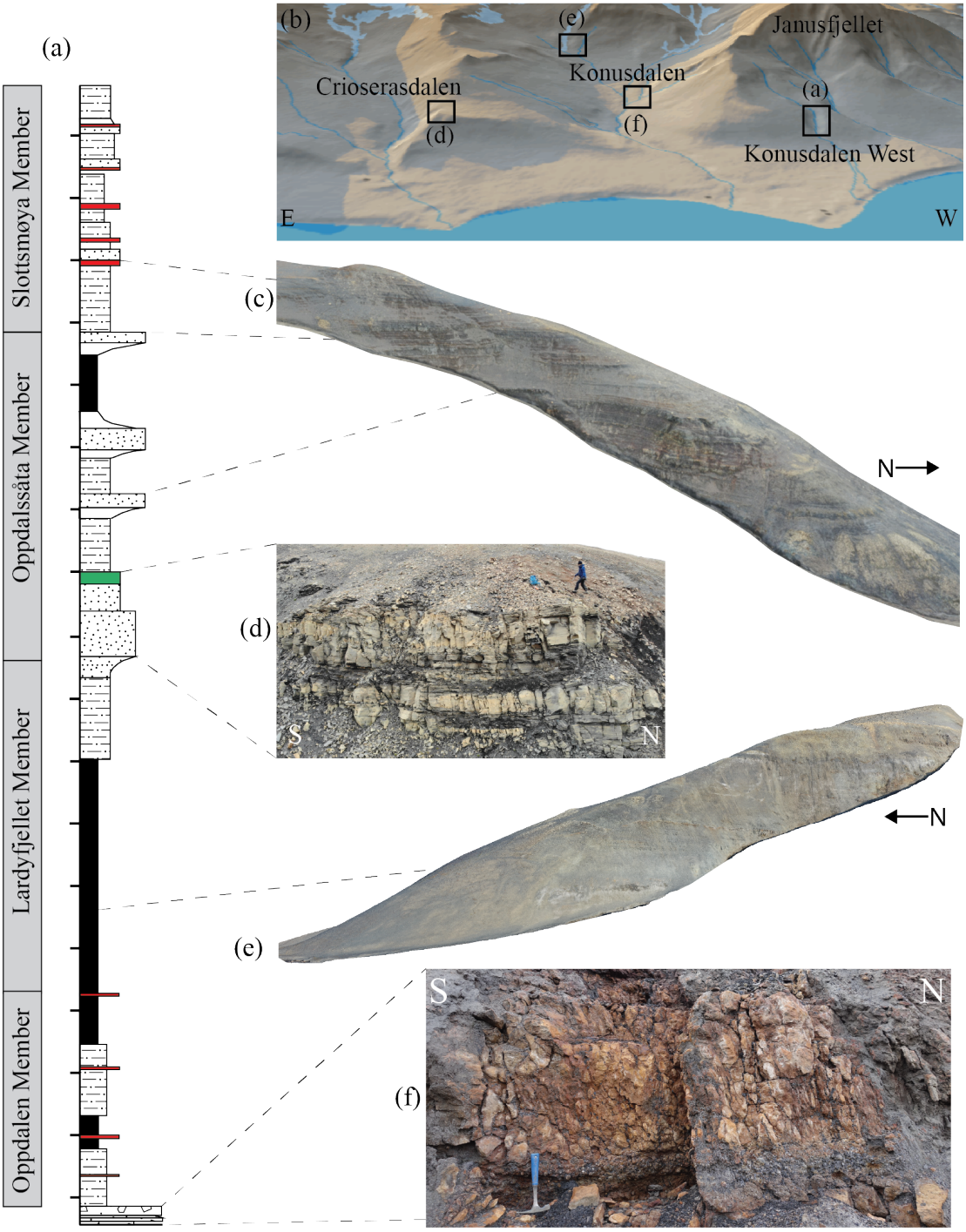

Figure 5.1: (a) Sedimentary log of the Agardhfjellet Formation modified from Koevoets et al. (2016). (b) 3D map of the study area (map retrieved from toposvalbard.no). (c) Virtual outcrop model of the siltstone dominated outcrop in Konusdalen West. (d) Oppdalssåta Member sandstones in Criacerasdalen. (e) Virtual outcrop model of shale dominated (Oppdalen and Lardyfjellet members) outcrops in Konusdalen. (f) Conglomerates of the Brentskardhaugen Bed which denote the base of the Agardhfjellet Formation. Dashed lines locate the vertical positions of (c)-(f) in the log.

5.2 Fault array in lower Agardhfjellet Formation

The results from one fault in the Lardyfjellet and Oppdalssåta members in Konusdalen West (Fig. 5.1b) and one in the Oppdalen and Lardyfjellet members in Konusdalen are presented herein. An additional fault array was identified in Crioserasdalen (see Mulrooney et al. (2019) and Ogata et al. (2014b)). No faults are identified from the drill cores in the lower interval of the Agardhfjellet Formation. However, zones of intense fracturing are observed, which are discussed to represent the presence of faults.

5.2.1 Konusdalen West fault array

Konusdalen West (western slope of Janusfjellet) presents two structural styles (5.2. The upper part of the outcrop, comprised by the Oppdalssåta and Slottsmøya members, is cut by a thrust fault (KW_T). Løvlie (2020) measured the thrust with a high dip angle (80 °), trending in a NNW-SSE-direction. However, mapping of the fault in a virtual outcrop model for this study, has estimated a maximum and minimum plausible fault strike. This presents the thrust as striking closer to northeast-southwest with a lower dip angle. The lower part of the outcrop, comprised by the Oppdalssåta Members, was analysed in detail for this study. This section is cut by a normal fault (KW_N) striking northeast-southwest and is dipping approximately 60 ° to the northwest (Fig. (5.2d). The strike of the normal fault is similar to what is suggested for the thrust fault for this study, but contradicts the suggested fault orientation by Løvlie (2020). The faults overlap in stratigraphy, but do not display any cross cutting relationships.

The detailed analysis of normal fault is presented in Figure 5.3. The dip angle varies along the fault and appears to be steeper in the more shale rich interval (5.3b). The main fault (KW_N) had a maximum offset of 8 meters, which decreased both up section and down section in the outcrop (Fig. 5.3d). Up section in the upper part of the Oppdalssåta Member, the fault splays into two small branches (KW_B1 and KW_B2) with further decreased in offset. In addition, two synthetic (KW_S1 and KW_S2) faults were identified in the foot wall of the main fault (Fig. 5.3b). The fault did not intersect with the main fault (KW_N) and display small offsets, estimated to be 10-20 centimeters. In the hanging wall, two antithetic faults (KW_A1 and KW_A2) were analysed. The antithetic faults intersected with the main fault and decreased in displacement upward. The fault array was not identified at the top plateau of the outcrop or the western side of the ridge.

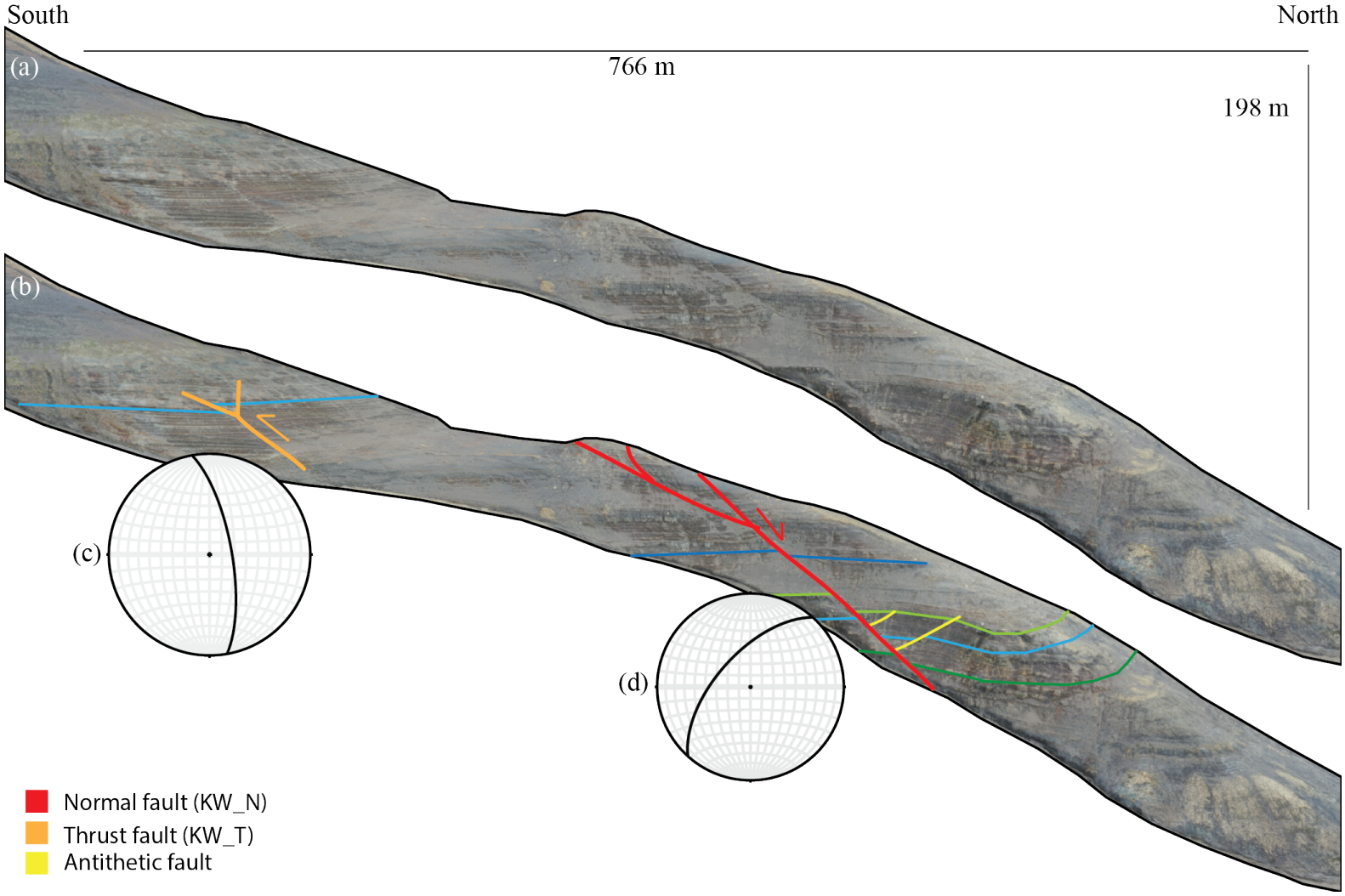

Figure 5.2: Two main faults present in the Konusdalen West outcrop; thrust fault in the Slottsmøya Member striking NNW-SSE (Løvlie, 2020), and a normal fault in the underlying Oppdalssåta Member striking northeast-southwest.

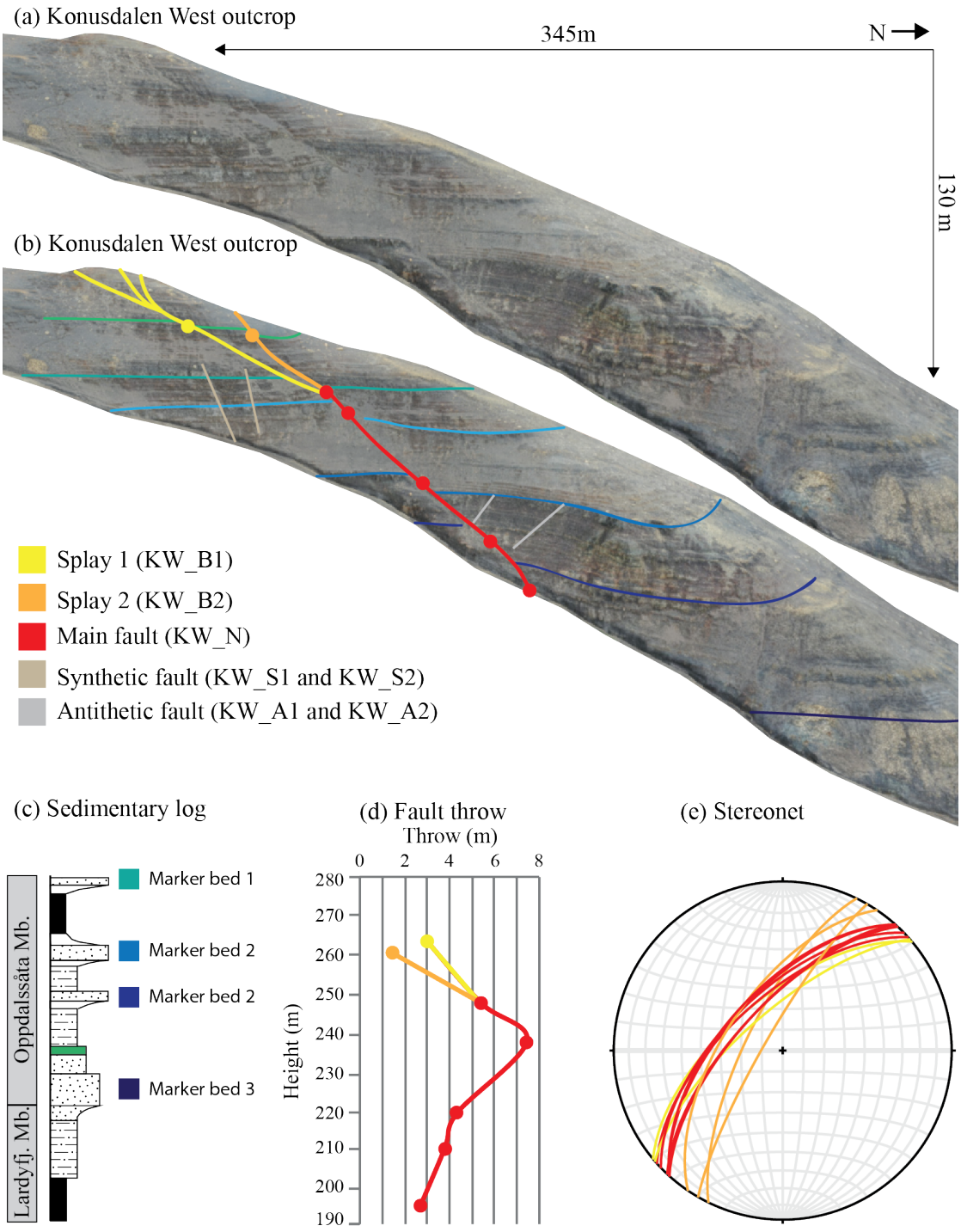

Figure 5.3: (a) Virtual outcrop model of Konusdalen West. (b) Virtual outcrop model with highlighted marker beds and faults. (c) Sedimentary log, modified from Koevoets et al. (2019). (d) Fault throw profile (circles in (b) indicates midpoint of the throw measurement. (e) Stereonet of the main fault (KW_N) and splay (KW_B1 and KW_B2).

5.2.2 Konusdalen West fault core architecture

The core of the main fault (KW_N) was characterized in three places, two of them presented in Figure 5.4. The core architecture, relative clay content of the shale gouge membranes (where present) and the core width varied along the fault plane. The fault core exhibits a width of 1.5 meter at the point of maximum displacement, whereas the lowermost section exhibit a core width of 10-15 centimeters. Membranes and lenses occurred at all investigated sections along the fault. In general, shale was more incorporated in the fault core as lenses and membranes. Discrete structures was predominantly analysed in the adjacent damage zone, presented in 5.3.1.

Shale gouge and fault breccia were the dominating membrane features in the fault core. The shale gouge exhibit several, 2 to 15 centimeter thick, continuous membrane intervals where the displacement were greater (Fig. 5.4b and c). Down section, where the displacement was lower, only one continuous shale gouge membrane of 10 centimeter was found (Fig. 5.4d and e). The membrane was splaying downsection into three thinner membranes separated by lenses and fault breccia between. Within the shale gouge, the clay content was at the highest where the displacement was greater. Patchy fault breccia membranes were also present in all sections along the fault.

Shale lenses were recorded at all analysed sections along thee fault. Lenses made up by the iron cemented carbonate beds were found in the lowermost investigated section, where the proximity of these beds were closer. The lenses are elongated parallel to the fault axis and are intensely fractured. In the shale lenses, the fractures are mostly anastemosing, while more swarm like in the iron cemented carbonate lenses.

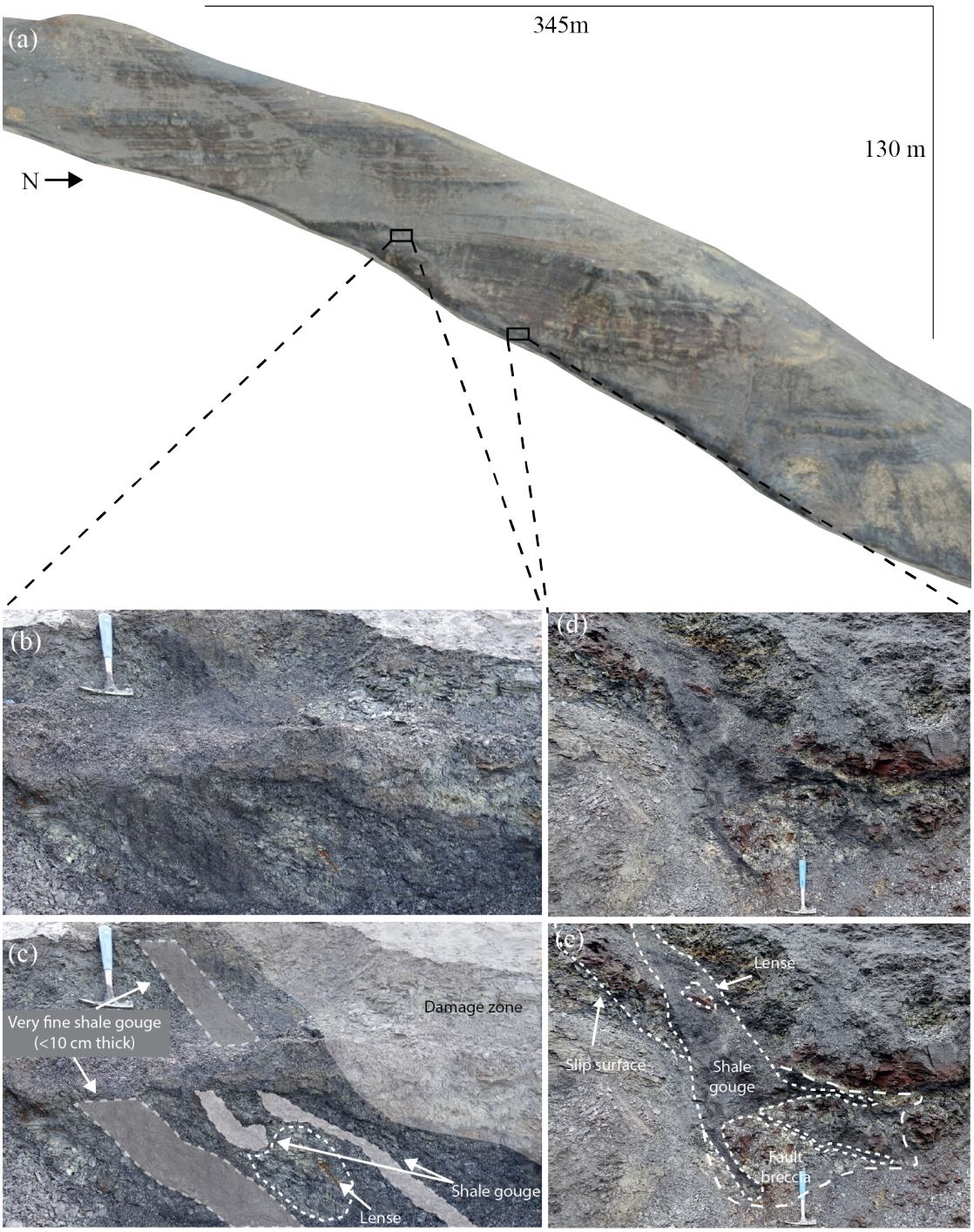

Figure 5.4: Fault core architecture of two of the analysed sections. (a) Virtual outcrop model of Konusdalen West outcrop with marked locations of the two presented sections. (b) and (c) show the fault core arcitecture at the greatest displacement recorded. (d) and (e) presents the architecture in the lowermost outcrop of the fault. Geological hammer for scale.

5.2.3 Konusdalen fault

The second normal fault was identified in the shale dominated interval comrising the Oppdalen and Lardyfjellet members in Konusdalen (Fig. 5.5). The fault plane strikes was estimated to northeast-southwest in a virtual outcrop model, dipping to the northeast (Fig. 5.5b). Maximum observed fault offset could not be definitively determined, but cross-fault marker beds indicate a throw of 5 meters. The vertical extent of the fault is also unknown, due to scree cover. Hanging wall strata show rotation towards the fault.

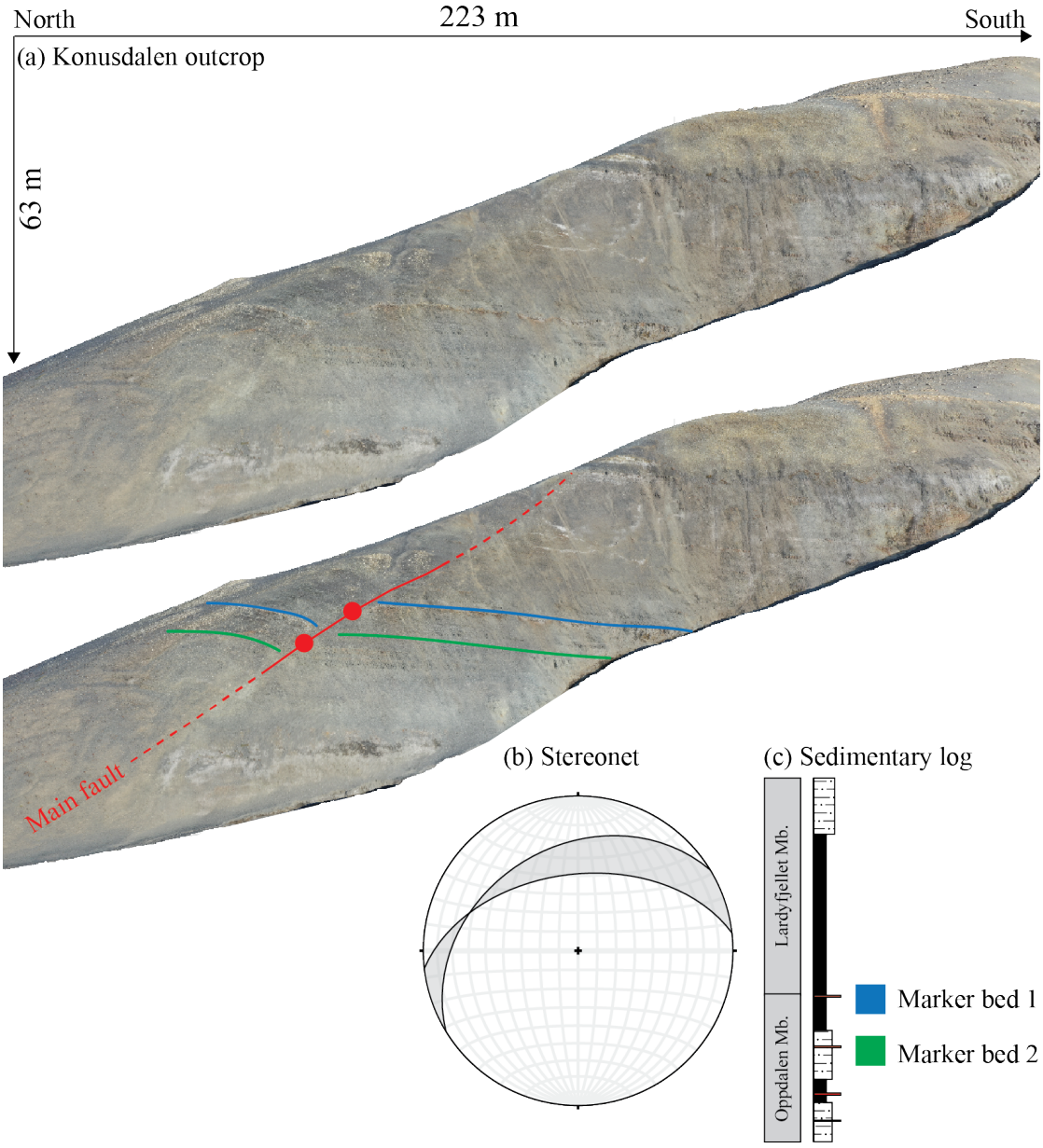

Figure 5.5: (a) Virtual outcrop model of Konusdalen with and without highlighted marker beds and normal fault. (b) Stereonet plotting the estimated fault plane. (c) Sedimentary log, modified from Koevoets et al. (2019).

5.3 Fracture networks in lower Agardhfjellet Formation

5.3.1 Fieldwork results

Seven scanlines are presented in Figure 5.7 and laterally span a total of 45 meters and comprise of 432 fracture measurements. Figure 5.7b and c presents three scanlines encompassing the main fault (KW_N). These are presented as scanline 1, 2 and 3 respectively. For these scanlines, the damage zone is defined to where higher fracture frequencies are presented compared to the adjacent rock. Additional fracture swarms of 5 to 25 centimeters of high fracture frequencies are interpreted as fault damage zone fracture corridors (Fig. 5.6b). Two scanlines were constructed in order to target the antithetic fault with greatest displacement (KW_A2)(Fig. 5.7d). The bed where scanline 3 and 4 was constructed was intensely fractured towards the fault plane on both sides of the fault. Therefore, quantitative measurements were not possible, and these intervals were defined as the damage zone. Figure 5.8e is a summary of data collected in a lenticular layer in the hanging wall of the main fault (KW_N). Finally, data from a scanline in the hanging wall of the main fault (KW_N) is presented in Figure 5.7f.
Shale dominated intervals were intensely fractured (Fig. 5.6a), whereas the fractures in the cemented beds were predominantly open to dense networks with some swarms of fractures (Fig. 5.6b).

Figure 5.6: (a) Intensely fractured shale dominated interval in the hanging wall of the main fault (KW_N). Dashed line indicates the fault core boundary. (b) Fracture swarm in cemented carbonate bed adjacent to the main fault (KW_N).

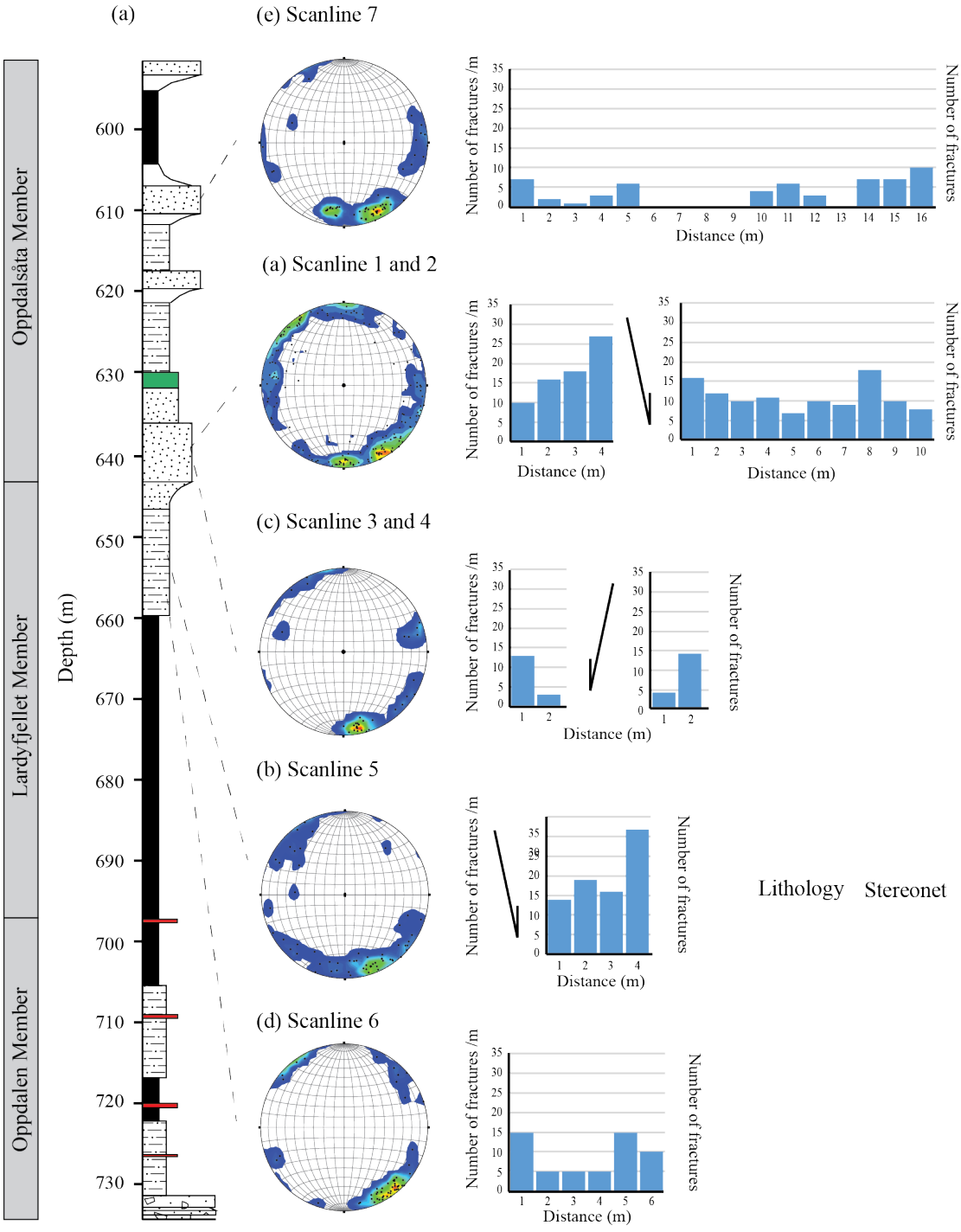

Figure 5.7: Summary of collected scanlines displaying number of fracture per meter. (a) scanline 7 (see location in Figure 5.12), (b) Scanline 1 and 2 across the main fault (see location in Figure 5.8), (c) scanline 3 and 4 across a antithetic fault (see location in Figure 5.9), (d) scanline 6 north of the main fault (see location in Figure 5.10) and (e) scanline 6 (see location in Figure 5.11)

(a) Virtual outcro

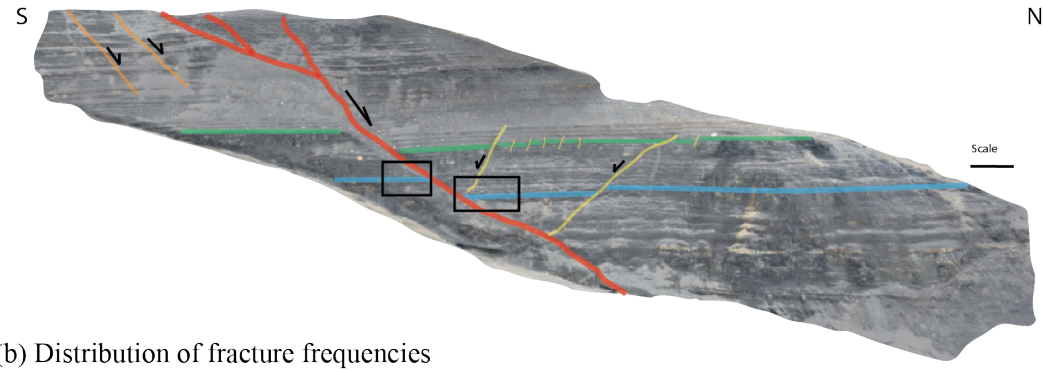

(b) Distribution of fracture frequencies

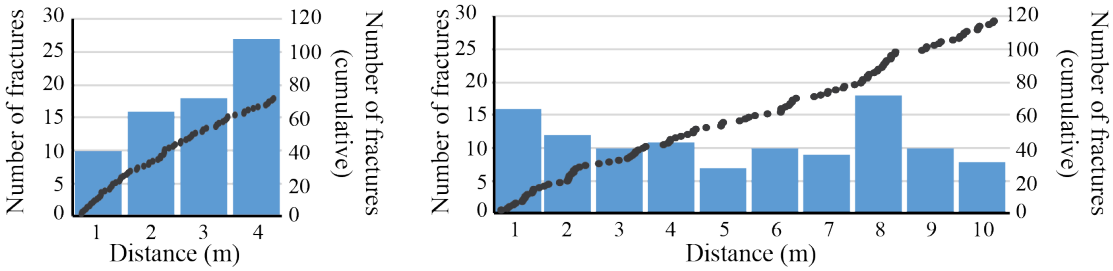

(c) Distribution of dip anlges

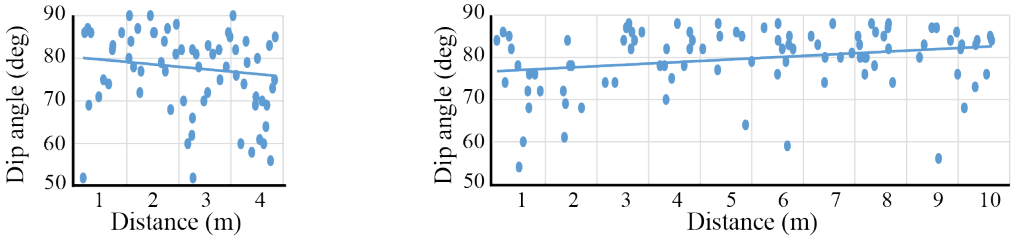

(d) Distribution of fracture orientations

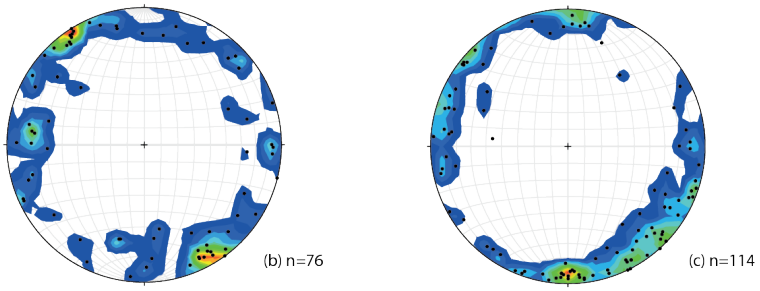

Figure 5.8: All data collected from scanline 1 and 2 in the foot wall and hanging wall of the main fault. (a) Virtual outcrop of Konusdalen West with location for each scanline. (b) Scanline 1 and 2 across the main fault, (c) distribution of dip angles, (d) stereonets.

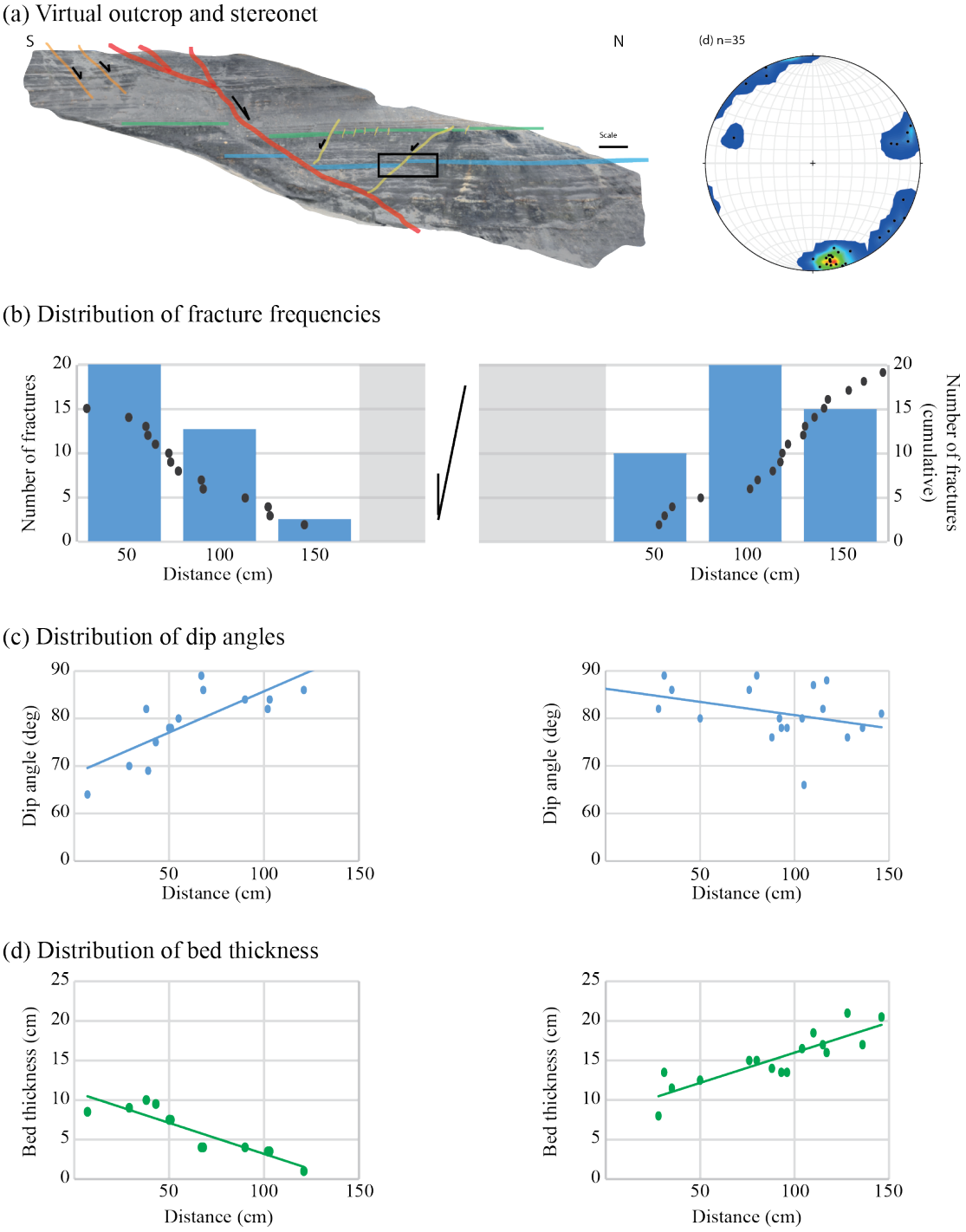

Figure 5.9: All data collected from scanline 3 and 4 in the foot wall and hanging wall of the main antithetic fault. (a) Virtual outcrop of Konusdalen West with location for each scanline. (b) Scanline 3 and 4 across the fault, where the grey areas indicate the absence of the marker bed (c) distribution of dip angles, (d) distribution of bed thickness.

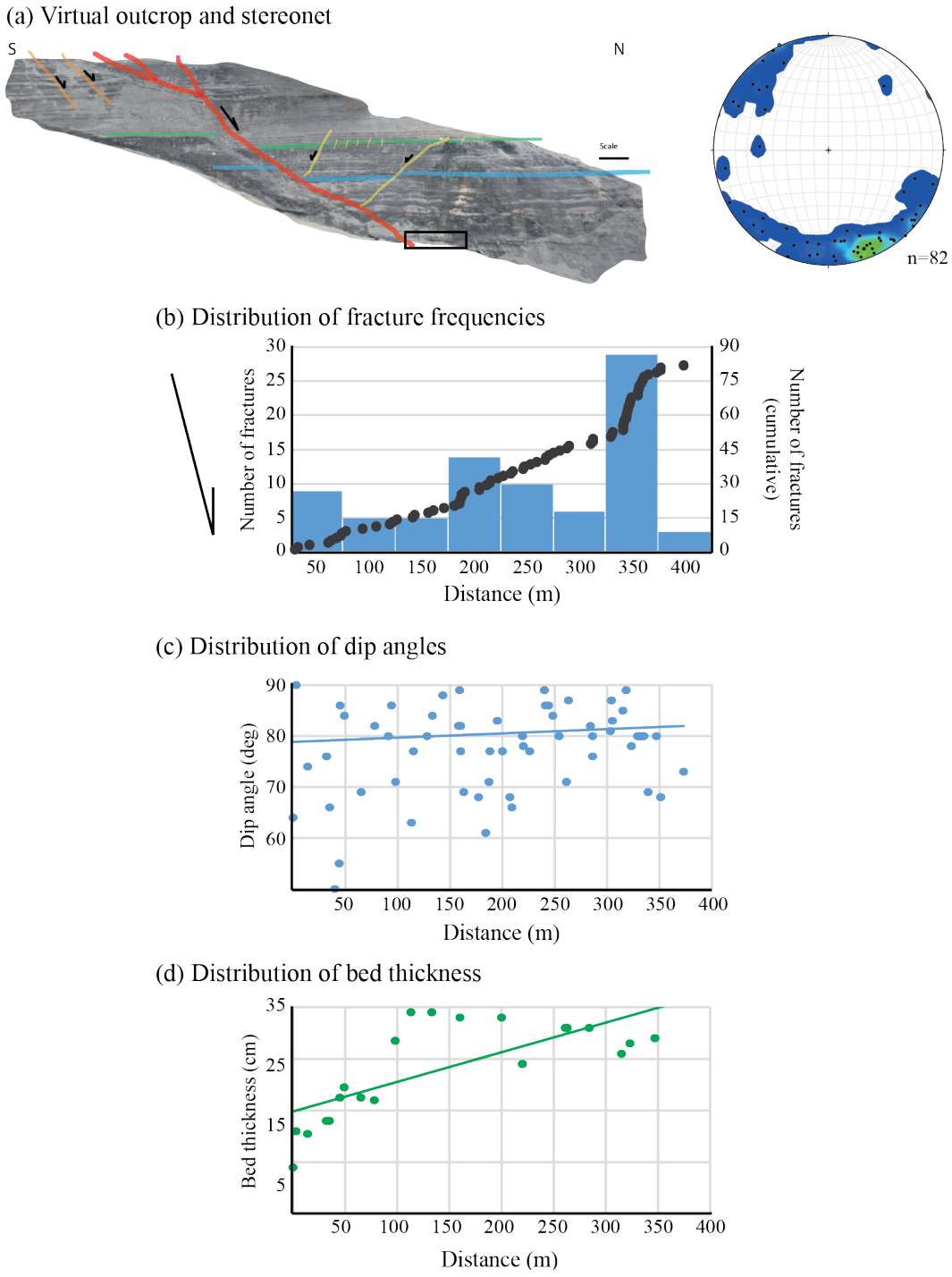

Figure 5.10: All data collected from scanline 5 in the hanging wall of the main fault. (a) Virtual outcrop of Konusdalen West with location for the scanline. (b) Scanline 5, (c) distribution of dip angles, (d) distribution of bed thickness.

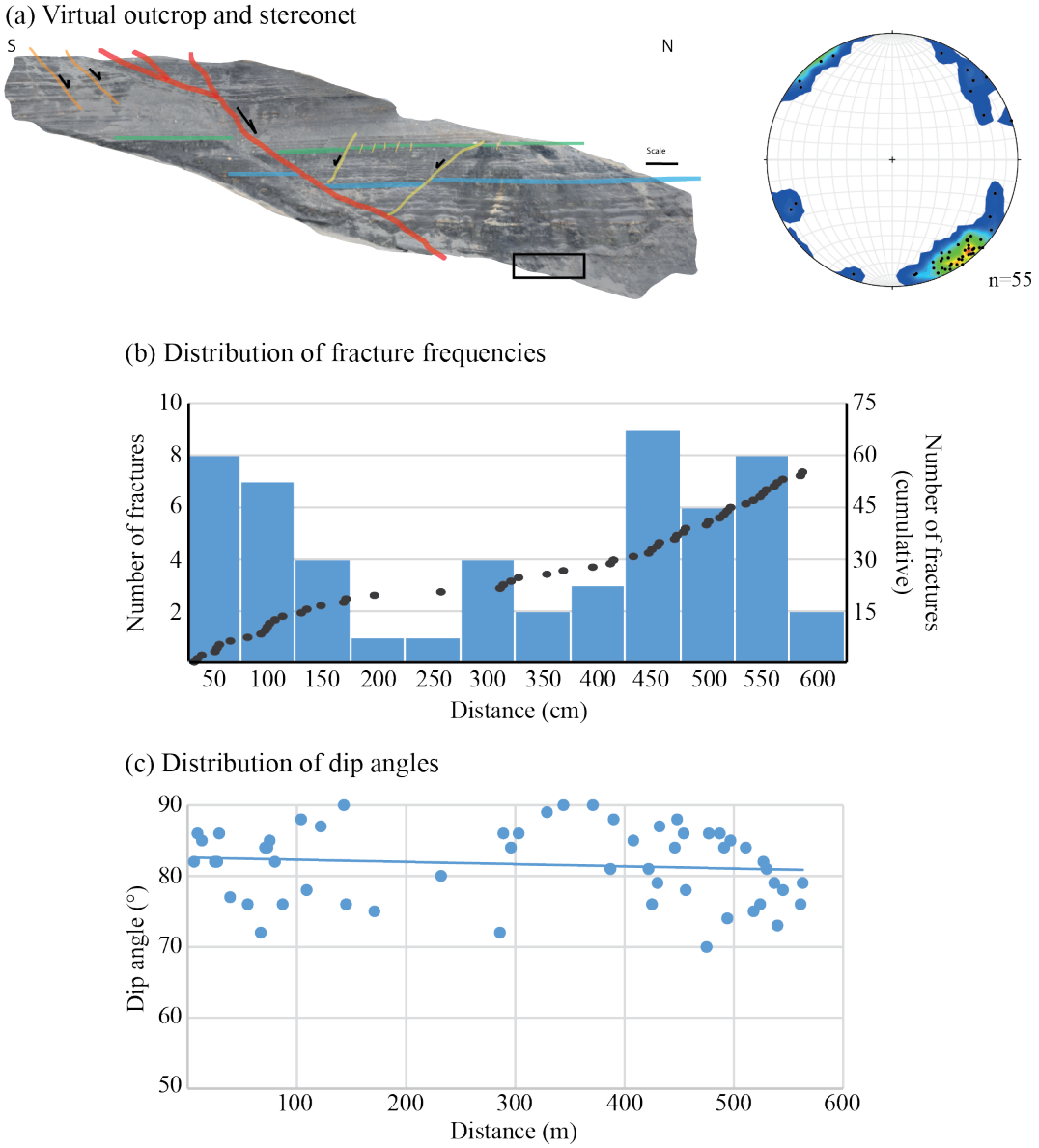

Figure 5.11: All data collected from scanline 6 in the hanging wall of the main fault. (a) Virtual outcrop of Konusdalen West with location for the scanline. (b) Scanline 6, (c) distribution of dip angles.

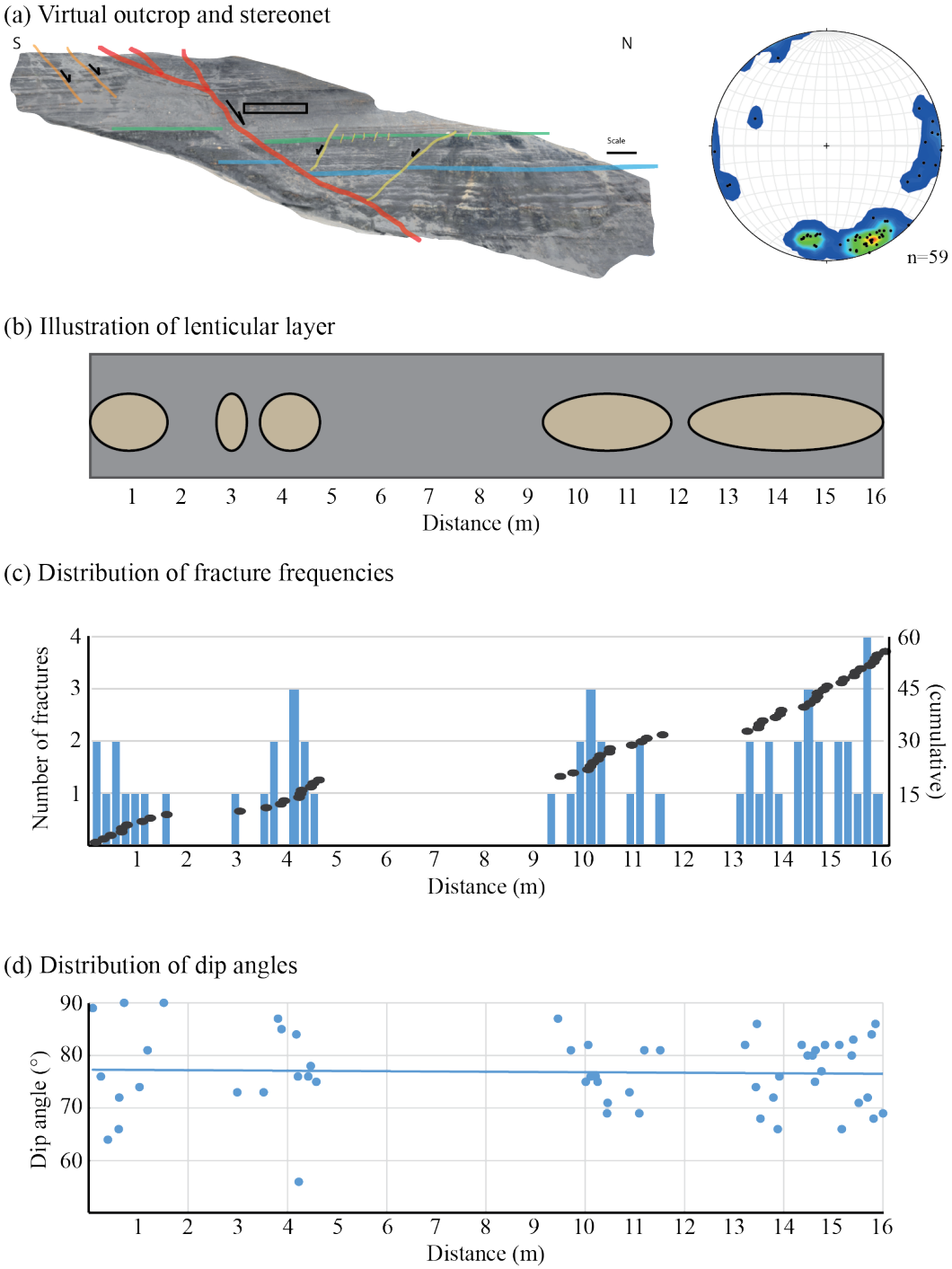

Figure 5.12: All data collected from scanline 7 in the hanging wall of the main fault. (a) Virtual outcrop of Konusdalen West with location for the scanline. (b) Illustration of the lenticular layer targeted (c) Scanline 7, (d) distribution of dip angles.

Detailed fracture description proved difficult in the field, due to heavily weathered outcrops. Where encountered, fracture surfaces for competent beds are generally steep dipping and gently undulating. They also exhibit minor asperities and small apertures of up to a few millimeters. Horizontal fractures proved difficult to identify. This is assumed to be due to the outcrop conditions. Further, horisontal fractures can have been misinterpreted as bedding. Only one fracture with slickenlines was recorded along scanline 5 (Fig. 5.13). Additionally, shear fractures were identified in stepping sandstone injectites at several location. These were however not analysed further.

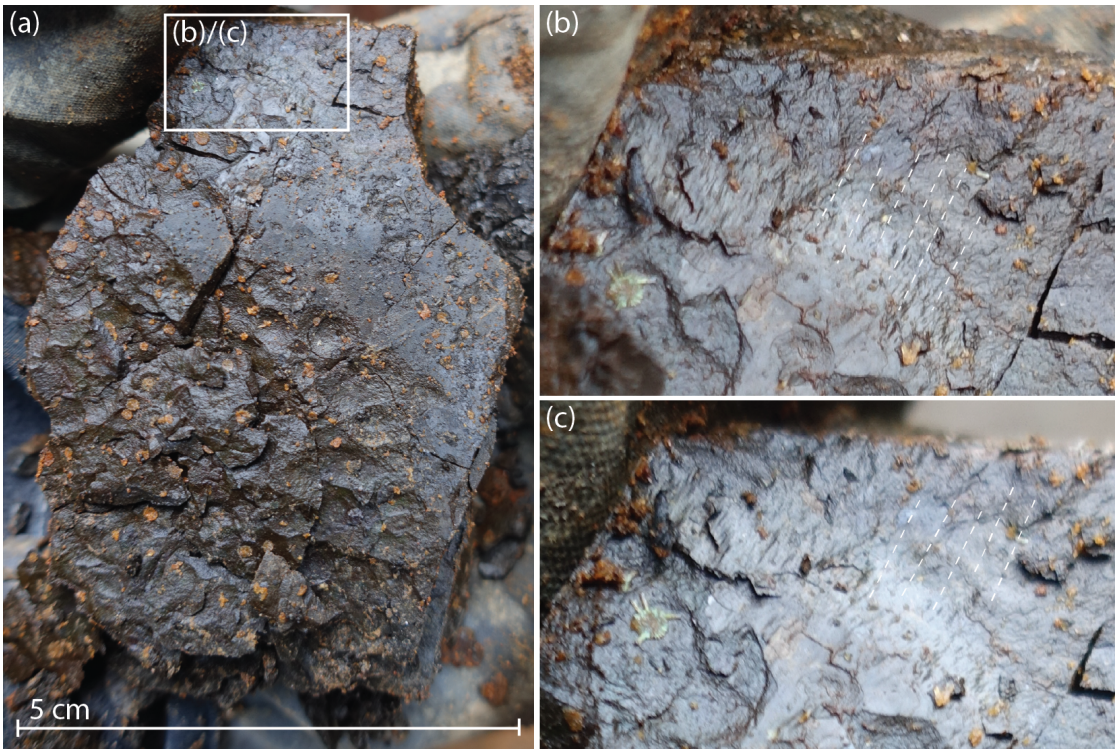

Figure 5.13: (a) Photo of the only sub-horizontal, shear fracture encountered. Additional photos of the slickenside in (b) and (c). Dashed lines indicate striations direction.

5.3.2 Drillcore results

Figure 5.16 presents the fracture logging from DH2 (conducted for this study) and DH4 (from Schaaf (2017)). The logs are derived from depths of 655-734m in DH2 and 580-668m in DH4. These intervals correspond to the two lowermost members of The Agardhfjellet Formation, the Lardyfjellet and Oppdalen members respectively. In total, 180 meters of core is presented in this study. The fracture analyses for this study present

detailed description of the fracture surfaces, whereas fracture frequencies and dip angles are presented from DH4.

Figure 5.16 presents all identified open and closed discontinuities identified from DH2 and DH4 (Fig. 5.16b and e), as well as their dip angle (Fig. 5.16c and f). Drilling induced fractures are excluded from the natural fractures presented in figure. These were distinguished by their consistent characteristics, i.e., they exhibit a horizontal, fresh, often grainy surface. The majority of the natural fractures exhibit polished, slickensided surfaces (mode 2 or 3) and closed discontinuities, defined as mineral filled mode 1 fractures. The differentiation is presented in Figure 5.14a, where a photo of a core box presents that only one natural fracture identified in the presented interval, where many drilling induced fractures were present. The amount of drilling induced fractures was very high compared to natural fractures, presented in subsection 5.3.3.

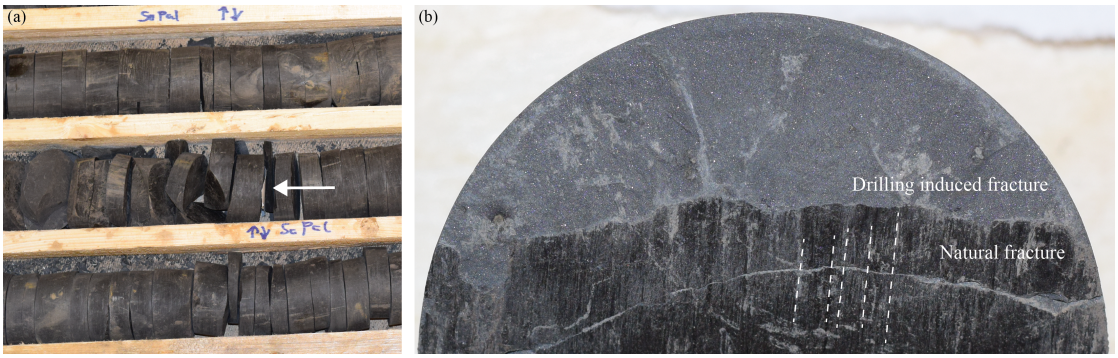

Figure 5.14: (a) Core box from DH2 to illustrate the abundance of drilling induced fractures. Aarrow highlighting a natural fractures, while the rest are drilling induced. (b) A fracture surface displaying a dipping discontinuity identified as a natural fracture (dashed lines are interpreted slickenlines), cut by a horizontal drilling induced fracture, which has a fresh and grainy appearance. Core diameter is 5 cm.

The distribution of the natural fractures and veins was uneven with some intervals being more fractured than others. The maximum number of fractures per meter is 9 in DH2 at 94 meters depth, whereas the average was 2.3 fractures per meter. For DH4, the maximum is 23 fractures per meter at 628 meters depth, with an average of 2.5 fractures per meter.

In order to determine controls on a specific type of fracturing, the distribution of fracture dips was plotted with a bin size of 10 °. (Fig. 5.15a and c). Fractures are also distinguished based on their host lithologies. In DH2, 51 meters of shale, 34 metres of silt and

11 meters of sandstone were logged. In DH4, 41 meters of shale,45 of siltstone and 5 meters of sandstone were logged. The dip angles in DH2 are skewed towards lower dip angles, especially for fractures identified in shale intervals (Fig. 5.15a). The majority of fractures in siltstone and sandstone are exhibit 20-40 ° dip. In DH4, the fractures identified in shale intervals are also skewed towards lower dip angles (Fig. 5.15c). The fractures in the siltstone interval are normalized around dip angles of 30-40 °. The diagrams show a different distribution of dip angles for DH2 and DH4, although (note the double axis for DH4). Figure (Fig. 5.15b and d present the distribution of the fractures in percentage identified for shale and siltstone intervals for DH2 and DH4 respectively. Both show an near equal distribution of natural fractures in shale and siltstone.

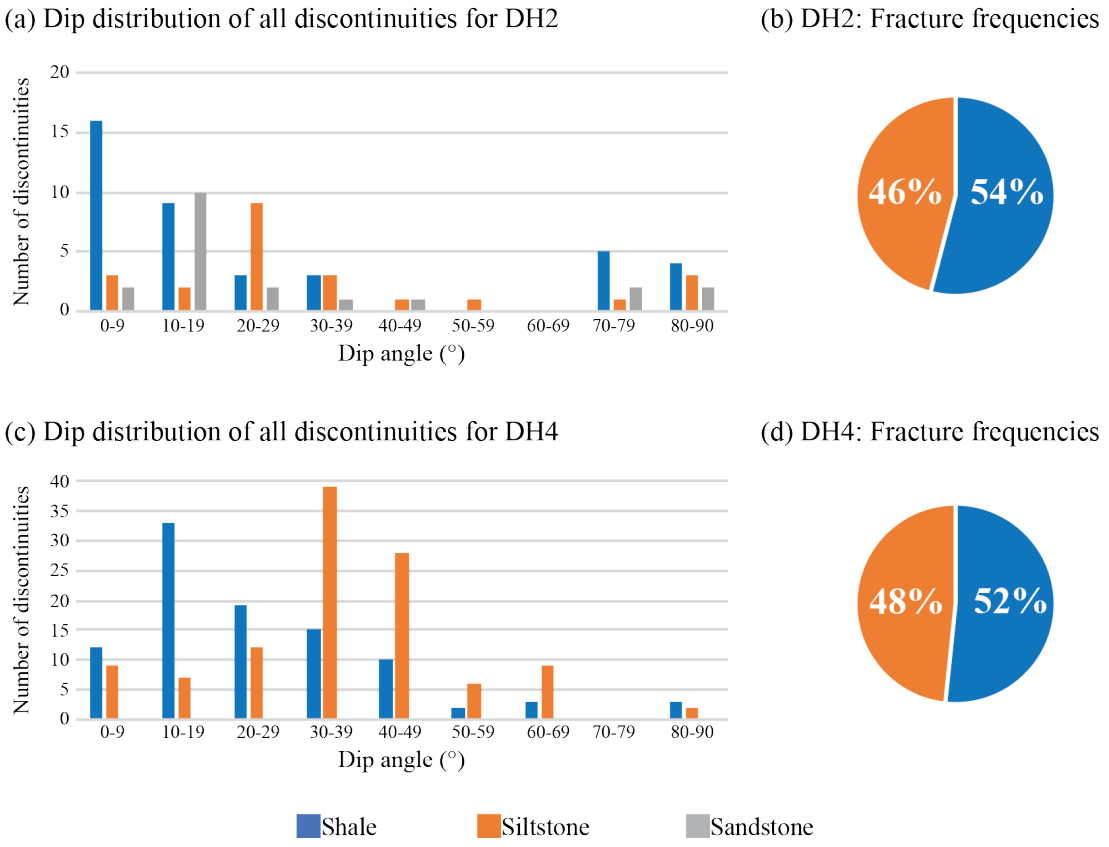

Figure 5.15: (a) Number of fractures for each dip interval with a bin size of 10 ° for each lithology in DH2. (b) Distribution of fracture identified for shale and siltstone in percentage from DH2. (c) Histogram showing fracture dip distribution for different lithologies in DH4 with a bin size of 10 °. (d) Distribution of fracture per lithology in percentage for DH4.

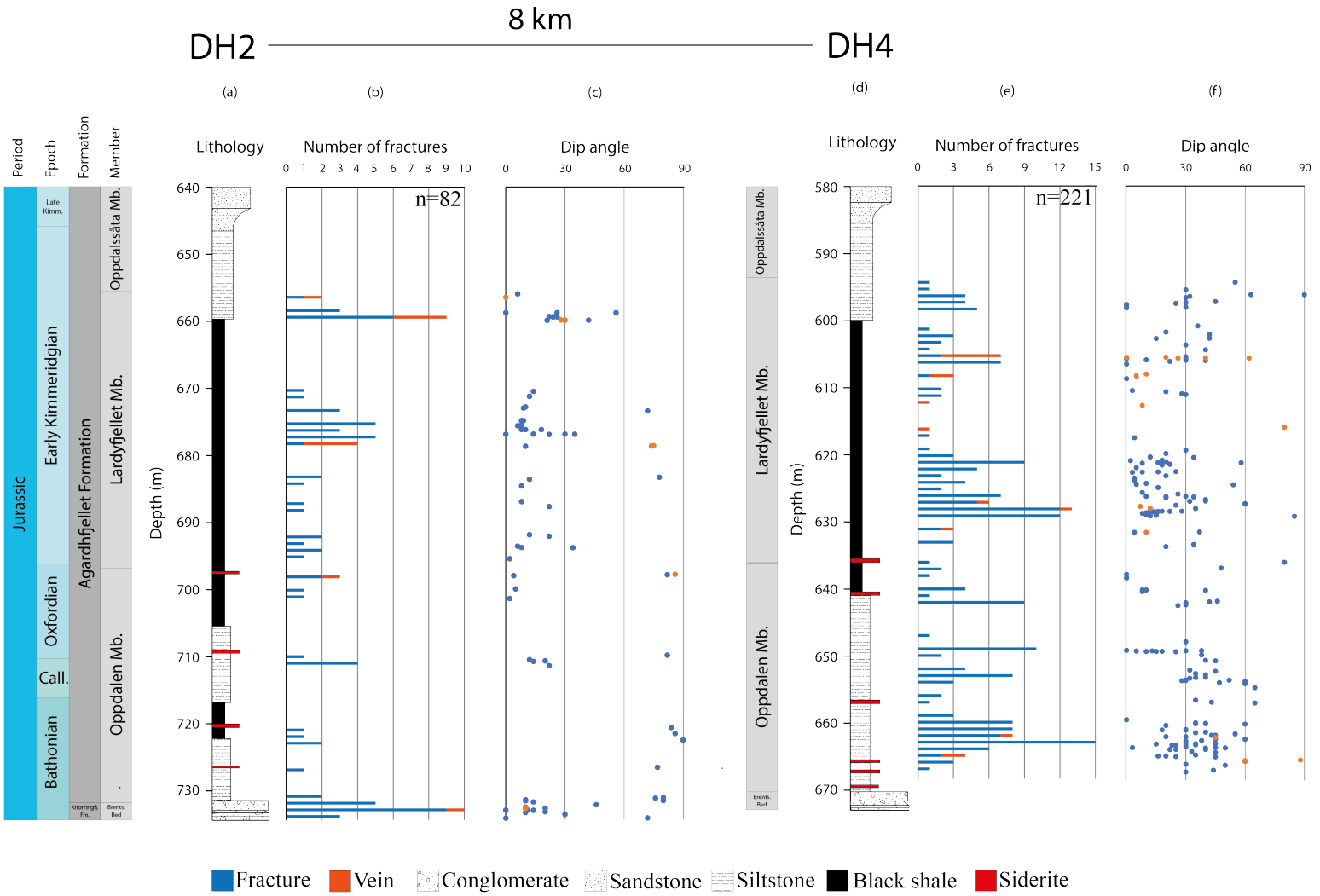

Figure 5.16: Overview of fracture distribution with regards to dip angle and lithology in DH2 and DH4, flattened on the top of the Lardyfjellet Member. (a) Sedimentary log from DH2, modified from Koevoets et al. (2016). (b) Number of natural fractures per meter in DH2. (c) Sedimentary log from DH4, modified from Koevoets et al. (2016). (d) Number of natural fractures per meter in DH4.

Fracture surface characteristics

All natural fractures in DH2 are classified by their fracture surface i.e. if they are smooth, textured or rough. In addition, calcite filled fractures are classified as veins. The majority of the logged core consisted of shale and siltstone, but a sandstone interval was also logged, which marks the transition from the Brentskarheugen Bed to the Oppdalen Member. In general, the fracture surfaces found in sandstones are rough and undulating (Fig. 5.17). Few of the fractures analysed from sandstone intervals exhibit polished spots with slickenlines (Fig. 5.17d and f).

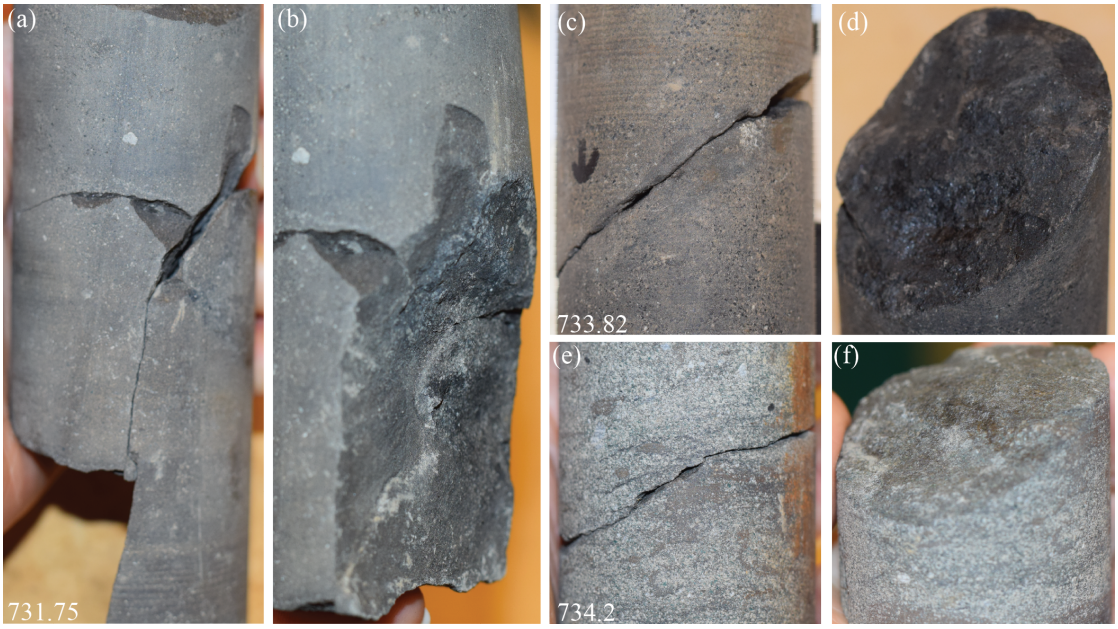

Figure 5.17: Fractures in sandstone. (a) Steep, rough fracture (midpoint at 731.75 m) and (b) the fracture surface. (c) Rough fracture from 733.82 m and (d) the fracture surface with partially lustrous spot (arrow). (e) Rough fracture from 734.20 m and (f) the fracture surface with partially shiny spot. Core diameter is 5cm.

Figure 5.18 displays steep fractures in DH2 and DH4. They are usually curved and cut the core in two parts (Fig 5.18a and b), terminate internally (Fig 5.18c) or against a drilling induced fracture (Fig 5.18d). These fracture surfaces are rough where no polished spots or striations have been identified.

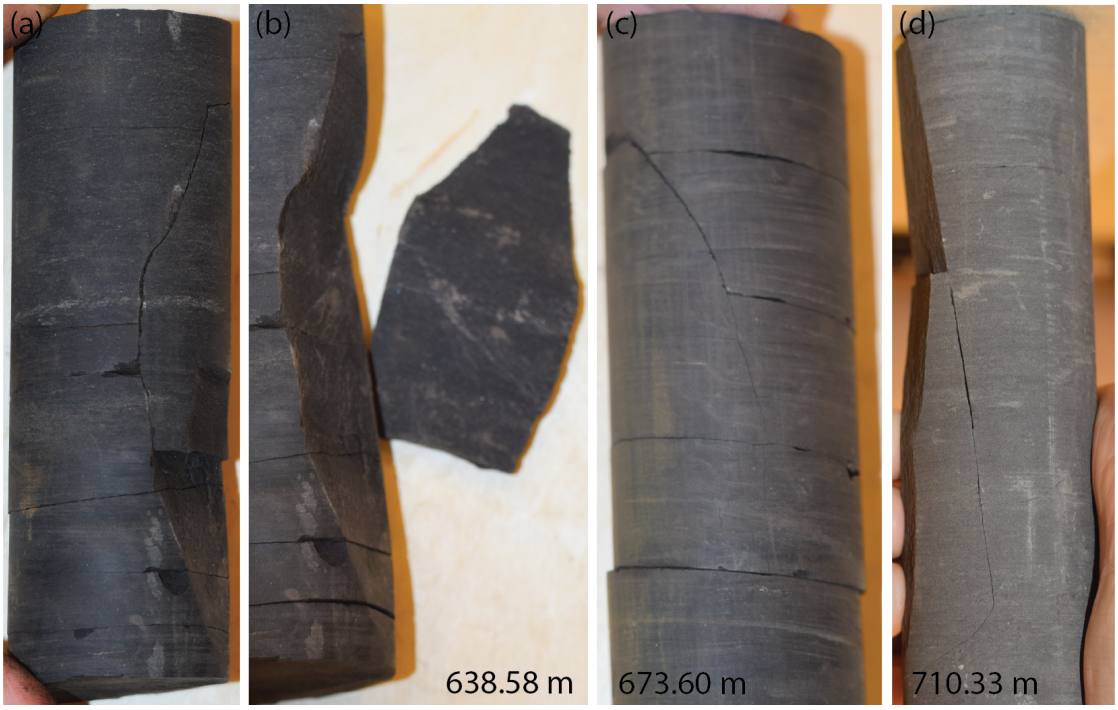

Figure 5.18: Steep fractures at midpoint (a) 638.58 m) and (b) the fracture surface, (c) 673.60 m and (d) 710.33 m. Core diameter is 5cm.

The fracture surfaces in Figure 5.19 are typical of the majority of fractures encountered in the drill cores. They are mainly identified in shale and have low dip angles, are polished and exhibit a lustre. Most have slickenlines that cover the surface entirely or partially. These fractures surfaces are classified as smooth. In some cases undulating surfaces are identified, e.g. Figure 5.19g.

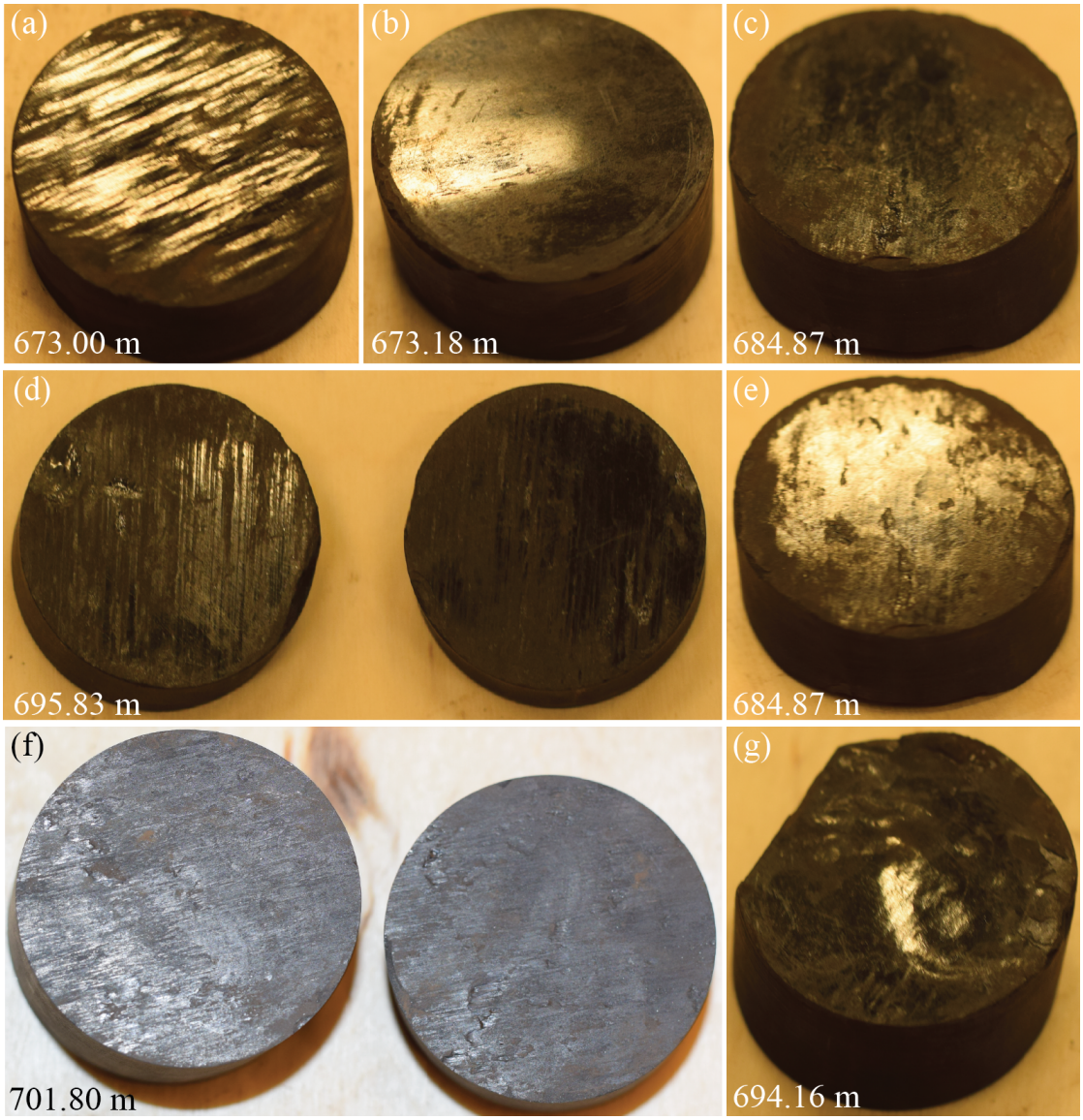

Figure 5.19: Polished fracture surfaces exhibiting polished, lustrous surfaces with slickenlines from (a) 670.00m, (b) 673.18m, (c) 684.87m, (d) 695.83m, (e) 684.87m, (f) 701.80m and (g) 694.16m. Core diameter is 5cm.

Figure 5.20 presents textured fracture surfaces. They differ from smooth fracture surfaces as they are more undulating or curved. Most of the textured surfaces are partially polished with slickenlines and are grainy, or not polished.

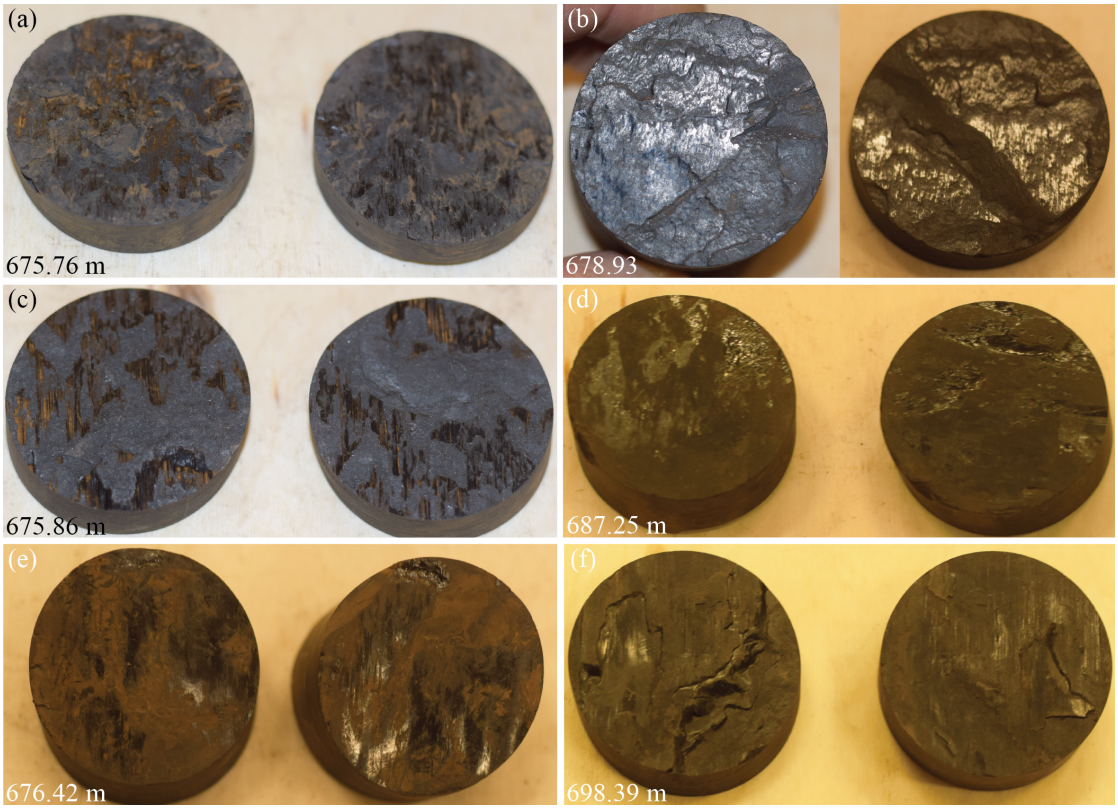

Figure 5.20: Textured fracture surfaces exhibiting undulating or curved surfaces, partially polished with slickenlines from (a) 675.76m, (b) 678.93m, (c) 675.80m, (d) 687.25m, (e) 676.42m and (f) 698.39m. Core diameter is 5cm.

The fractures in Figure 5.21 display fracture with rough surfaces. These surfaces are more heterogeneous and can be grainy, uneven, matt or greasy in appearance. Polished areas with slickenlines are uncommon, but some occur.

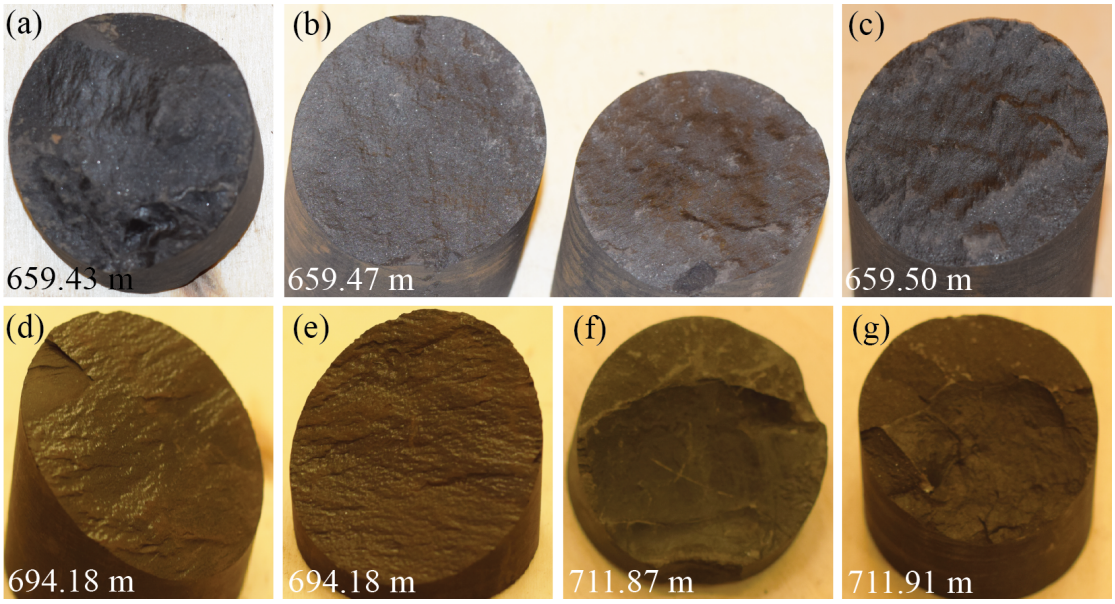

Figure 5.21: Rough surfaces encountered at (a) 659.43m, (b) 659.47m, (c) 659.50m, (d) 694.18m, (e) 694.18m, (f) 711.87 and (g) 711.91m. Core diameter is 5cm.

Some fractures have calcite mineralisation on the surface that occurred in curved or uneven areas (Fig. 5.22).

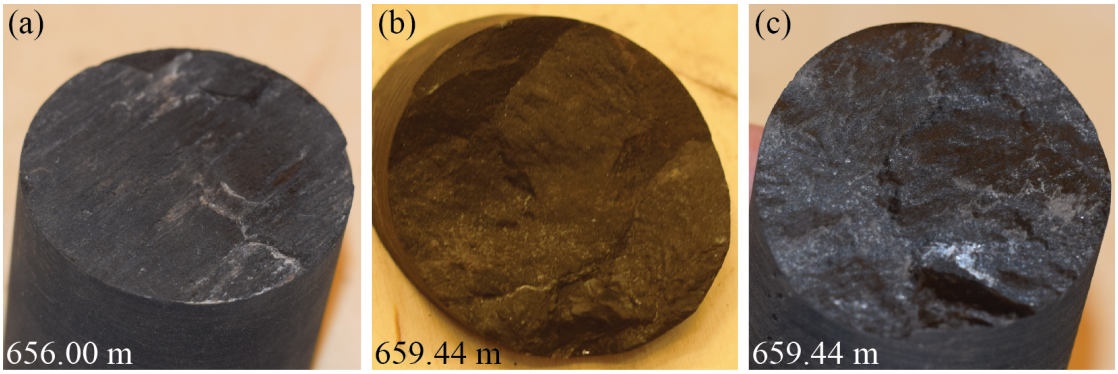

Figure 5.22: Partially mineralised fracture surfaces at (a) 656.00m, (b) 659.44m and (c) 659.44m. Core diameter is 5cm.

Most areas with high fracture frequencies are the result of fracture swarms, i.e., they are not uniformly distributed throughout. Two examples are presented in Figure 5.23 and Figure 5.24. Firstly, two low angled fractures (Fig. 5.23d and e) intersects a fracture dipping 60° (Fig. 5.23b and c). All of the fractures display polished parts with slickenlines. The steepest fracture has slickenlines plunging, while the two latter have

slickenlines with the same direction as the dip angle.

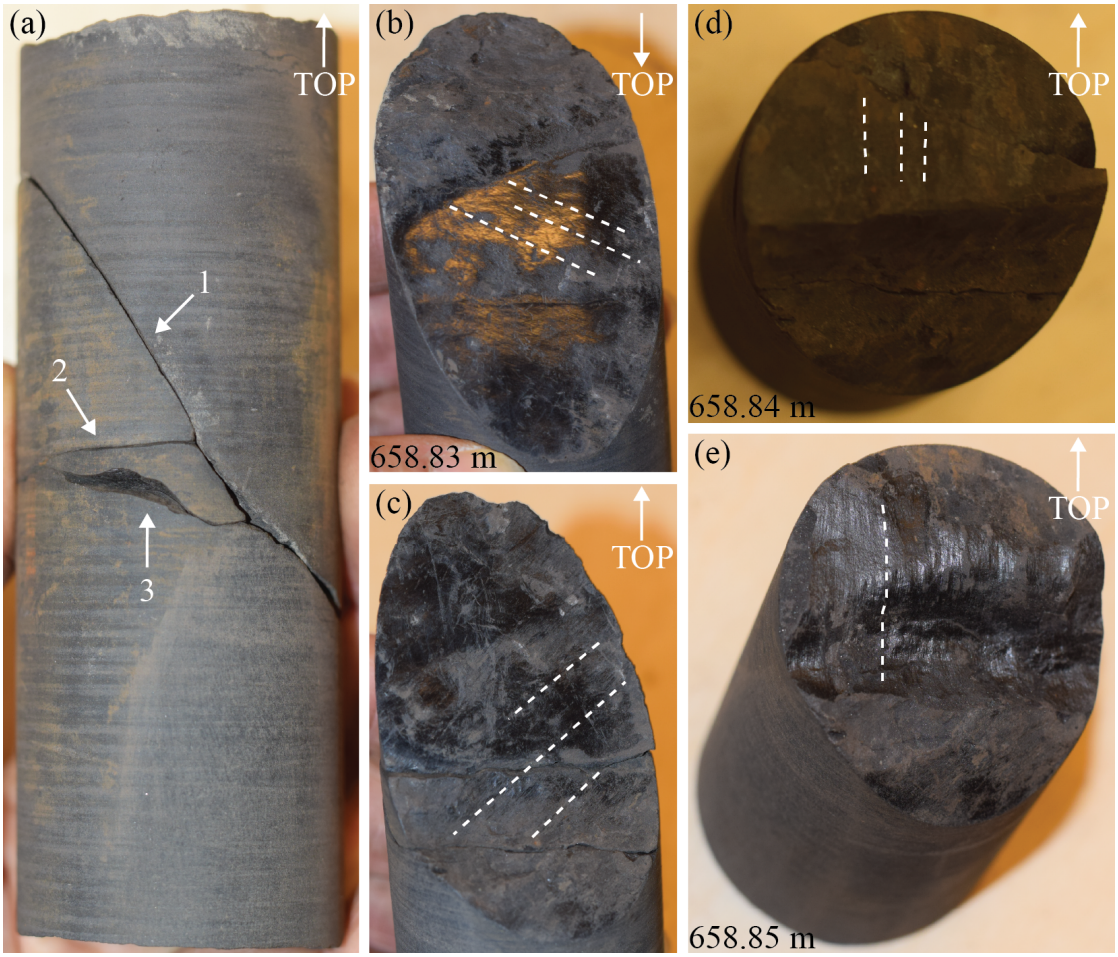

Figure 5.23: (a) Example of closely spaced fractures at (b) 658.83m top, (c) 658.83m bottom, (d) 658.84m and (e) 658.85m. Dashed lines indicate slickenlines. Core diameter is 5cm.

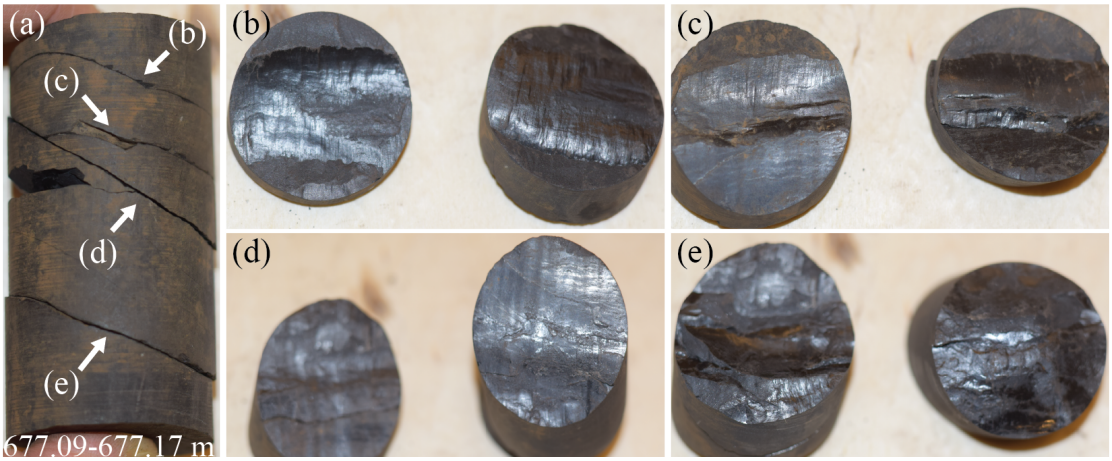

Figure 5.24: (a) Example of closely spaced fractures at 677.09-677.17m. Fracture surface at depth (b) 677.09m, (c) 677.12m, (d) 677.13m and (e) 677.17m. All surfaces are polished with slickensides. Core diameter is 5cm.

Veins are less abundant than fractures (Fig. 5.16). Only 9 have been identified in DH2 and 15 in DH4 and examples from DH2 are presented in Figure 5.25. In Figure 5.25e and f, three large veins are shown, while there is a swarm of minor fracture splaying from these. Also, at the bottom of the thickest mineral infill, there is a smooth slip surface. All mineral infills react to hydrocloric acid and have been interpreted as calcite.

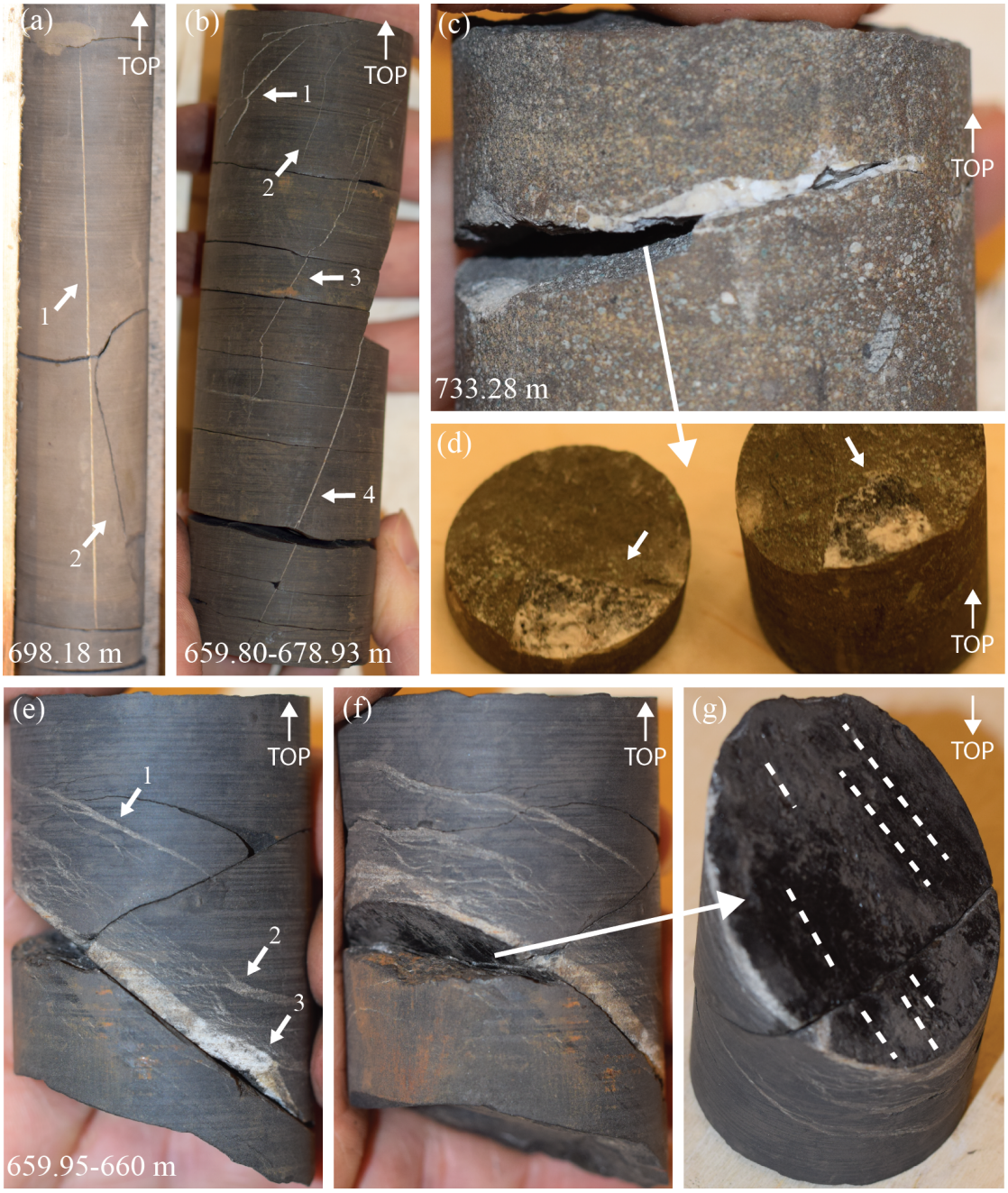

Figure 5.25: Examples of veins from DH2. (a) One sub-vertical vein with midpoint at 698.18m (1) and one steep-dipping, open fracture (2) with midpoint at 698.23m. (b) Five thin, undulating veins. (c) Sub-horizontal fracture exhibiting a 8mm cavity from 733.28m. (d) Fracture surfaces from the latter fracture, showing partially mineral infill of the cavity. (e) Three 'major' (1, 2 and 3) adjacent to a swarm of 'minor' veins at midpoint 659.95m, 659.95m and 659.96 respectively. (f) The same core as shown in (e), but from a different angle. (g) Slip surface at the bottom of the calcite infill. Core diameter is 5cm.

Figure 5.26 presents all fractures identified in DH2 categorized by their surface characteristics. Comparison of fracture abundance grouped by surface characteristics, to dip angle (Fig. 5.26a) and the lithology in which they occur (Fig. 5.26b) shows that generally, the fractures are low angled, less than 30 °. Fractures with smooth surfaces tend to occur in shale and exhibit low dip angles. Textured fracture surfaces are less abundant and only occur at low dip angles. Rough fractures are more common in coarser lithologies and mostly exhibit low angles, 10-30 °. In addition, rough surfaces dominate the high angled fractures.

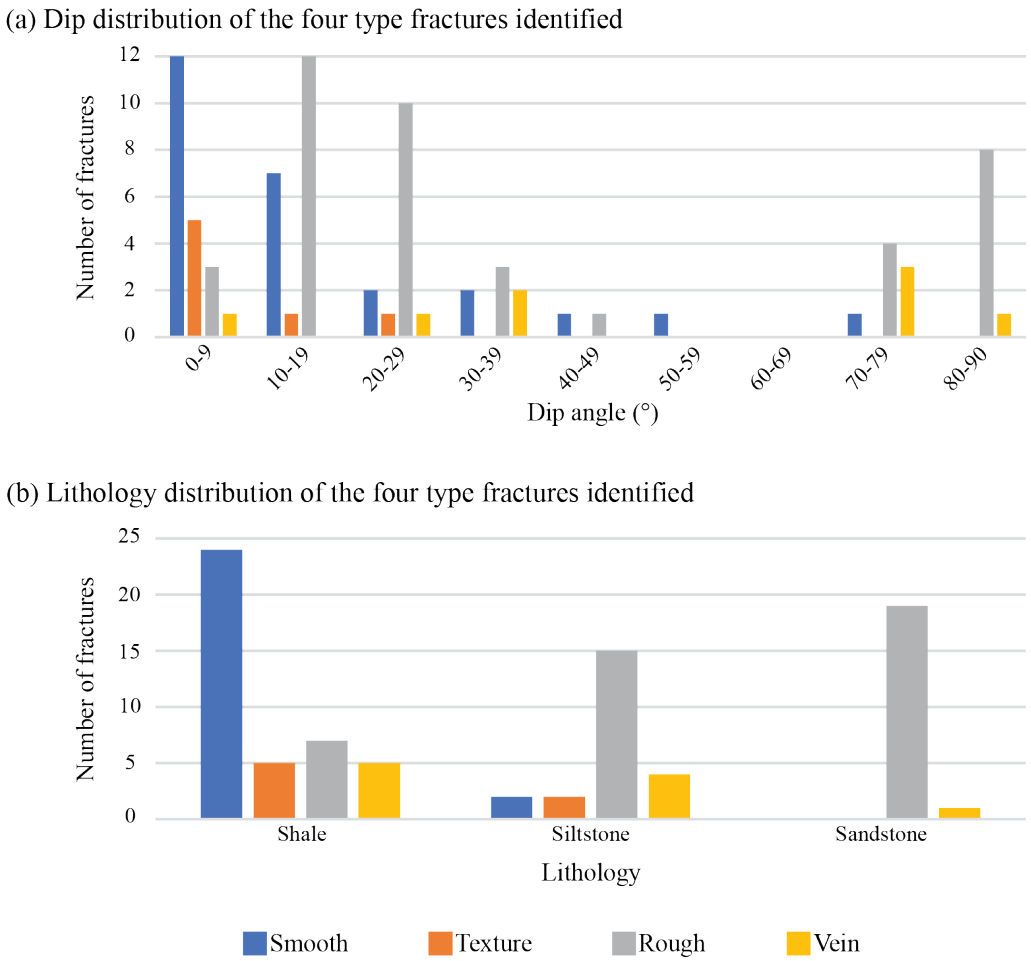

Figure 5.26: Fracture abundance categorised by surface characteristics compared to (a) dip angles and (b) types of lithology.

Striated fracture tend to occur in shale intervals, display low dip angles and exhibit smooth fracture surfaces (Fig. 5.27).

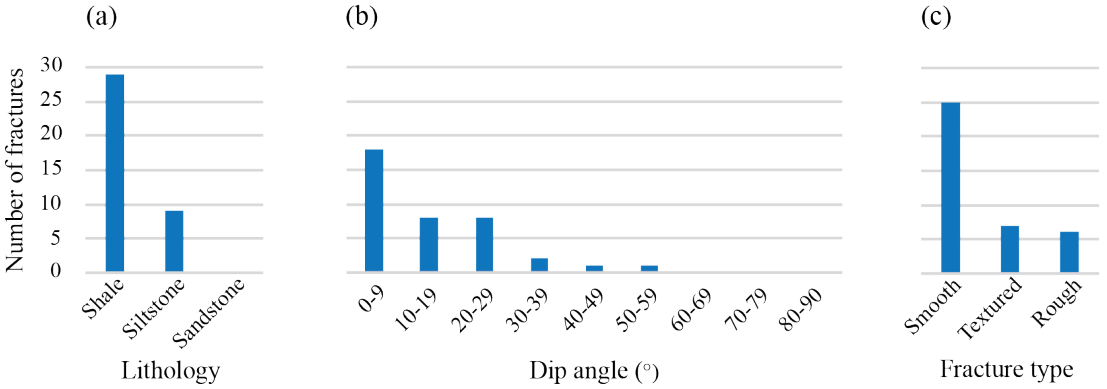

Figure 5.27: Abundance of fracture with slickensides plotted against (a) lithology, (b) dip angle and (c) surface type.

Open and closed discontinuities

The amount of veins versus fractures is generally lower in DH4, compared to DH2. DH2 has 11% closed, whereas DH4 has 7% closed (Fig. 5.28a and b). Most of the veins are encountered in certain intervals for both drill cores (Fig. 5.16). Figure 5.28c and d presents the lithological distribution of veins and fractures. The relative contribution of veins versus fractures is plotted against dip angel for both drill cores in Figure 5.28e and f. A higher percentage of closed discontinuities is discernible for higher dip angels. Kinematic apertures range from 1 millimeter to 0.7 cm.

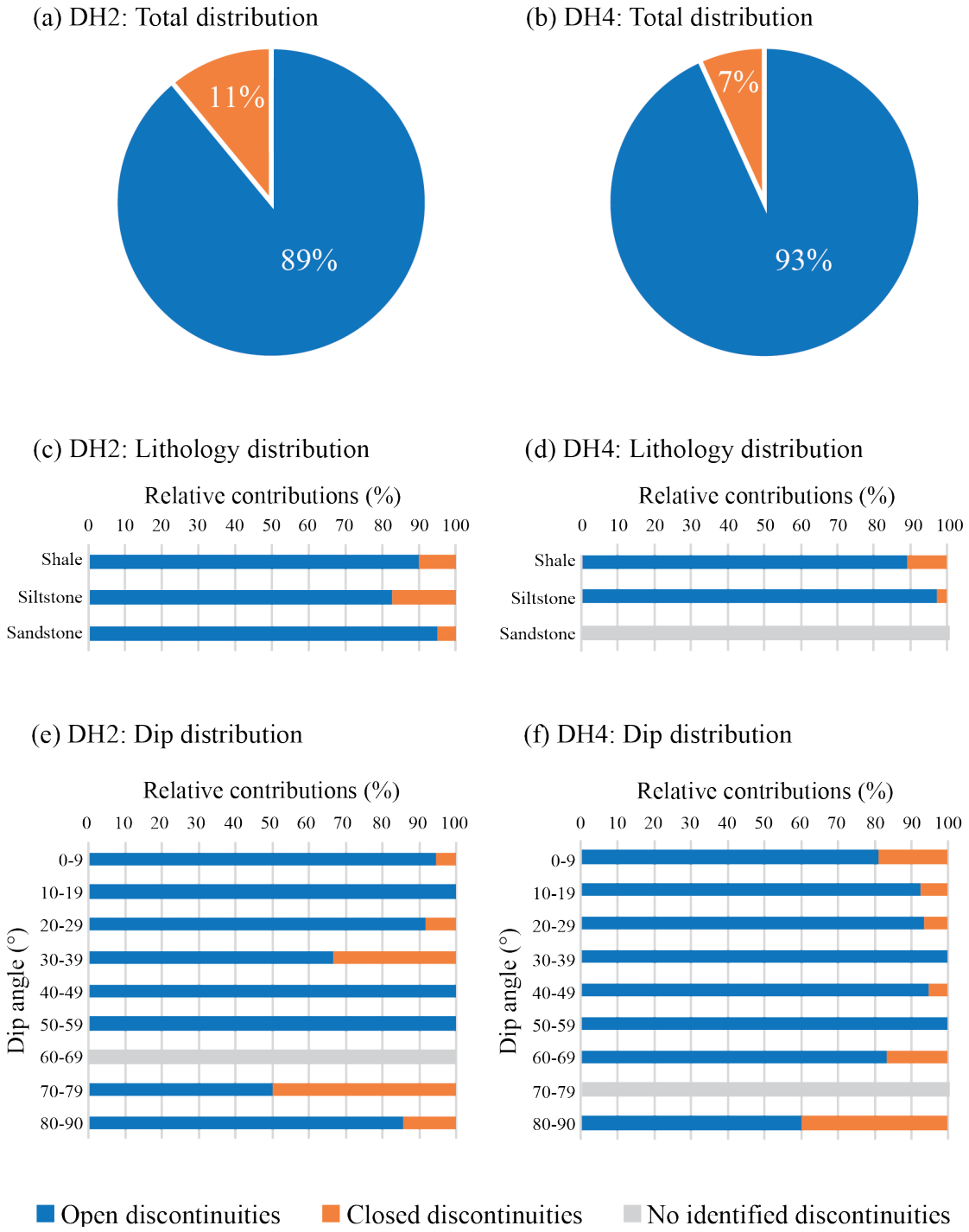

Figure 5.28: (a) Relative abundance of open and closed discontinuities in DH2. (b) Relative abundance of open and closed discontinuities in DH4 (c) Lithological distribution for DH2. (d) Lithological distribution for DH4. (e) Dip angle distribution for DH2. (f) Dip angle distribution for DH4.

5.3.3 Integrated results

Additional fracture data presented herein is derived from the UNIS CO2 Lab. Interpretation of fractures from core box photos (see Braathen et al. (2012)) include all encountered discontinuities, not differentiating between drilling induced and natural fractures. Further, acoustic televiewer data was derived from DH4 (Elvebakk, 2010). Fracture abundance from the interpreted photos by dip angle is presented in Figure 5.29a. 98% of the encountered fractures in DH2 show low dip angles, where 81% in DH4. The televiewer collected fracture orientation, presented in Figure 5.29b.

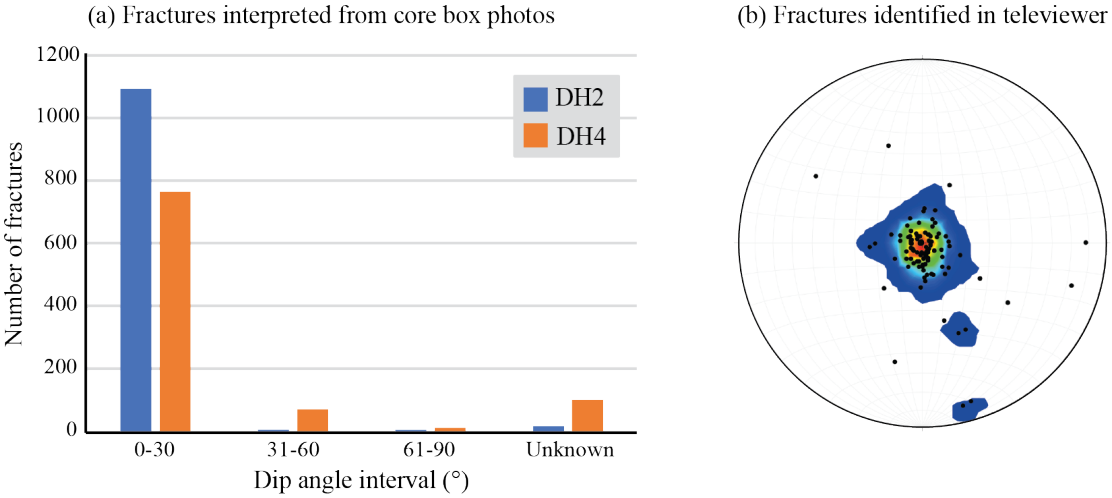

Figure 5.29: (a) Fracture abundance by dip angle intervals for the interpreted core box photos (UNIS CO2 Lab). Fractures primarily show log dip angles. (b) Data from DH4 televiewer presented in stereonet (UNIS CO2 Lab). The majority of the encountered fractures are subhorisontal.

Comparison of all fracture data for the same stratigraphic interval for DH2 and DH4 are plotted in Figure 5.30 and 5.31. A strong correlation was identified between the drilling induced fractures and interpreted fractures from core box photos in DH2 and DH4 (Fig. 5.32). Higher fracture frequencies were seen in drilling induced fractures in DH2, totalling 2462 more fractures than in DH4. In DH2, the drilling induced fractures exhibit very high frequencies in shale intervals, varying between 30 and 80 fractures per meter (Fig. 5.32a and b). In DH4, drilling induced fractures and interpreted fractures from core box photos present higher fracture frequencies in the deepest siltstone interval (Fig. 5.32c and d).

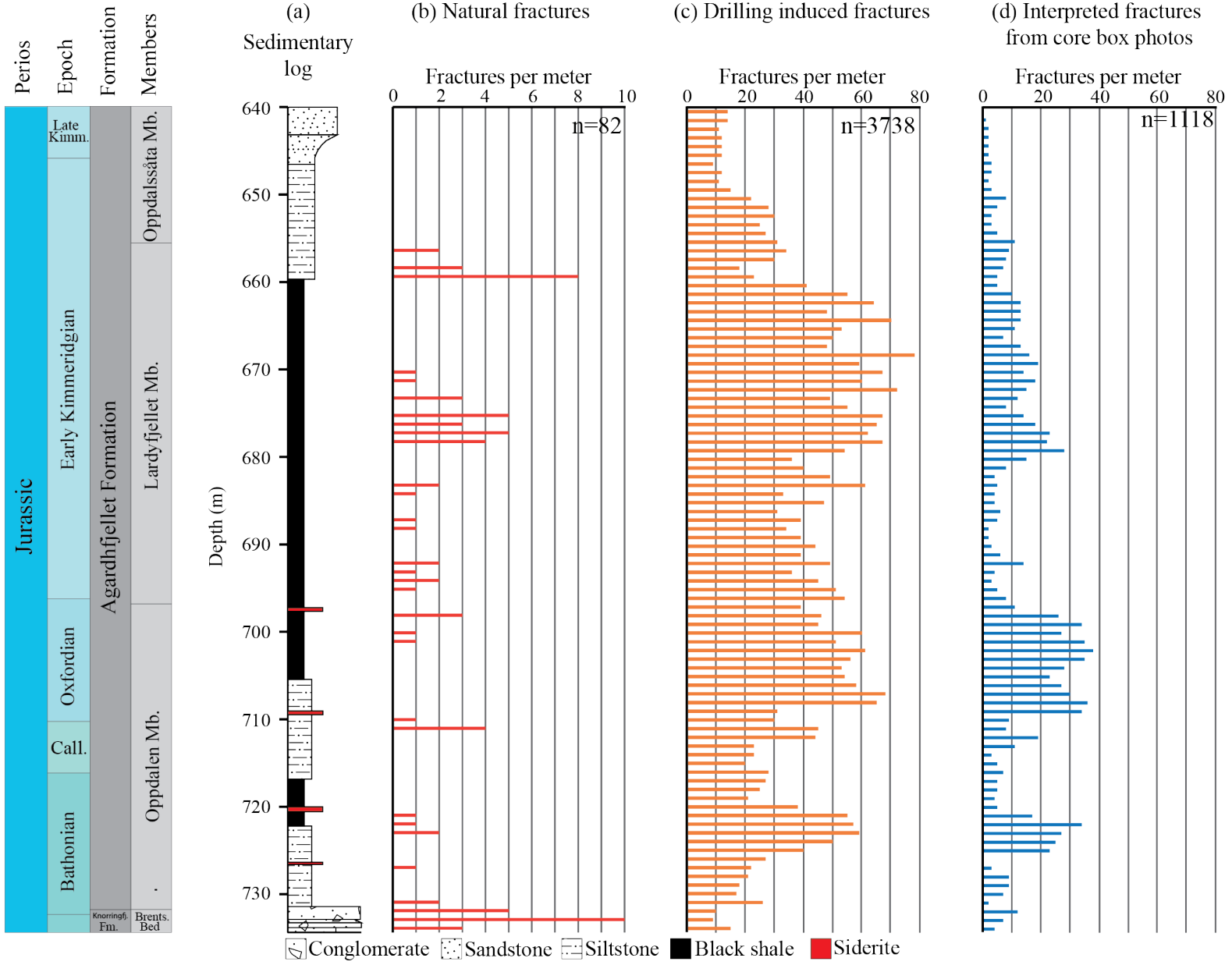

Figure 5.30: Fracture frequency per meter, for DH2. (a) Sedimentary log modified from Koevoets et al. (2016). Fractures per meter of (b) natural fractures (this study), (c) drilling induced fractures (this study) and (d) fractures from interpreted core box photos (Braathen et al., 2012).

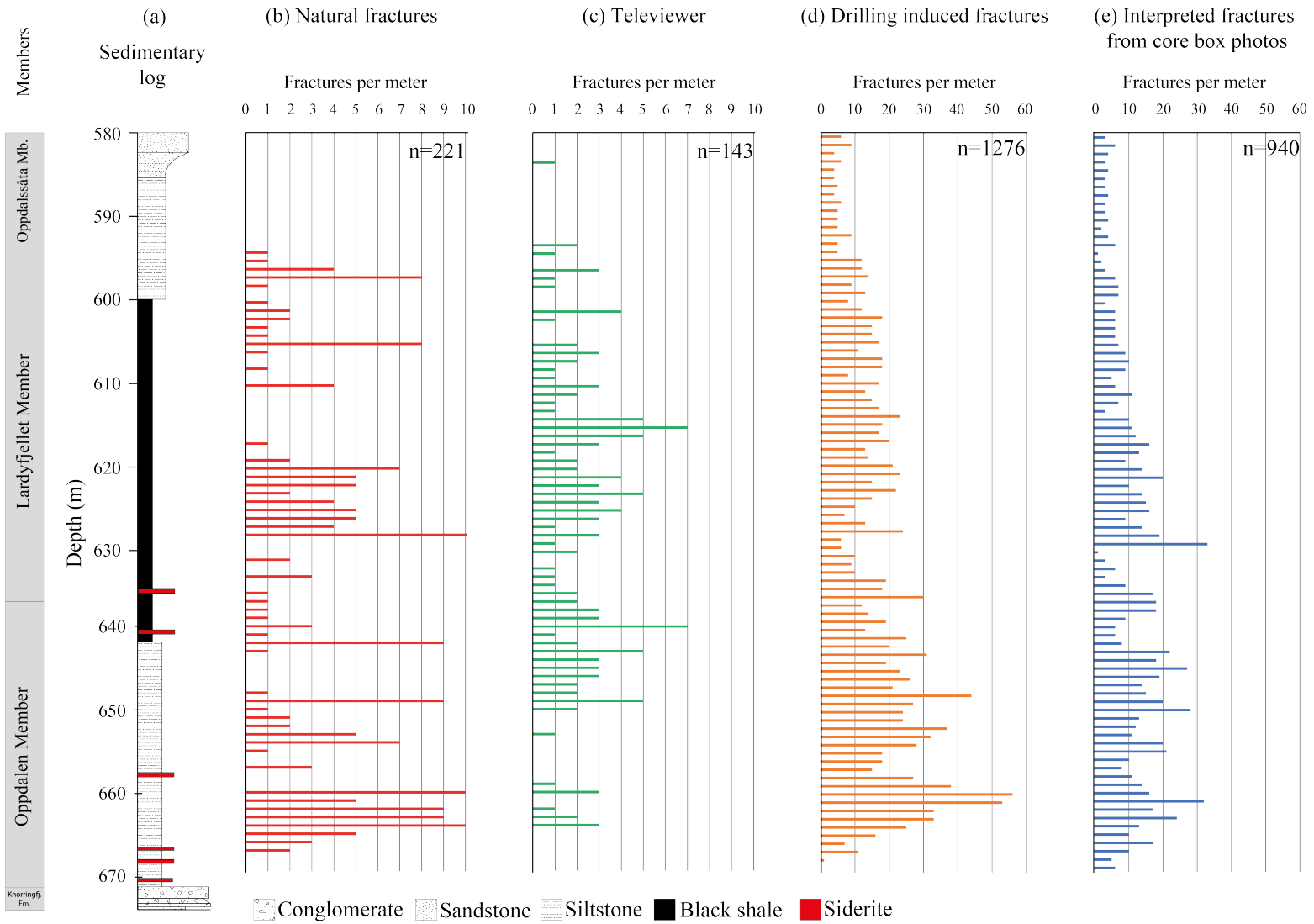

Figure 5.31: Fracture frequency per meter, for DH4. (a) Sedimentary log modified from Koevoets et al. (2016). Fractures per meter of (b) natural fractures (this study), (c) drilling induced fractures (this study), (d) fractures from interpreted core box photos (Braathen et al., 2012). and (e) fractures identified in televiewer (Elvebakk, 2010).

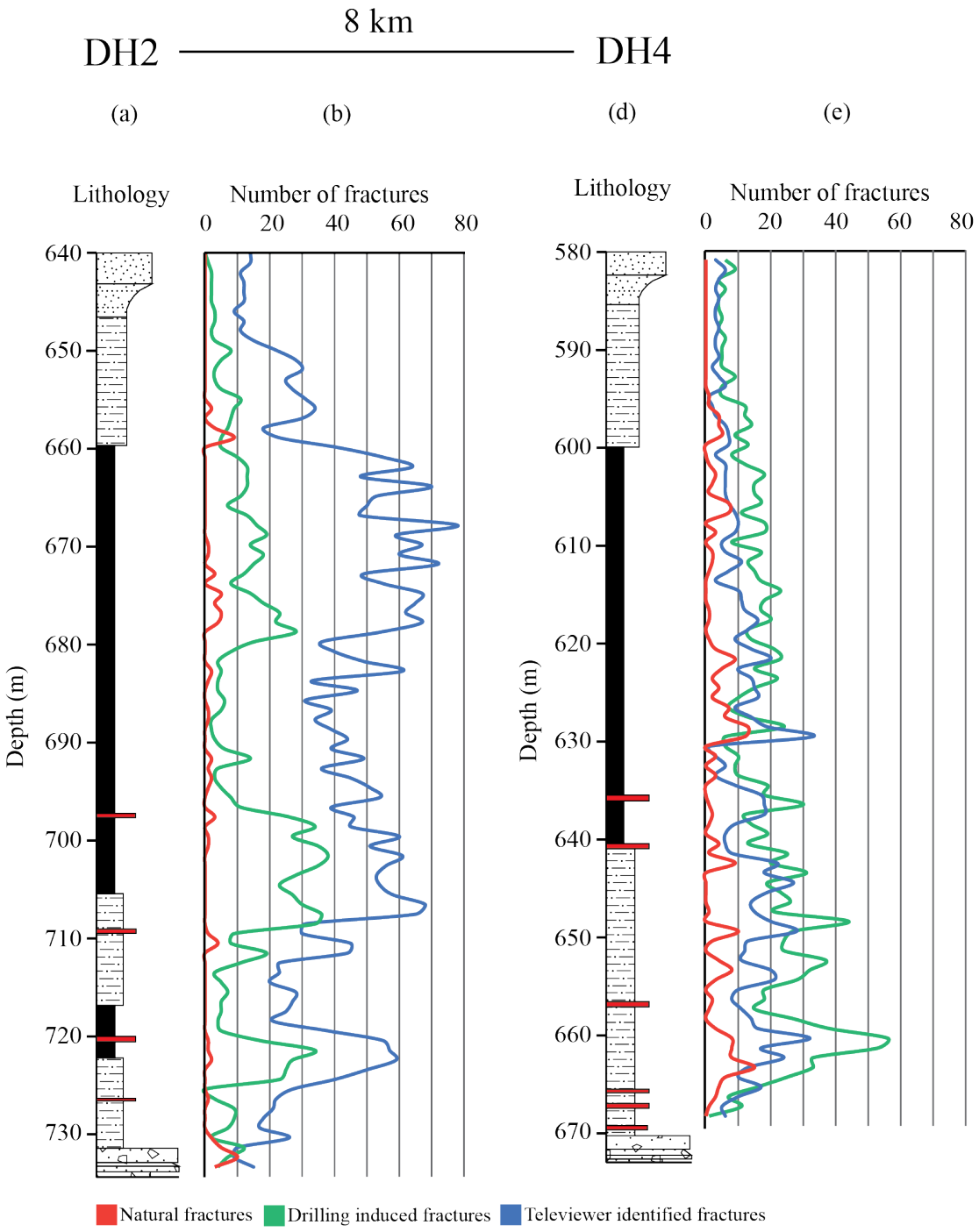

Figure 5.32: Sedimentary log modified from Koevoets et al. (2016) for (a) DH2 and (c) DH4. All fracture data plotted in graphs for (b) DH2 and (d) DH4. In DH2, drilling induced fractures and fractures interpreted from core box photos increase in abundance in shale intervals. In DH4, there is a stronger correlation with the natural fractures and other fracture data than in DH2. More fractures are encountered in siltstone for DH4.

Comparing fieldwork and drill core results

Figure 5.33 summarises the distribution of dip angles, fracture spacing and fracture orientation presented herein. The fractures collected in field are steeper than thos from drill cores (Fig. 5.33a). Further, the fracture spacing is much closer in the drill cores than in outcrops. Lastly, the distribution of fracture orientation from outcrops and televiewer is plotted in Figure 5.33c.

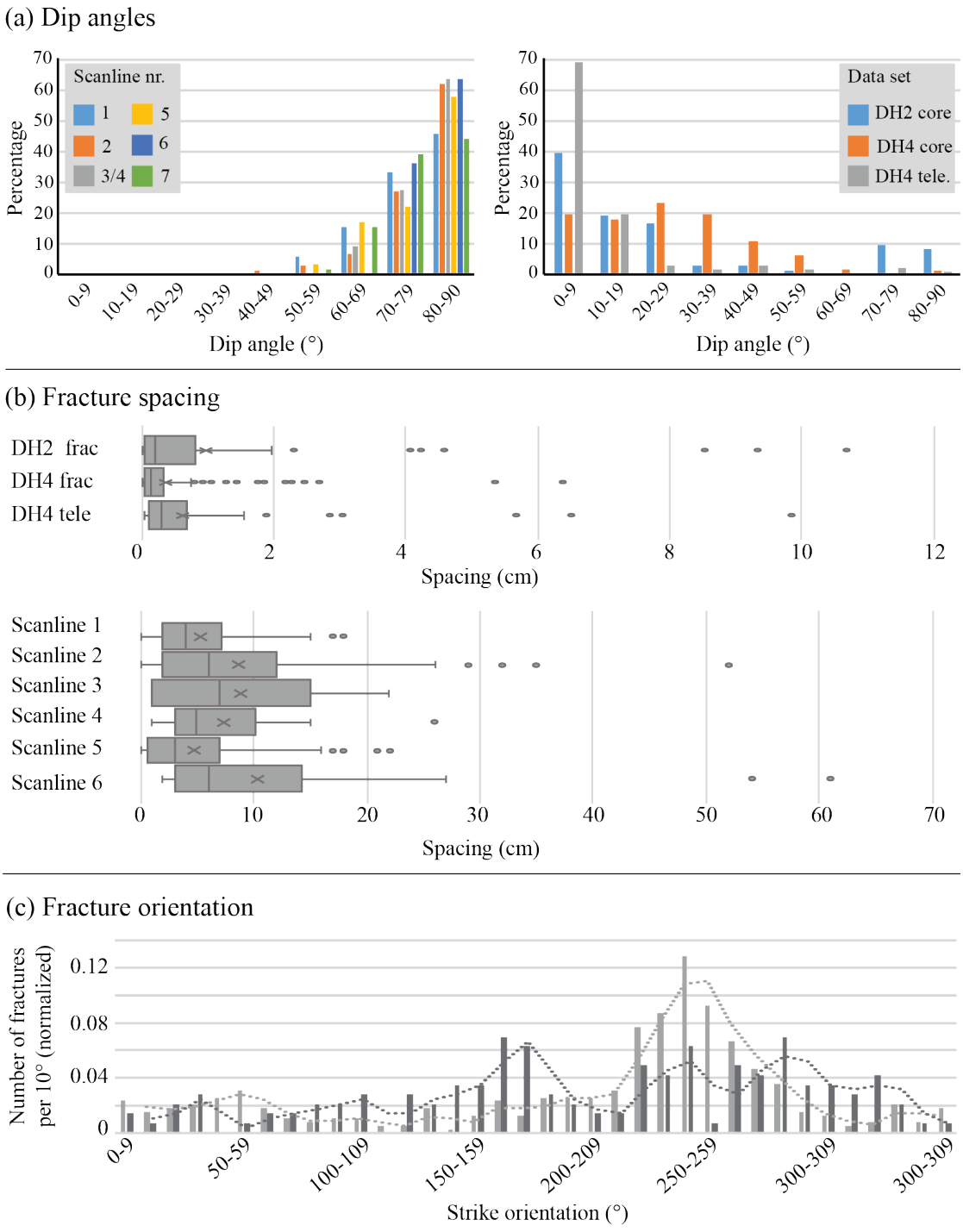

Figure 5.33: Summary of main findings in fracture abundance from fieldwork and drill core results. (a) Distribution of dip angles plotted with a bin size of 10 ° from fieldwork scanlines and drill core and televiewer data. Histograms are given in percentage. (c) Interquartile box-and-whisker plots of fracture spacing for drill cores and fieldwork scanlines. (d) Orientation comparison of the fractures from outcrop (dark grey) and DH4 televiewer (light grey). The histograms are normalised.

Chapter 6

Discussion

In this chapter, the development of the analysed structures from drill cores and outcrop is discussed. Firstly, the faults and fractures analysed near Deltaneset is considered in relation to the tectonic evolution of central Spitsbergen. Further, the caprock integrity of the lower Agardhfjellet Formation is discussed, based on analysed fractures from drill cores and Konusdalen West. Finally, challenges and source of errors, and suggestions for further work are presented.

6.1 Development of fracture networks and extensional faults in the lower Agardhfjellet Formation

All structures analysed in central Spitsbergen presented herein provide information on the kinematics responsible for their development. A northeast-southwest-trending normal fault array affected an interval from the Lardyfjellet Member to the lowermost stratigraphy of the Slottsmøya Member, observed in three locations, Konusdalen West, Konusdalen and Criocerasdalen respectively. Further, the normal fault in Konusdalen West was analysed in an outcrop down-section from two thrust faults in the uppermost Slottsmøya Member. For this study they were estimated to strike northwest-southeast, whereas Løvlie (2020) measured the faults to strike NNW-SSE. In addition, the analysed fracture network in Konusdalen West presented dominant ENE-WSW-trending opening fractures.

The northeast-southwest orientation of the normal fault array suggest northwest-southeast extension. However, based on the established knowledge of tectonic evolution of central Spitsbergen after deposition of the Agardhfjellet Formation, no tectonic event fits this suggested paleo stress regime (Dallmann et al., 2015; Maher et al., 2020). Therefore, three known phases of tectonism are discussed in relation to the development of the extensional regime that has affected the lower Agardhfjellet Formation in central Spitsbergen. The structural styles exhibited by the adjacent rock are considered when assessing the potential formation mechanism of the normal faults in the lower Agardhfjellet Formation. This is considered important, as the underlying storage formation of

the Wilhelmøya Subgroup host extensional faults (Mulrooney et al., 2019; Ogata et al., 2014b), whereas the upper Agardhfjellet and Rurikfjellet formations show a dominance of contractional structures, such as thrusts, back-thrusts, duplexes and a regional detachment zone (Andresen et al., 1992; Haremo et al., 1990; Løvlie, 2020). Additionally, a second detachment is found in the shale dominated Botneheia Formation underlying the storage formation. Hence, the storage formation and lower Agardhfjellet Formation is positioned between two detachments. Therefore, contrasts in stratigraphic competence is suggested as an explanation for the styles of deformation that occur, as well as the progressive deformation depending on the temporal and spatial evolution of tectonic events.

The first post-deposition event that may have affected the Agardfjellet Formation is the Early Cretaceous HALIP event. Evidence from this event is found as a suite of dolorite intrusion and a major hiatus in the lower Cretaceous succession in Svalbard (Dörr et al., 2012; Jochmann et al., 2019; Smelror[1] and Larssen, 2016). Thermal uplift an subsequent erosional unloading in response to this event should in theory be coupled by opening fractures and potentially normal faulting (Engelder, 1985; Gabrielsen and Kløvjan, 1997), but no evidence of faults related to this event has been reported from Svalbard. A second major uplift event is associated with Quaternary deglaciation, uplifting central Spitsbergen (Dimakis et al., 1998; Wangen et al., 2016). Again, decompaction associated with this event could in theory be coupled with local extensional structures. However, none of these two geological events are the most likely explanation for the normal faults in the lower Agardhfjellet Formation.

Results herein indicate the Paleogene WSFTB is the most probably cause of extensional faults and fractures in the lower Agardhfjellet Formation. Many authors have investigated the kinematics and deformation style of contractional structures associated with the WSFTB (Andresen et al., 1992; Braathen and Bergh, 1995; Braathen et al., 1999b,a). Extensional faults, however, such as those described herein, have only been briefly discussed (Ogata et al., 2014b; Mulrooney et al., 2019; Lubrano-Lavadera et al., 2019). The kinematics of the causal tectonic event are evaluated using orientations of fractures, normal faults , thrust faults and the detachment that is present in the Mid-Triassic Botneheia and upper Agardhfjellet formations. Three possible scenarios that could have lead to development of localized extension as seen in central Spitsbergen are illustrated in Figure 6.1. The faults can be a result of (1) a purely extensional phase, that characterises the final stage of the WSFTB evolution (Braathen and Bergh, 1995), (2) transpressional strike-slip faulting, which has been reported in the dextral Isfjorden-Ymerbukta Fault

Zone (Braathen et al., 1999a) or (3) extension occurring from contraction (only) due to space constraints in the hanging wall of thrusts between detachments.

After purely contractional stages, the WSFTB has a fourth stage where central Spitsbergen was deformed according to a northeast-southwest-trending, transpressional, dextral fault zone (Braathen et al., 1999a). The strike-slip fault zone, referred to as Isfjorden-Ymerbukta fault zone, is present 30 kilometers northwest of Deltaneset. Normal faults striking northwest-southwest are described in Braathen et al. (1999a), similar to the orientation of the normal faults near Deltaneset. Hence, the development of the normal faults analysed for this study can be a result of extension sub-parallel to the maximum principal stress, developing during progressive transpression (Krantz, 1995). Secondly, Braathen and Bergh (1995) suggest that post-orogenic rifting between Svalbard and Greenland which post-dates the WSFTB lead extension. Normal faults could develop in response to this separation. However, these two suggestion of the development of normal faults do not constrain the normal faulting only to the lower Agardhfjellet Formation and underlying storage formation.

Another mechanism that could constrain local extension in the lower Agardhfjellet Formation and underlying storage formation, is the relative movement of the decollement zones in the Botneheia and Agardhfjellet formations. Depending on which level of detachment was active or moving faster relative to one other, extension could occur to compensate for the space constrains. I.e. if the detachment in upper Agardhfjellet Formation was the only active detachment or moving faster than the detachment in Botneheia Formation, duplexes could develop to accommodate for the progressive deformation. Subsequently, if the detachment in Botneheia Formation was the only detachment moving (or moving faster than the detachment in Agardhfjellet Formation), local extension can accommodate space problems adjacent to a duplex. This would place the formation in a contractional phase of the WSFTB. The contraction vary from SSW-NNE to WSW-ENE shortening. Hence, the detachments would have an overall trend parallel to the main principal stress and structures forming in relation to this would likely strike perpendicular to the direction of movement (i.e. NNW-SSE to WNW-SSE). However, this does not fit with the northeast-southwest-trending normal fault analysed for this study.

The steeply dipping fractures analysed herein are interpreted as mode I fractures with a dominant ENE-WSW orientation. The fractures likely represent the orientation of

the maximum paleo-stress (Fig. 6.1). This indicates that mode I fractures developed during the same tectonis event as the normal faults that intersect the lower Agardhfjellet Formation. This finding is supported by analyses of fractures in the underlying storage formation (Wærum, 2011; Lord, 2013; Ogata et al., 2014b; Mulrooney et al., 2019). All authors suggest a dominant fracture orientation ENE-WSW to have formed during WSFTB. Further, the fractures from DH2 and DH4 are mostly shear fractures with low dip angles. This fits with the logged cores from the upper interval of the Agardhfjellet Formation by Løvlie (2020), where several intensely fractured to crushed intervals interpreted as detachment zones are recorded in the Slottsmøya Member.

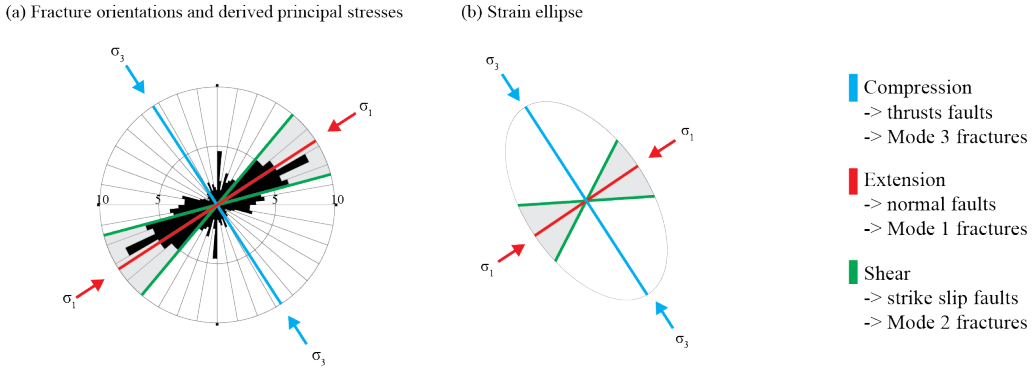

Figure 6.1: (a) Rose diagram showing fracture orientation and causal principal paleo-stresses. (b) Strain ellipse showing fracture modes.

6.2 Caprock integrity

The intention of the UNIS CO_2 Lab was to inject CO_2 into the Triassic storage formation comprised of the Wilhelmøya Subgroup, capped by the upper Jurassic to Cretaceous Agardhfjellet and Rurikfjellet formations. The discussion herein will address the significance of structural discontinuities in the lower Agardhfjellet Formation in central Spitsbergen as potential migration pathway. Fluid flow implications of preexisting structures will be emphasised, firstly through collected fracture type and abundance, secondly for the analysed fault architecture. Further, risk of caprock failure during CO_2 injections will be discussed. Finally, other features presenting potential seal bypass systems that can compromise the caprock integrity are addressed.

6.2.1 Integrating fracture network from drill core and outcrop

The fractures analysed in drill cores and outcrops in this study are contrasting. The vast majority of fractures in drill cores are low angled shear fractures (mode II or III). Natural fractures from drill cores presented higher fracture frequencies in the shale and siltstone intervals (i.e. Oppdalen and Lardyfjellet members), compared to sandstone intervals that comprise the Oppdalssåta Member (Fig. 5.16). Further, higher fracture frequencies correlate well with the siderite intervals in DH2. There are more identified fractures in DH4 than DH2, which can be a result of local impacts of e.g. faults. The analysis near Deltaneset confirms the presence of a normal fault array in the lower Agardhfjellet Formation and increased fracture frequencies in relation to the faults. Hence, higher fracture frequencies in DH4 could suggest influence an adjacent fault. The fractures measured in Konusdalen West are dominantly steeply dipping mode I fractures, trending ENE-WSW. Fracture spacing recorded from the drill cores is much closer than those from outcrops (Fig. 5.33).

The detailed characterisation from DH2 herein present fractures with lower dip angles in shale and dominating dip angles of 20-40°in siltstone. Further, the steep fractures that were analysed either terminate at a bedding plane, another fracture or taper out. A higher portion of calcite veins occurred in fractures with higher dip angles. The observation herein suggests that some veins are reactivated with a component of shear. Cross cutting relationship of veins and shear fractures, constrain the steep fracture as opening, mineral precipitation from fluid flow and subsequent sub-horizontal shearing, displacing the initial opening fracture.

The fractures in the lower Agardhfjellet Formation are mostly open, which can cause preferential migration pathways. Hence, the confirmed presence of fractures which exhibit all dip angles from drill cores and steeply dipping fractures from outcrops, is considered a potential risk of forming a fracture network preferential for fluid flow, if the fractures connect laterally and vertically.

6.2.2 Comparing fractures identified in drill core and televiewer

This study analysed the natural and drilling induced fractures, where fractures identified in televiewer and core box photos were obtained from Elvebakk (2010) and Braathen et al. (2012) respectively. Braathen et al. (2012) presents all encountered discontinuities in the drill cores without distinguishing between natural fractures and drilling induced

fractures. Most of the fractures analysed for this study were interpreted as drilling induces fractures. The drilling induced fractures from this study and those interpreted from core box photos (Braathen et al., 2012) correlate, as they are the same encountered discontinuities (Fig. 5.32). The drilling induced fractures are generated either during drilling or as a result of decompaction when retrieved the cores. Hence, interpreting all discontinuities in drill cores will overestimate the abundance of fracture actual present in the subsurface significantly. This is also suggested by Braathen et al. (2012).

The biggest discrepancy occurs between the quantitative amount of natural fractures encountered in drill core an televiewer in DH4 (Fig. 5.31). The fracture frequencies identified in televiewer are predominantly from the shale dominated interval comprising the Lardyfjellet Member. In total, there are 78 more fractures identified in televiewer than in the drill core in the 90 meter interval. The mean distribution of fractures per meter is 2.5 for televiewer versus 1.6 for the natural fractures from drill cores. It is therefore suggested that the televiewer overestimates the presence of fractures in the lowermost caprock succession. If only utilizing televiewer data when assessing the presence of fractures in the subsurface, the caprock can be considered compromised incorrectly. However, compared to the 940 fractures interpreted from core box photos, where all encountered discontinuities are presented as fractures, televiewer presents a better proxy for the actual fracturing of the lower Agardhfjellet Formation. Further, the televiewer can orient fractures which is preferential when predict connectivity of fractures, but fails to identify fractures with higher dip angles (Fig. 5.33).

6.2.3 Fault characteristics

The normal faults in the lower Agardhfjellet Formation in central Spitsbergen analysed in this study show offset of up to 8 meters. Detailed fault characteristics presented herein were all from Konusdalen West. A normal fault cut through the Oppdassåta Member and splays up-section into the lowermost Slottsmøya Member. Two antithetic faults (KW_A1 and KW_A2) intersecting the main fault in the hanging wall were analysed, showing decreased displacement upward. Additional synthetic faults (KW_S1 and K_S2) were present in the foot wall. The faults are quite discrete structures, i.e., a narrow zone of deformation, and the highly fractured nature of the host rock is not discernible from a possible damage zone. However, presence of numerous fracture swarms adjacent to the fault confirm high strain of the host rock. The fault core width increased with fault displacement. The fault core was predominantly made up by intensely fractured shale

lenses, shale gouge membranes and fault breccia. The shale gouge membranes were numerous and thicker within the fault where maximum displacement was recorded.

When compared to maximum displacement to length relationships (Kim and Sanderson, 2005), these displacements are not sufficient to result in lengths where the normal faults would link laterally. In addition, they do not appear to be hard-linked with faults in the underlying storage formation, when assessing displacement as dissipating down-section. This is also supported by Lubrano-Lavadera et al. (2019) and Mulrooney et al. (2019). However, there are potentially faults with greater displacement in the lower Agardhfjellet Formation that are not observed in central Spitsbergen.

The splay from the main fault is evidence of an active process zone where the fault dies out (McGrath and Davison, 1995; Skar et al., 2017). Splay faults and fractures commonly develop in the hanging wall around the tips of propagating fault (Perrin et al., 2016). The antithetic faults (KW_A1 and KW_A2) nucleate near the main fault and propagate upwards. These findings are supported by experimental studies summarised in Withjack et al. (1995). The same author also discusses synthetic faults and concludes these often have smaller offsets than the antithetic faults, which is also what is observed in the Konusdalen West outcrop. All faults that are identified in relation to the main fault (KW_N) are considered to accommodate space constraints.

The fault core width increase and number of thicker membranes with fault displacement, likely develop as more slip is accommodated for in these sections. This is a common observation in normal faults, (e.g., Peacock and Xing (1994); Braathen et al. (2009) and Torabi and Berg (2011). The increased membrane thicknesses decrease porosity and permeability of the fault. Hence, the normal fault in Konusdalen West (KW_N), is considered sealing. This is due to membranes present in the fault core acting as a baffle, which would prevent across fault migration (Færseth et al., 2007). This is considered important, as fluids flowing through fractures in the damage zones create preferential migration pathways for fluids causing along fault migration. This is supported by Faulkner et al. (2010); Ogata et al. (2014a). Further, due to the presence of normal faults in the reservoir (Lubrano-Lavadera et al., 2019; Mulrooney et al., 2019; Ogata et al., 2014b) and in the upper part of the caprock (Løvlie, 2020), there is a potential risk of these structures to connect and facilitate vertical migration. As such connectivity of structures throughout the Agardhfjellet Formation is considered the main risk for the caprock integrity.

6.2.4 Risk of hydraulic fracturing

Pressure build-up during CO_2 injection would change the stress acting on the lowermost caprock succession. The current stress field and recorded pore pressure needs to be assessed in order to predict potential failure in the lower Agardhfjellet Formation by hydraulic fracturing during CO_2 injections. Preexisting healed (or sealed) fractures represent weaknesses and will reopen prior to generation of new fractures. Bohloli et al. (2014) conducted mechanical laboratory tests and injections tests of the UNIS CO_2 Lab wells to evaluate the risk of hydraulic fracturing of the caprock. They conclude that the presence of preexisting fractures in combination with high tensile strength of pristine rocks makes it very unlikely to generate hydraulic fractures in response of rising pressure in the storage formation. I.e. the additional pressure needed to generate new fractures compared to shearing of preexisting fractures, is considered very high. With the current stress state of the caprock, with only slightly higher vertical stress compared to horizontal stress in the lower Agardhfjellet Formation (Bohloli et al., 2014), it is not sufficient to conclude on vertical or horizontal fractures as more likely to reactivate during CO2 injections.

Pore pressure measurements presented in Bohloli et al. (2014) exhibit severe under pressure in the storage formation and the lowermost interval of the Agardhfjellet Formation. Hence, the tolerance of rising pressure during CO_2 injections is considered greater than if the the formations followed the hydrostatic gradient. In contrast, over pressure was recorded for a sandstone aquifer overlying the entire caprock succession (i.e. the Agardhfjellet and Rurikfjellet formation). The inability to equalise pressure between the storage formation and an aquifer overlying the caprock indicate an effective seal. This interpretation is supported by Bohloli et al. (2014) and Braathen et al. (2012).

6.2.5 Additional seal bypass systems

Two additional features are considered a risk for the caprock integrity, as they can result in seal bypass systems. Firstly, the Early Cretaceous intrusions cause networks of cooling joints within the intrusion and syn-emplacement fractures in the host rocks adjacent to the intrusions (Senger et al., 2014a; Ogata et al., 2014b). As these are reported to commonly intrude the weaker lithologies on Svalbard, including the Agardhfjellet Formation, these are considered to have an impact where they occur locally. Secondly, sandstone injectites are observed in the lower Agardhfjellet Formation near Deltaneset (Ogata et al., 2014b). These form a direct fluid pathway, which could potentially

transport fluids through the caprock, depending on their extent.

6.2.6 Concluding remarks on caprock integrity

The lower Agardhfjellet Formation exhibit significantly impacts from tectonic deformation. The normal fault array analysed near Deltaneset is present in stratigraphy from the Oppdalen Member to the lowermost interval of the Slottsmøya Member. The high abundance of steep dipping, open fractures adjacent to the faults presented herein is considered the main risk of enabling fluid flow through the lowermost caprock succession. All features identified as potential risks for caprock integrity (i.e. migration pathways) are summarised in Figure 6.2.

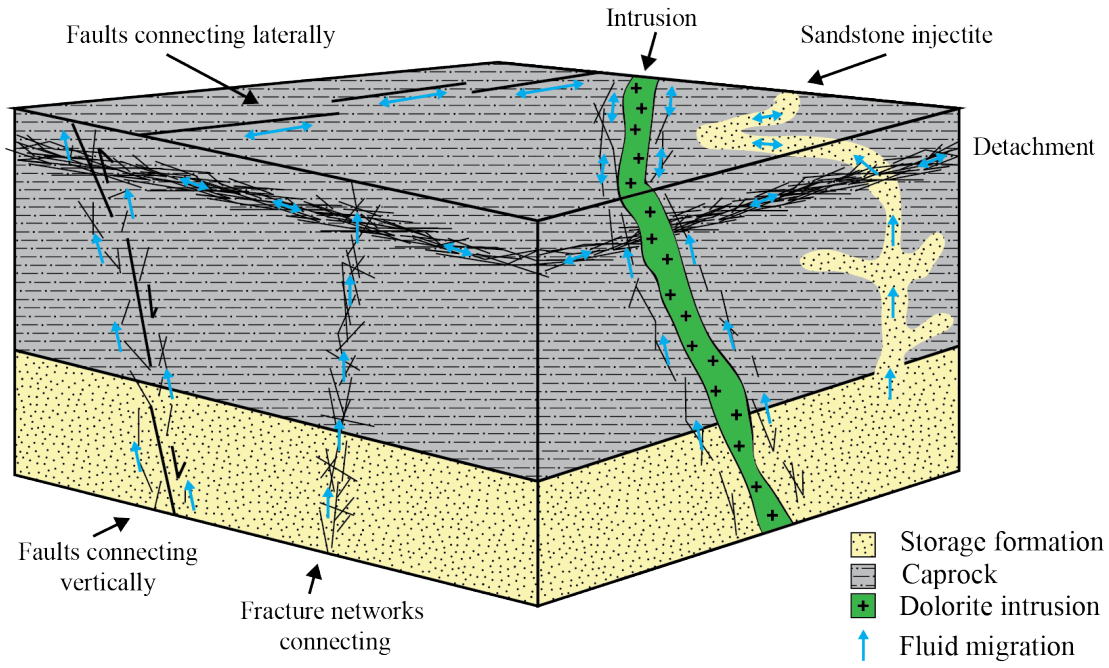

Figure 6.2: Will change figure, but the idea is to make a figure to illustrate the potential migration pathways.

The contrasting pore pressures recorded in the lower Agardhfjellet Formation and sandstone aquifer overlying the complete caprock interval in central Spitsbergen (Bohloli et al., 2014), indicate a caprock without continuous migration pathways. This is in accordance with the seal assessment conducted by Bohloli et al. (2014); Braathen et al. (2012) and Ogata et al. (2014b). As such, the caprock comprised of the Agardhfjellet and Rurikfjellet formations is argued to be an efficient seal for CO_2 sequestration purposes.

6.3 Challenges and sources of errors

There were challenges related to fieldwork for this study. Several polar bear encounters happened in field campaigns in 2018 and 2019, which lead to evacuation from the field site, which lead to a significant reduction in field days. However, a sufficient data set is considered to have been collected in order to adress the research objectives of the study.

Outcrop geometries do not display the faults as the 3D features that they are. This can make interpretations challenging and inaccurate. In addition, when assessing the extent of the fault, one must base this on the maximum displacement of a fault, which might not be what is exposed in the outcrop.

There are two biases to take into account for the fracture analyses conducted in this study. Firstly, the fracture analysis from the field is biased towards coarser lithologies and not divided into bed confined and thoroughgoing. This is due to an inability to conduct scanlines in heavily weathered outcrops comprised of black shales. Secondly, the analyses from vertical drill cores represent, by definition, a significant bias towards low angled fractures. All drill cores analysed for this study were 5 centimeter in diameter, which will not intersect the majority of the vertical fractures. Hence, the presence and extent of vertical fracture sets will not be captured. If systematically connecting vertical fractures from fieldwork to lithology, this bias could be minimized.

6.4 Future work

Some suggestions to further complete the caprock integrity analysis include conducting more detailed sedimentology analyses, mineralogy and clay analysis, to determine lithological control on fracturing. Furthermore, the presence of sandstone injectites is confirmed near Deltaneset in the Agardhfjellet Formation. The implications of which for caprock integrity should be explored. Finally, a more detailed fracture network model could be defined for the entire caprock succession, i.e., the Agardhfjellet and Rurikfjellet formations. The connectivity of fractures could lead to migration networks through the caprock. For this, the Oppdalssåta Member would have to be analyzed in cores and in the field.

Chapter 7

Conclusion

This study concludes on the nature and development of geological structures in the lower Agardhfjellet Formation. Implication of the structures in relation to caprock integrity is assessed and has the following concluding remarks:

- A southwest-northeast-trending normal fault array in the lower Agardhfjellet Formation developed in Central Spitsbergen during the Paleogene Western Spitsbergen fold-and-thrust-belt. The local extension developing in an overall contractional regime, constrained to the underlying storage formation and lower Agardhfjellet Formation.
- The analysed faults are not hard-linked to underlying storage formation or contractional structures in the upper Agardhfjellet Formation.
- Damage zones in relation to the faults exhibit steep dipping, open fractures, preferential for fluid migration. Predominantly WSW-ENE-trending open fractures exhibit high fracture frequencies adjacent to the analysed fault with additional fracture swarms.
- The fractures from the drill cores and outcrop represent different styles of deformation. Shear fractures were encountered in drill cores, whereas the fractures measured in outcrop were steep, opening fractures, both of which can be caused by contraction during formation of the WSFTB.
- The potential of fluids migrating through preexisting structures in the lower Agardhfjellet Formation is considered the main risks when assessing the structures implication on caprock integrity.
- The caprock succession as a whole (i.e. the Agardhfjellet and Rurikfjellet Formation) is an efficient seal for CO_2 storage purposes.

Bibliography

Abay, T., Karlsen, D., Lerch, B., Olaussen, S., Pedersen, J., and Backer-Owe, K. (2017). Migrated petroleum in outcropping mesozoic sedimentary rocks in spitsbergen: Organic geochemical characterization and implications for regional exploration. *Journal of Petroleum Geology*, 40(1):5–36.

Ameen, M. S. (1995). Fractography: fracture topography as a tool in fracture mechanics and stress analysis. an introduction. *Geological Society Special Publication*, (92):1–10.

Anderson, E. M. (1905). The dynamics of faulting. *Transactions of the Edinburgh Geological Society*, 8(3):387–402.

Andresen, A., Haremo, P., Swensson, E., and Bergh, S. G. (1992). Structural geology around the southern termination of the lomfjorden fault complex, agardhdalen, east spitsbergen. *Norsk Geologisk Tidsskrift*, 72(1):83–91.

Aplin, A. C., Fleet, A. J., and Macquaker, J. H. (1999). Muds and mudstones: Physical and fluid-flow properties. *Geological Society, London, Special Publications*, 158(1):1–8.

Bäckström, S. A. and Nagy, J. (1985). *Depositional history and fauna of a Jurassic phosphorite conglomerate (the Brentskardhaugen Bed) in Spitsbergen.*

Bælum, K. and Braathen, A. (2012). Along-strike changes in fault array and rift basin geometry of the carboniferous billefjorden trough, svalbard, norway. *Tectonophysics*, 546:38–55.

Bergh, S. G. and Andresen, A. (1990). Structural development of the tertiary fold-and-thrust belt in east oscar ii land, spitsbergen. *Polar Research*, 8(2):217–236.

Bergh, S. G., Braathen, A., and Andresen, A. (1997). Interaction of basement-involved and thin-skinned tectonism in the tertiary fold-thrust belt of central spitsbergen, svalbard. *AAPG bulletin*, 81(4):637–661.

Birkenmajer, K., Pugaczewska, H., and Wierzbowski, A. (1982). The janusfjellet formation (jurassic-lower cretaceous) at myklegardfjellet, east spitsbergen. *Palaeontologia Polonica*, 43:107–140.

Bjærke, T. et al. (1980). Mesozoic palynology of svalbard v. dinoflagellates from the agardhfjellet member (middle and upper jurassic) in spitsbergen. *Norsk Polarinstitutt Skrifter*, 172:145–167.

Bohloli, B., Skurtveit, E., Grande, L., Titlestad, G. O., Børresen, M., Johnsen, Ø., and Braathen, A. (2014). Evaluation of reservoir and cap-rock integrity for the longyearbyen co2 storage pilot based on laboratory experiments and injection tests.

Braathen, A., Bælum, K., Christiansen, H. H., Dahl, T., Eiken, O., Elvebakk, H., Hansen, F., Hanssen, T. H., Jochmann, M., Johansen, T. A., et al. (2012). The longyearbyen co 2 lab of svalbard, norway—initial assessment of the geological conditions for co 2 sequestration. *Norwegian Journal of Geology/Norsk Geologisk Forening*, 92(4).

Braathen, A., Bergh, S., Karlsen, F., Maher, H., Andresen, A., Hansen, A.-I., and Bergvik, A. (1999a). Kinematics of the isfjorden-ymerbukta fault zone: a dextral oblique-thrust ramp in the tertiary fold-thrust belt of spitsbergen. *Norsk Geologisk Tidsskrift*, 79(4):227–240.

Braathen, A. and Bergh, S. G. (1995). Kinematics of tertiary deformation in the basement-involved fold-thrust complex, western nordenskiøld land, svalbard: tectonic implications based on fault-slip data analysis. *Tectonophysics*, 249(1-2):1–29.

Braathen, A., Bergh, S. G., and Maher Jr, H. D. (1999b). Application of a critical wedge taper model to the tertiary transpressional fold-thrust belt on spitsbergen, svalbard. *Geological Society of America Bulletin*, 111(10):1468–1485.

Braathen, A., Tveranger, J., Fossen, H., Skar, T., Cardozo, N., Semshaug, S., Bastesen, E., and Sverdrup, E. (2009). Fault facies and its application to sandstone reservoirs. *AAPG bulletin*, 93(7):891–917.

Brekke, H., Sjulstad, H. I., Magnus, C., and Williams, R. W. (2001). Sedimentary environments offshore norway—an overview. In *Norwegian Petroleum Society Special Publications*, volume 10, pages 7–37. Elsevier.

Childs, C., Manzocchi, T., Walsh, J. J., Bonson, C. G., Nicol, A., and Schöpfer, M. P. (2009). A geometric model of fault zone and fault rock thickness variations. *Journal of Structural Geology*, 31(2):117–127.

Corfu, F., Polteau, S., Planke, S., Faleide, J. I., Svensen, H., Zayoncheck, A., and Stolbov, N. (2013). U–pb geochronology of cretaceous magmatism on svalbard and franz josef land, barents sea large igneous province. *Geological Magazine*, 150(6):1127–1135.

Dallmann, W. (1999). *Lithostratigraphic lexicon of Svalbard*. Norwegian Polar Institute.

Dallmann, W. K., Elvevold, S., Gerland, S., Hormes, A., Majka, J., Ottemöller, L., Pavlova, O., and Sander, G. (2015). Geoscience atlas of svalbard.

Dimakis, P., Braathen, B. I., Faleide, J. I., Elverhøi, A., and Gudlaugsson, S. T. (1998). Cenozoic erosion and the preglacial uplift of the svalbard–barents sea region. *Tectonophysics*, 300(1-4):311–327.

Dörr, N., Lisker, F., Clift, P., Carter, A., Gee, D. G., Tebenkov, A., and Spiegel, C. (2012). Late mesozoic–cenozoic exhumation history of northern svalbard and its regional significance: Constraints from apatite fission track analysis. *Tectonophysics*, 514:81–92.

Dypvik, H. (1984). Jurassic and cretaceous black shales of the janusfjellet formation, svalbard, norway. *Sedimentary Geology*, 41(2-4):235–248.

Dypvik, H., Eikeland, T., Backer-Owe, K., Andresen, A., Johanen, H., Elverhøi, A., Nagy, J., Haremo, P., and Biærke, T. (1991). The janusfjellet subgroup (bathonian to hauterivian) on central spitsbergen: a revised lithostratigraphy. *Polar Research*, 9(1):21–44.

Dypvik, H. and Harris, N. B. (2001). Geochemical facies analysis of fine-grained siliciclastics using th/u, zr/rb and (zr+ rb)/sr ratios. *Chemical Geology*, 181(1-4):131–146.

Elvebakk, H. (2010). Results of borehole logging in well lyb co2, dh4 of 2009, longyearbyen, svalbard.

Engelder, T. (1985). Loading paths to joint propagation during a tectonic cycle: an example from the appalachian plateau, usa. *Journal of Structural Geology*, 7(3-4):459–476.

Engelder, T. and Lacazette, A. (1990). Natural hydraulic fracturing. *Rock joints*, pages 35–44.

Færseth, R. B., Johnsen, E., and Sperrevik, S. (2007). Methodology for risking fault seal capacity: Implications of fault zone architecture. *AAPG bulletin*, 91(9):1231–1246.

Faleide, J. I., Bjørlykke, K., and Gabrielsen, R. H. (2010). Geology of the norwegian continental shelf. In *Petroleum Geoscience*, pages 467–499. Springer.

Faulkner, D., Jackson, C., Lunn, R., Schlische, R., Shipton, Z., Wibberley, C., and Withjack, M. (2010). A review of recent developments concerning the structure, mechanics and fluid flow properties of fault zones. *Journal of Structural Geology*, 32(11):1557–1575.

Freund, L. B. (1998). *Dynamic fracture mechanics*. Cambridge university press.

Gabrielsen, R. and Kløvjan, O. (1997). Late jurassic—early cretaceous caprocks of the southwestern barents sea: fracture systems and rock mechanical properties. In *Norwegian Petroleum Society Special Publications*, volume 7, pages 73–89. Elsevier.

Gabrielsen, R. H. and Clausen, J. A. (2001). Horses and duplexes in extensional regimes: A scale-modeling contribution. *Geological Society of America Memoirs*, 193:207–220.

Gale, J. F., Laubach, S. E., Olson, J. E., Eichhubl, P., and Fall, A. (2014). Natural fractures in shale: A review and new observationsnatural fractures in shale: A review and new observations. *AAPG bulletin*, 98(11):2165–2216.

Gasser, D. (2014). The caledonides of greenland, svalbard and other arctic areas: status of research and open questions. *Geological Society, London, Special Publications*, 390(1):93–129.

Hanks, C. L., Lorenz, J., Teufel, L., and Krumhardt, A. P. (1997). Lithologic and structural controls on natural fracture distribution and behavior within the lisburne group, northeastern brooks range and north slope subsurface, alaska. *AAPG bulletin*, 81(10):1700–1720.

Haremo, P. and Andresen, A. (1992). Tertiary décollement thrusting and inversion structures along billefjorden and lomfjorden fault zones, east central spitsbergen. In *Structural and tectonic modelling and its application to petroleum geology*, pages 481–494. Elsevier.

Haremo, P., Andresen, A., Dypvik, H., Nagy, J., Elverhøi, A., Eikeland, T. A., and Johansen, H. (1990). Structural development along the billefjorden fault zone in the area between kjellströmdalen and adventdalen/sassendalen, central spitsbergen. *Polar Research*, 8(2):195–216.

Hubbert, M. K. and Willis, D. G. (1972). Mechanics of hydraulic fracturing.

Ingram, G. M. and Urai, J. L. (1999). Top-seal leakage through faults and fractures: the role of mudrock properties. *Geological Society, London, Special Publications*, 158(1):125–135.

Jochmann, M. M., Augland, L. E., Lenz, O., Bieg, G., Haugen, T., Grundvåg, S. A., Jelby, M. E., Midtkandal, I., Dolezych, M., and Hjálmarsdóttir, H. R. (2019). Sylfjellet: a new outcrop of the paleogene van mijenfjorden group in svalbard. *arktos*, pages 1–22.

Kim, Y.-S., Peacock, D. C., and Sanderson, D. J. (2004). Fault damage zones. *Journal of structural geology*, 26(3):503–517.

Kim, Y.-S. and Sanderson, D. J. (2005). The relationship between displacement and length of faults: a review. *Earth-Science Reviews*, 68(3-4):317–334.

Koevoets, M., Abay, T., Hammer, Ø., and Olaussen, S. (2016). High-resolution organic carbon–isotope stratigraphy of the middle jurassic–lower cretaceous agardhfjellet formation of central spitsbergen, svalbard. *Palaeogeography, Palaeoclimatology, Palaeoecology*, 449:266–274.

Koevoets, M. J., Hammer, Ø., Olaussen, S., Senger, K., and Smelror, M. (2019). Integrating subsurface and outcrop data of the middle jurassic to lower cretaceous agardhfjellet formation in central spitsbergen. *Norwegian Journal of Geology*, 99(2):219–252.

Krajewski, K. (1990). Phosphoritization in a starved shallow shelf environment: the brentskardhaugen bed (toarcian-bajocian) in spitsbergen. *Polish Polar Research*, pages 331–344.

Krajewski, K. P. (2004). Carbon and oxygen isotopic survey of diagenetic carbonate deposits in the agardhfjellet formation (upper jurassic), spitsbergen: preliminary results. *Polish Polar Research*, pages 27–43.

Krajewski, K. P., ŁACKA, B., KUŹNIARSKI, M., ORŁOWSKI, R., and PREJBISZ, A. (2001). Diagenetic ori- gin of carbonate in the marhogda bed (jurassic) in spitsbergen, svalbard. *Pol. Polar Res*, 22:89–128.

Krantz, R. (1995). The transpressional strain model applied to strike-slip, oblique-convergent and oblique-divergent deformation. *Journal of Structural Geology*, 17(8):1125–1137.

Kulander, B. R., Dean, S. L., and Barton, C. C. (1977). *Fractographic Logging for Determination of Pre-core and Core-induced Fractures, Nicholas Combs No. 7239 Well,*

Hazard, Kentucky. Energy Research and Development Administration, Morgantown Energy Research ....

Laubach, S. E., Olson, J. E., and Gross, M. R. (2009). Mechanical and fracture stratigraphy. *AAPG bulletin*, 93(11):1413–1426.

Leever, K. A., Gabrielsen, R. H., Faleide, J. I., and Braathen, A. (2011). A transpressional origin for the west spitsbergen fold-and-thrust belt: Insight from analog modeling. *Tectonics*, 30(2).

Lord, G. S. (2013). Steep fracture patterns and their characteristics within the triassic de geerdalen formation on svalbard: An emphasis on regional trends, local variations and lithological controls. Master's thesis, Institutt for geologi og bergteknikk.

Lubrano-Lavadera, P., Senger, K., Lecomte, I., Mulrooney, M. J., and Kühn, D. (2019). Seismic modelling of metre-scale normal faults at a reservoir-cap rock interface in central spitsbergen, svalbard: implications for co2 storage. *Norwegian Journal of Geology*, 99(2):329–347.

Løvlie, K. (2020). Structural deformation and mineralogy of the agardhfjellet and rurikfjellet formations in central spitsbergen, svalbard. Master's thesis, UiO.

Maher, H., Senger, K., Braathen, A., Mulrooney, M. J., Smyrak-Sikora, A., Osmundsen, P. T., and Ogata, K. (2020). Mesozoic-cenozoic regional stress field evolution in svalbard. *Tectonics*, 39(4):e2018TC005461.

Maher, Jr, H. D. (2001). Manifestations of the cretaceous high arctic large igneous province in svalbard. *The Journal of Geology*, 109(1):91–104.

Maher Jr, H. D., Braathen, A., Bergh, S., Dallmann, W., and Harland, W. B. (1995). Tertiary or cretaceous age for spitsbergen's fold-thrust belt on the barents shelf. *Tectonics*, 14(6):1321–1326.

McGrath, A. G. and Davison, I. (1995). Damage zone geometry around fault tips. *Journal of Structural Geology*, 17(7):1011–1024.

Mcwhae, J. R. H. (1952). The major fault zone of central vestspitsbergen. *Quarterly Journal of the Geological Society*, 108(1-4):209–232.

Metz, B., Davidson, O., De Coninck, H., et al. (2005). *Carbon dioxide capture and storage: special report of the intergovernmental panel on climate change*. Cambridge University Press.

Midtkandal, I., Nystuen, J. P., and Nagy, J. (2007). Paralic sedimentation on an epicontinental ramp shelf during a full cycle of relative sea-level fluctuation; the helvetiafjellet formation in nordenskiöld land, spitsbergen. *Norwegian Journal of Geology/Norsk Geologisk Forening*, 87(3).

Minakov, A., Mjelde, R., Faleide, J. I., Flueh, E. R., Dannowski, A., and Keers, H. (2012). Mafic intrusions east of svalbard imaged by active-source seismic tomography. *Tectonophysics*, 518:106–118.

Mørk, A., Dallmann, W., Dypvik, H., Johannessen, E., Larssen, G., Nagy, J., Nøttvedt, A., Olaussen, S., Pchelina, T., and Worsley, D. (1999a). Mesozoic lithostratigraphy. *Lithostratigraphic lexicon of Svalbard. Upper Palaeozoic to Quaternary bedrock. Review and recommendations for nomenclature use*, pages 127–214.

Mørk, A., Elvebakk, G., Forsberg, A. W., Hounslow, M. W., Nakrem, H. A., Vigran, J. O., and Weitschat, W. (1999b). The type section of the vikinghogda formation: a new lower triassic unit in central and eastern svalbard. *Polar research*, 18(1):51–82.

Mulrooney, M. J., Larsen, L., Van Stappen, J., Rismyhr, B., Senger, K., Braathen, A., Olaussen, S., Mørk, M. B. E., Ogata, K., and Cnudde, V. (2019). Fluid flow properties of the wilhelmøya subgroup, a potential unconventional co2 storage unit in central spitsbergen. *Norwegian Journal of Geology*, 94(1):121–154.

Nejbert, K., Krajewski, K. P., Dubinska, E., and Pecskay, Z. (2011). Dolerites of svalbard, north-west barents sea shelf: age, tectonic setting and significance for geotectonic interpretation of the high-arctic large igneous province. *Polar Research*, 30(1):7306.

Nelson, R. (2001). *Geologic analysis of naturally fractured reservoirs*. Elsevier.

Nicol, A., Childs, C., Walsh, J., Manzocchi, T., and Schöpfer, M. (2017). Interactions and growth of faults in an outcrop-scale system. *Geological Society, London, Special Publications*, 439(1):23–39.

Ogata, K., Senger, K., Braathen, A., and Tveranger, J. (2014a). Fracture corridors as seal-bypass systems in siliciclastic reservoir-cap rock successions: Field-based insights from the jurassic entrada formation (se utah, usa). *Journal of Structural Geology*, 66:162–187.

Ogata, K., Senger, K., Braathen, A., Tveranger, J., and Olaussen, S. (2014b). Fracture systems and mesoscale structural patterns in the siliciclastic mesozoic reservoir-caprock succession of the longyearbyen co 2 lab project: Implications for geological

co 2 sequestration in central spitsbergen, svalbard. *Norwegian Journal of Geology*, 94(1):121–154.

Peacock, D. and Mann, A. (2005). Evaluation of the controls on fracturing in reservoir rocks. *Journal of Petroleum Geology*, 28(4):385–396.

Peacock, D. and Xing, Z. (1994). Field examples and numerical modelling of oversteps and bends along normal faults in cross-section. *Tectonophysics*, 234(1-2):147–167.

Perrin, C., Manighetti, I., and Gaudemer, Y. (2016). Off-fault tip splay networks: A genetic and generic property of faults indicative of their long-term propagation. *Comptes Rendus Geoscience*, 348(1):52–60.

Polteau, S., Hendriks, B. W., Planke, S., Ganerød, M., Corfu, F., Faleide, J. I., Midtkandal, I., Svensen, H. S., and Myklebust, R. (2016). The early cretaceous barents sea sill complex: distribution, 40ar/39ar geochronology, and implications for carbon gas formation. *Palaeogeography, Palaeoclimatology, Palaeoecology*, 441:83–95.

Rismyhr, B., Bjærke, T., Olaussen, S., Mulrooney, M. J., and Senger, K. (2019). Facies, palynostratigraphy and sequence stratigraphy of the wilhelmøya subgroup (upper triassic–middle jurassic) in western central spitsbergen, svalbard.

Rotevatn, A., Jackson, C. A.-L., Tvedt, A. B., Bell, R. E., and Blækkan, I. (2019). How do normal faults grow? *Journal of Structural Geology*, 125:174–184.

Schaaf, N. W. (2017). Towards characterization of natural fractures in a caprock shale: An integrated borehole-outcrop study of the agardhfjellet formation, svalbard, arctic norway.

Schultz, R. A. and Fossen, H. (2008). Terminology for structural discontinuities. *AAPG bulletin*, 92(7):853–867.

Senger, K., Planke, S., Polteau, S., Ogata, K., and Svensen, H. (2014a). Sill emplacement and contact metamorphism in a siliciclastic reservoir on svalbard, arctic norway. *Norwegian Journal of Geology/Norsk Geologisk Forening*, 94.

Senger, K., Tveranger, J., Ogata, K., Braathen, A., and Planke, S. (2014b). Late mesozoic magmatism in svalbard: A review. *Earth-Science Reviews*, 139:123–144.

Singhal, B. B. S. and Gupta, R. P. (2010). *Applied hydrogeology of fractured rocks*. Springer Science & Business Media.

Skar, T., Berg, S. S., Gabrielsen, R. H., and Braathen, A. (2017). Fracture networks of normal faults in fine-grained sedimentary rocks: examples from kilve beach, sw england. *Geological Society, London, Special Publications*, 439(1):289–306.

Skogseid, J., Planke, S., Faleide, J. I., Pedersen, T., Eldholm, O., and Neverdal, F. (2000). Ne atlantic continental rifting and volcanic margin formation. *Geological Society, London, Special Publications*, 167(1):295–326.

Smelror[1], M. and Larssen, G. B. (2016). Are there upper cretaceous sedimentary rocks preserved on sørkapp land, svalbard? *Norwegian Journal of Geology*, 96(2).

Steel, R., Gjelberg, J., Helland-Hansen, W., Kleinspehn, K., Nøttvedt, A., and Rye-Larsen, M. (1985). The tertiary strike-slip basins and orogenic belt of spitsbergen.

Stoker, M. S., Stewart, M. A., Shannon, P. M., Bjerager, M., Nielsen, T., Blischke, A., Hjelstuen, B., Gaina, C., McDermott, K., and Ólavsdóttir, J. (2017). An overview of the upper palaeozoic–mesozoic stratigraphy of the ne atlantic region. *Geological Society, London, Special Publications*, 447(1):11–68.

Torabi, A. and Berg, S. S. (2011). Scaling of fault attributes: A review. *Marine and Petroleum Geology*, 28(8):1444–1460.

Torabi, A., Gabrielsen, R., Fossen, H., Ringrose, P., Skurtveit, E., Ando, E., Marinelli, E., Viggiani, G., Braathen, A., Hovland, A., et al. (2015). Strain localization in sandstone and its implications for co2 storage. *first break*, 33(7):81–92.

Torsvik, T. H., Carlos, D., Mosar, J., Cocks, L. R. M., and Malme, T. (2002). Global reconstructions and north atlantic paleogeography 440 ma to recent. *BATLAS–Mid Norway plate reconstruction atlas with global and Atlantic perspectives. Geological Survey of Norway, Trondheim*, 18:39.

Wærum, G. O. (2011). Bruddmønstre i øvre triaslagrekken ved vindodden på svalbard: opptreden, geometri og dannelsesmekanismer samt betydning for co2 lagring. Master's thesis, Universitetet i Tromsø.

Wangen, M., Souche, A., and Johansen, H. (2016). A model for underpressure development in a glacial valley, an example from adventdalen, svalbard. *Basin Research*, 28(6):752–769.

Welbon, A. I. and Maher Jr, H. D. (1992). Tertiary tectonism and basin inversion of the st. jonsfjorden region, svalbard. *Journal of Structural Geology*, 14(1):41–55.

Westoby, M. J., Brasington, J., Glasser, N. F., Hambrey, M. J., and Reynolds, J. M. (2012). 'structure-from-motion'photogrammetry: A low-cost, effective tool for geoscience applications. *Geomorphology*, 179:300–314.

Withjack, M. O., Islam, Q. T., and La Pointe, P. R. (1995). Normal faults and their hanging-wall deformation: an experimental study. *AAPG bulletin*, 79(1):1–17.

Worsley, D. (1986). *The geological history of Svalbard: Evolution of an Arctic archipelago*. Den norske stats oljeselskap as.